Master Thesis in Geosciences

Velocity Anisotropy of shales and sandstones from core sample and well log on the Norwegian Continental shelf

Meseret Taye Melaku

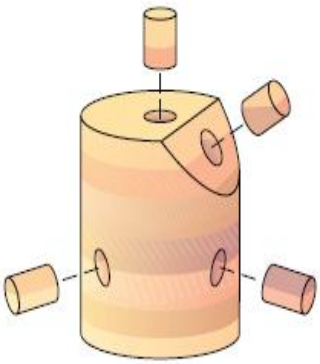

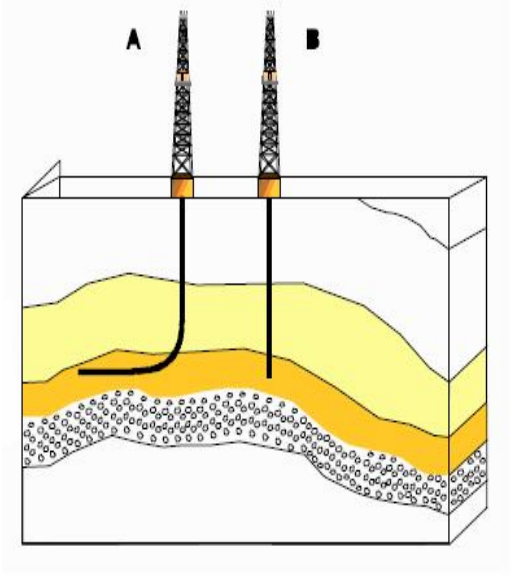

UNIVERSITY OF OSLO
FACULTY OF MATHEMATICS AND NATURAL SCIENCES

Velocity Anisotropy of shales and sandstones from Core Samples and well logs on the Norwegian Continental Shelf

Meseret Taye Melaku

Master Thesis in Geosciences

Discipline: Petroleum Geology and Geoscience

Department of Geosciences

Faculty of Mathematics and Natural Sciences

UNIVERSITY OF OSLO

[June 2007]

Abstract

Velocity anisotropy referse the directional inequality of velocity on the subsurface. Often sedimentary rocks are anisotropic and occurse at all scales from core plugs to reservoirs. In this thesis velocity anisotropy of shale and sandstone was analysed from core sample and well log data. The core sample was taken at a shallow and intermediate depth from the northern North Sea (Gullfaks and Statfjord Fileds) and deeply buried, the Haltenbanken Area. The well log data were vertical and deviated well bore from Statfjord Field. The estimated velocity anisotropy from the core sample varied from weak (ε=0.11 and γ= 0.11) for immature source rock type Draupne Formation, ε=0.02 and γ= 0.07 for calcite cemented Broom Formation (Brent Group) and ε=0.15 and γ= 0.27 for cap rock type Lange Formation from the Haltenbanken Area. Velocity anisotropy from the well log data also show evidence of anisotropy on the Statfjord Field shale formations. The predicted velocity anisotropy from the well log data was substantial due to layer induced anisotropy (~ ε=0.15 - 0.25 and ~γ= 0.43 - 0.531) shale formations. The observed degree of anisotropy from the core sample and well log data was dependent on: the volume and type of clay minerals, the provenance, the depositional environment, diagensis, compaction, kerogen (TOC) content. This study also observed how velocity anisotropy can make huge difference to a reservoir performance and subsurface imaging by emplmenting the estimated anisotropic parameters.The methods and the results obtained on this study may be used as potential indicator of remote detection of source rock, reservoir rock and cap rock.

ACKNOWLEDGMENTS

I sincerely thank my advisors, Professor Knut Bjørlykke and Associate Professor Jens Jahren their inspiring advice, scientific discussions, teaching, and continuous support for completion of this master thesis.

I would like to express my gratitude to Professors Leiv-J. Gelius for providing constructive suggestions on rockphysics side of my study.

I would like to give thanks to Dr Michel Heeremans for providing well log data

I would like to give thanks for PhD student and research fellows, Nazmul Haque Mondol, Øyvind Marcussen, Christer Bertel Peltonen, Olav Antonio Blaich, Boukili Mourad, their great deal of help, during my study here and help with editing my thesis

Last but not least, I thank my parents and relative and friends for their support and encouragement during my study.

Oslo 01.06.07

Meseret Taye

Table of Contents

Objective of the thesis

Introduction……1

Chapter 1. Evidence of Velocity Anisotropy……3

1.1 What is Anisotropy

1.2 The type of Anisotropy

1.3 Scale of Anisotropy

1.4 Symmetry of Anisotropy

1.5 Anisotropy of Shale

1.6 Anisotropy of Sandstones

1.7 Anisotropy of deviated wells

Chapter 2. Quantification of Anisotropy for TIV media……17

2.1 Elastic parameters of Transverse Isotropy

2.2 Phase velocities in a Transverse Isotropic Medium

2.3 Group Velocity and Anisotropic Wave Propagation

2.4 Elliptical anisotropy (Polar) anisotropy

2.5 Anisotropy well log

2.6 Backus Averaging for layer induced anisotropy

2.7 Anisotropy relations

Chapter 3: The Geology of the Study Area……..35

3.1 The Geology of northern North Sea

3.2 The Geology of Haltenbanken

Chapter 4: Velocity Anisotropy Analysis from Core samples……..45

4.1 Northern North Sea Core Samples

4.2 Haltenbanken Area Core Sample

4.3 Discussion

Chapter 5: Velocity Anisotropy from well log…….69

5.1 Database

5.2 Model Description

5.3 Results

5.3.1 Velocity Anisotropy from comparison of Vertical and Deviated well Logs.

5.3.2 Velocity versus well deviation angle

5.3.4 Quantification of the observed velocity anisotropy

5.3.5 Pure shale velocity anisotropy and formation parameters

5.4 Discussion

5.4.1 Velocity Anisotropy from comparison of Vertical and Deviated well Logs.

5.4.2 Velocity versus well deviation angle

5.4.4 Quantification of the observed velocity anisotropy

5.4.5 Pure shale velocity anisotropy and formation parameters

5.4.6 The relationship of P-and S-wave velocity with porosity and volume of Shale

Chapter 6: The Use of Anisotropy for Exploration and Exploitation……99

6.1 Anisotropic Depth Migration (ADM)

6.2 Anisotropy AVO analyses

Chapter 7: Conclusions…….109

References……123

Abbreviations

Objective of this study

The objective of this thesis is to address three main concepts in the explorations and productions of hydrocarbon. The first to look at the evidence, origin and causes of velocity anisotropy in shale and sandstones. The evidence (source) of velocity anisotropy will presented in accordance with previous studies of anisotropy in laboratory and field data. The second objective will deal about the best way of measurement, quantification and documentation of the detected or observed anisotropy. Data from core sample and well log will be used to quantify the degree of velocity anisotropy for shale and sandstone from the Norwegian Continental Shelf. The third will be the application of anisotropy; i.e how and when will be use anisotropy in general for exploration and exploitation in particular for subsurface seismic imaging, reservoir characterization and description. A practical example will be used to how anisotropy is important in subsurface imaging and reservoir characterization.

Introduction

Sedimentary rocks are anisotropic. Velocity anisotropy is the variation of velocity on measurement directional. There are two type of anisotropy: intrinsic and induced. The intrinsic anisotropy is the result of preferential orientation of the sediment grains and pores that can be created by sediment composition, grain size and shape, and deposition and compaction. Intrinsic anisotropy in sedimentary rocks is normally in the form of transverse isotropy. Most shale is intrinsically transversely isotropic. The induced anisotropy is caused by the strain associated with applied stress, fractures and mainly diagensis. Stress anisotropy preferentially aligns pores, grains, cracks, and fractures so that an otherwise isotropic rock becomes seismically anisotropic.

Anisotropy is then one of the few indicators of variations in rock that can be studied with wavelengths longer than the scale of the variations. Anisotropy, for example, can be detected only when the observing wavelength is larger than the ordering of elements creating the anisotropy. For example at ultrasonic scale can detect anisotropy at centimetre scale, at wireline (sonic) can detect at meter scale, and at seismic scale (frequency ~500 -900 kHz), reservoir beds can be detected.

The two types of anisotropy which is resulted due the styles of alignment in earth materials are: horizontal alignment with vertical axis of symmetry-vertically transverse isotropy (VTI) and vertical alignment with horizontal axis of symmetry - vertically transverse isotropy (HTI). Two oversimplified but convenient models have been created to describe how elastic properties, such as velocity or stiffness, vary in the two types.

In VTI waves generally travel faster horizontally, along layers, than vertically. Detecting and quantifying this type of anisotropy are important for correlation purposes, such as comparing sonic logs in vertical and deviated wells, and for bore hole and surface seismic imaging and studies of amplitude variation with offsets(AVO).

In HTI medium waves travelling along the fracture direction but within the competent rock generally travel faster than wave crossing the fractures. Identifying and measuring this kind of anisotropy yield information about the rock stress and fracture density and orientation. These parameters are important for designing hydraulic fracture jobs and for understanding horizontal and vertical permeability anisotropy.

From the literature review of sections, the work of many authors presented on anisotropic properties of shale and sandstone based on laboratory and field data (Jones and Wang, 1981, Hornby et al, 1994, Vernik and Liu, 1997, Wang, 2002). All the measured

shales show a substantial degree of seismic anisotropy, ranging from a few percent to as high as 50%. Massive sands are intrinsically isotropic.

This thesis will use core sample and well log to for velocity anisotropy of shale and sandstone. The thesis consists of seven chapters and they organized in the following:

Chapter 1. The chapter will try to address possible causes of velocity anisotropy, their origin on the subsurface. Scale of which detect anisotropy and the symmetry of the anisotropy medium will also be discussed.

Chappter2. The chapter will deal about the basics of the method of quantification and documenting velocity anisotropy for data from both ultrasonic laboratory and field data measurements.

Chapter 3. The short review of the geological settings of study area will be presented. Mostly the description focus on the lithology type and depositional environment of formations and groups.

Chapter 4. Using the method from chapter 3, the ultrasonic laboratory core sample velocity anisotropy will be analyzed for sample from the northern North Sea and the Haltenbanken Area. The core sample data was obtained from Norwegian Geotechnical Institute (NGI) in summarized sheet

Chapter 5: This chapter will present velocity anisotropy from the comparison between vertical and deviated well logs. Additionally the velocity versus well angle deviation will be for shale formation will be presented.

Chapter 6. Based on the observed anisotropy from chapter 4 and 5, the use of Velocity anisotropy for exploration and production (exploitation) will be discussed by two practical problems.

Chapter7: The major outcomes of this research will be reviewed and recommendations for further study will be given.

Chapter 1

1. Evidence of Velocity Anisotropy

1.1 What is Anisotropy?

Anisotropy: Variation of one or more properties of a homogeneous material with direction. The requirement of homogeneity makes the term specific and, in particular, disallows application to materials which are heterogeneous on the scale of the wavelengths used to probe them(Winsterstein, 1990).

Velocity anisotropy*:* Variation of wave speed with direction of wave travel in a homogeneous material, where homogeneity extends over distances on the order of, or exceeding, a wavelength (Winsterstein, 1990). A medium that displays this directional dependence is referred to as an anisotropic medium

1.2 Source of Anisotropy

Sedimentary rocks are often found to be anisotropic. In sedimentary rocks there are many sources of velocity anisotropy, some of them are: (Koesoemadinata and McMechan, 2004).

- aligned crystals,
- direct stress-induced anisotropy,
- lithologic anisotropy (i.e., aligned grains),
- aligned fractures, cracks and pores, and the nature of their infilling material (e.g. clays, hydrocarbons, water, etc.)
- structural anisotropy (i.e., fine layering) and

The first four source of anisotropy could be detected at micro scale and the last source of anisotropy at a sonic scale.

1.3 Type of Anisotropy

Two types of anisotropy exist: intrinsic and induced. Intrinsic anisotropy is the result of preferential orientation of the sediment grains and pores that can be created by sediment composition, grain size and shape, and deposition, whereas induced anisotropy is caused by the strain associated with applied stress, fractures, and diagensis (Wang, 2001)

Intrinsic Anisotropy

Anisotropy in the earth develops during deposition and during processes that take place after deposition. In clastic sediments, anisotropy can arise during and after deposition. In carbonates, anisotropy is controlled mostly by fractures and diagenetic processes, and so tends to arise after deposition (Anderson et al, 1994). In nature there is stratification, as a form of

intrinsic anisotropy, in many sedimentary structures such as river deposits, streams, fan deltas, estuarine and tidal deposits, beaches and shelves, slope and deep sea deposits, and eolian sand dunes (Ruiz, 2004).

Anisotropy for clastic rock during deposition develops when the rocks have some degree of uniformity and homogeneity, i.e. five fundamental properties of its grain -composition, size, shape, orientation and packing (Figure 1). The directionality of these properties of clastic material will develop intrinsic anisotropy.

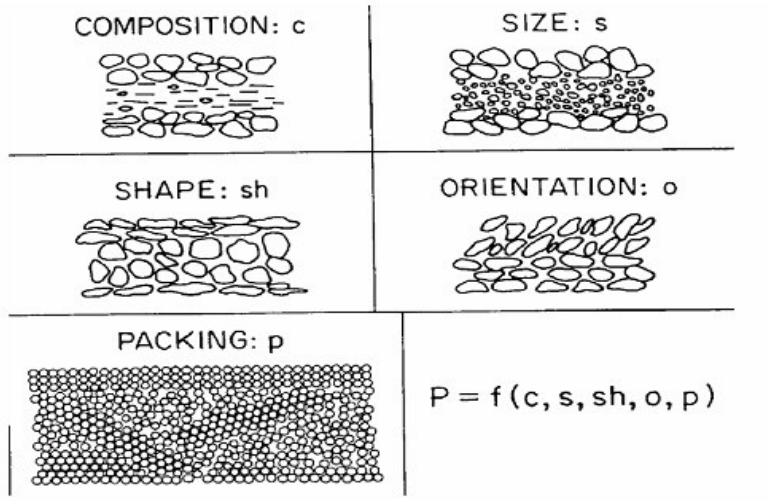

Figure 1: show the origin of anisotropy from five possible causes, such as grain - composition, size, shape, orientation and packing

In all depositional setting (deposition and transportation of clastic rocks), variations in transport energy produces variation in the degrees of grain orientation, packing and sorting. Because topography varies laterally, so does transport energy. This produces lateral gradient in sediment texture, composition and geometry. Over time, stacking of lateral gradients produces a vertical gradient (Anderson et al, 1994).

Induced Anisotropy

Many causes of anisotropy induced after depositions are lumped under the heading of diagenesis- the physical, chemical or biological alteration of sediment after deposition and during and after lithification (Anderson et al, 1994, Koesoemadinata and McMechan, 2004). Compaction by overburden pressure can cause rotation of grain axes into the horizontal plane. Compaction and dewatering of mud cause clay platelet alignment that give rise to pronounced anisotropy of shale. Realignment, grain pressure solution (dissolution of grains at their contact point) also contributes for anisotropy.

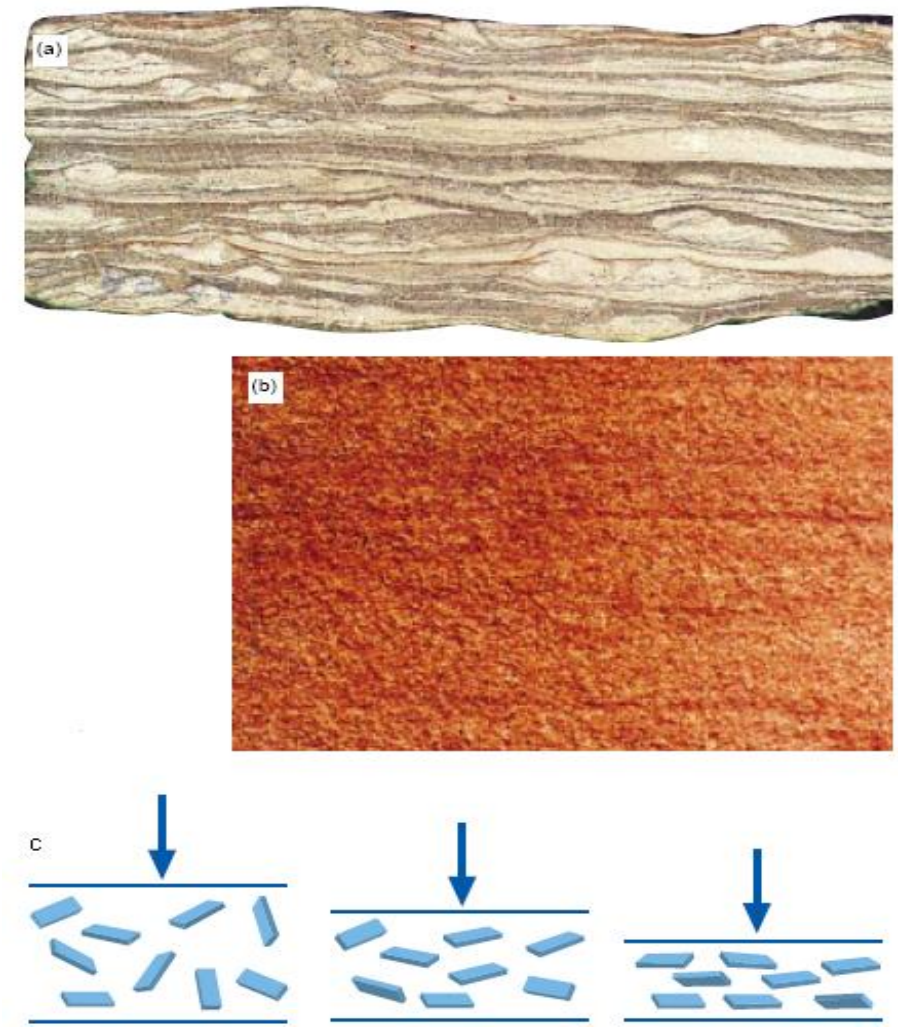

Figure 2: sedimentary layering and associated processes lead to anisotropy. The irregular layering in the siltstone (a) and the more regular layers in the sandstone (b) reflect variations in depositional environment, original mineralogy and grain size or diagenetic events. The clay grains (c) sediments have a random distribution at deposition. However, as the weight of accumulating sediment increases in the early stages of diagenesis, the grains are rotated to develop a rock fabric which exhibits elastic anisotropy. All of these factors will combine to give these rocks very different degrees of anisotropy (modified from Armstrong, 1994).

1. 4 Scale of Anisotropy

Anisotropy is then one of the few indicators of variations in rock that can be studied with wavelengths longer than the scale of the variations (Helbig, 1994). For example, using 30 m (100 ft) wavelengths seismic waves, we can examine rock structure down to the particle scale. However, seismic wave are unable to determine whether the anisotropy is due to alignment at the particle scale or at a scale nearer the length of the wave. In the words of one anisotropy specialist, ‘’ the seismic wave is a blunt instrument in that it cannot tell us whether anisotropy is from large or small structures (Winsterstein ,1990). Concept of scale is

fundamental for evaluating the source of anisotropy. The three common scales of measurements (wave length) which can reveal the anisotropic nature of rocks are: ultrasonic scale (mill meter), sonic scale (decimetre) and borehole seismic (tens of meter) wavelength. The following sections describe how anisotropy is being used to investigate rock properties at each of those scales based on the discussion of Armstrong et al (1994).

At the Ultrasonic scale : wave length in most sedimentary rocks are small which is the order of 0.25–5 mm for 250kHz ultrasonic laboratory experiments, and they are four times smaller at 1 MHz. Ultrasonic laboratory experiments on cores show evidence for both layering and fracture related anisotropy in different rock types.

Since ultrasonic laboratory measurements at of 0.25–5 mm wavelength detect anisotropy, this indicates that the spatial scale of the feature causing the anisotropy is much smaller than the wave length. The main cause of elastic anisotropy in shales appears to be layering of clay platelets on the micron scale due to geotropism and compaction. A good example of anisotropy due to clay platelet layering is shown in Figure 3.

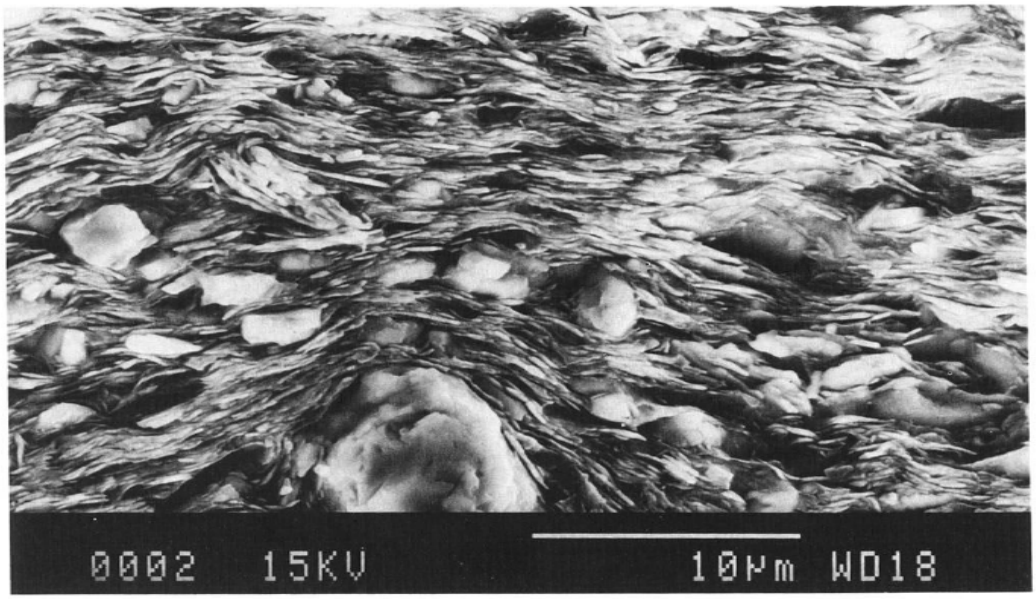

Figure 3: Scanning electron microphotograph of a shale. The platey particles are clay minerals while the larger, nearly spherical, particles are silt. (Hornby et al, 1994).

Ultrasonic measurements also able to detect anisotropy developed due to micro cracks. These microcracks may formed due to applied or unloading when a core is taken and in the subsiding basin microcracks are rarely

Laboratory experiment also show the effect of directional stresses on ultrasonic velocities, conforming that compressional waves travel faster in the direction of applied stress (Figure 4). One explanation of this may be that all rocks contain some distribution of microcracks, random or otherwise. As the stress applied, cracks oriented normal to the direction of greatest stress will close, while cracks aligned with the stress direction will open. In most cases, waves travel fastest when their particle motion is aligned in the direction of the opening cracks.

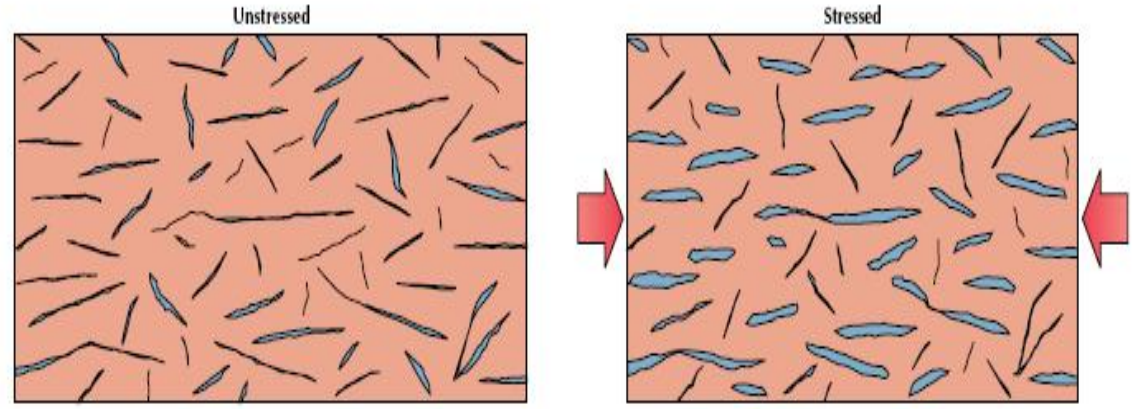

Figure 4: Effect of nonuniform compressive stress on microcracks. In rocks with randomly oriented microcracks (left), cracks normal to the direction of maximum compressional stress will close, while cracks parallel to the stress direction will open or remain open. Elastic waves in such a rock will travel faster across closed cracks in the direction of maximum stress than across open cracks (Armstrong et al, 1994).

At the sonic scale: ccurrently available technology can detect and characterize fine layering and fractures at the well bore scale (centimeters to meters). At this scale the most common evidence for TVI layering anisotropy comes from different P-wave velocities measured in vertical and highly deviated or horizontal wells in the same formation. Then the velocity will be higher in the horizontal than vertical direction for the same formations. In the case of S-wave the same can be said but the wave split in the fast and slow shear wave.

At the bore hole scale: most of the experiments designed to capture in-situ elastic properties have been vertical seismic profiles (VSPs), at the 10 m wave length scale. More sophisticated walkaways VSPs, called walkaways for short, can measure elastic properties of layered anisotropic rocks in way no others can.

1.5 Symmetry of Anisotropy medium

Transverse isotropy is defined as having the same property (e.g. velocity, stiffness, permeability, resistively) when measured within a plane that is normal to an axis, but having a different value when measured at some other angle to that axis (Winsterstein, 1990). This axis is a direction, designated as the symmetry axis and normal to alignment direction of subsurface.

There are two styles of alignment in earth materials: horizontal with vertical axis of symmetry and vertical with horizontal axis of symmetry. These two type of alignments (symmetries) give rise to two types of anisotropy: transverse isotropic with vertical axis of symmetry (VTI) and transversely isotropic with horizontal axis of symmetry (HTI). Two oversimplified but convenient models have been created to describe how elastic properties, such as velocity or stiffness, vary in the two types.

Vertically transverse isotropic (VTI): if the individual layer thickness is much less than the wave length of the passing wave, horizontally bedded fine layered sedimentary rocks can be modelled as transversely isotropic media with vertical axes of symmetry (Backus, 1962). In this type of simplest horizontal, or layered, case, elastic properties may vary vertically, such as from layer to layer, but not horizontally (Figure 5 left). Such a material is called transverse isotropic with vertical axis of symmetry (VTI).

Waves generally travel faster horizontally, along layers, than vertically. Detecting and quantifying this type of anisotropy are important for correlation purposes, such as comparing sonic logs in vertical and deviated wells, and for bore hole and surface seismic imaging and studies of amplitude variation with offsets(AVO). Around petroleum reservoir of interest, sandstone, shales, or shale-rich sequences generally exhibits transverse isotropy due to their layered characters. Transverse isotropy is chosen as the focus of this research because of its widespread occurrence in the sedimentary rocks commonly encountered in oil exploration.

Many exploration geophysicists have worked on transverse isotropy, for example, Helbig (1994), Thompsen (1986), Tsvankin (1996). Thompsen (1986), which is the single most cited article in the history of Geophysics proposed a convenient five parameter model to describe seismic wave propagation in a transversely isotropic medium. This model has been widely used in research into transversely isotropy.

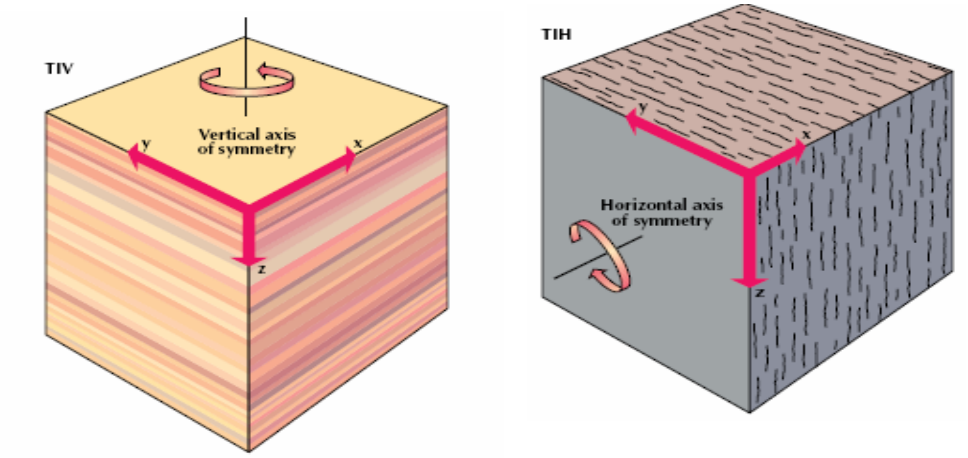

Figure 5: Simple geometries assumed for elastic anisotropy. In layered rocks (left vertically transverse isotropic), elastic properties are uniform horizontally within a layer, but may vary vertically and from layer to layer. In vertically fractured rocks (right, horizontally transverse isotropic), elastic properties are uniform in a vertical planes parallel to the fractures, but may vary in the direction perpendicular to the fractures, and across the fractures(modified from Armstrong et al ,1994).

Horizontally transverse isotropic (HTI): The simplest case of the second type of anisotropy corresponds to material with aligned vertical weaknesses such as cracks or fractures, or with unequal horizontal stresses (Winterstein, 1990). Elastic properties vary in the direction crossing the fractures, but not along the plane of the fractures. Such a material is called transversely isotropic with horizontal axis of symmetry (HTI) as shown in Figure 5, (right). Waves travelling along the fracture direction but within the competent rock generally travel faster than wave crossing the fractures. Identifying and measuring this kind of anisotropy yield information about the rock stress and fracture density and orientation. These parameters are important for designing hydraulic fracture jobs and for understanding horizontal and vertical permeability anisotropy. More complex cases, such as dipping layers, fractured layered rocks or rocks with multiple fracture sets, may be understood in terms of superposition of the effects of the individual anisotropies.

Layered rocks may have angle of dip from the horizontal direction. If so, the symmetry axis may not be vertical, .i.e. it may have an angle of dip to tilt from the vertical direction (Armstrong et al, 1994). Such a medium will be termed a tilted transversely isotropic (TTI) medium having a tilted symmetry axis. Knowledge of the angle of inclination of the symmetry axis is very important in understanding the fine structure of rocks, such as fracture orientation or local bedding directions.

The TTI is common feature when the geology is disturbed by tectonic activity. Whether the tectonic activity is compressional, extensional, or resulting from salt flows (Figure 6), the

resulting dipping layers have a tilted symmetry axis or bedding-plane normal. Several researchers have observed lateral position errors on structures below TTI media (Alkhalifah, 1995, Vestrum and Muenzer, 1997, and the reference therein).

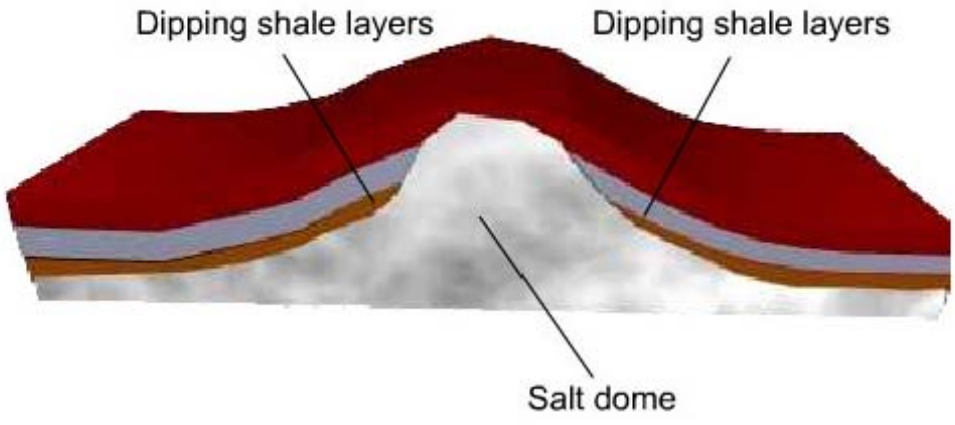

Figure 6: An example of Tilted transverse isotropy (TTI), the symmetric axis is tilted with respect to the horizontal. The TTI is due to the salt dome.

1.6 Anisotropy in Shale

Shales and silts are the most abundant sedimentary rocks in the earth's crust and have been estimated to comprise approximately two-thirds of all sedimentary rocks. In petroleum geology, organic shales are source rocks as well as seal rocks that trap oil and gas. In reservoir engineering, shales are flow barriers. In drilling, the bit often encounters greater shale volumes than reservoir sands. In seismic exploration, shales are seismic reflectors. As a result, seismic and petrophysical properties of shales and the relationships among these properties are important for both exploration and reservoir management. The existing database of shale velocities suggests that seismic propagation through shale is a function of intrinsic anisotropy of the constituent of clay minerals and their microstructures (Rai and Hanson 1988; Vernik and Nur 1992; Sayers 1994; Vernik and Liu 1997).

Anisotropy may also be studied in the laboratory using ultrasonic waves. In general ssuccessful imaging of subsurface features in the earth depends on knowledge of the behavior of the wave propagation through overlying strata, which is shale. Clearly, the inherent anisotropy of shales must be taken into account, both for structural imaging of subsurface features and for more advanced techniques such as amplitude variation with offset (AVO) analysis of hydrocarbon-bearing reservoirs (Hornby et al, 1994).

Previous studies of Shale Anisotropy

One of the first experimental studies on the physical properties of shale was by Kaarsberg (1958), who measured compressional wave velocity in both artificial and natural shale samples in three mutually perpendicular directions. Two cores were taken in the plane of bedding and one was taken perpendicular to bedding. Velocity was measured at atmospheric pressure as a function of drying time. The samples were determined to be transversely isotropic (hexagonal symmetry), due to preferred mineral orientation.

Jones and Wang (1981) reported compressional and shear wave velocities of Cretaceous shale as a function of confining pressure. Velocity measurements were made to 400 MPa at angles parallel and perpendicular to bedding, as well as at 45^0 to bedding, on both saturated and unsaturated cores. They found that velocities with vibration directions parallel to bedding were higher than those parallel to bedding, and concluded that this was due to preferred mineral orientation.

Banik (1983) studied the shale anisotropy from North Sea basin well log data. He used 21 well data sets and found a strong correlation between the occurrence of the depth error and the presence of shales in the subsurface. The error is caused by the elliptical velocity anisotropy of shales. From the depth correction, the plot result of the anisotropy of shaly sections as a function the depth section showed anisotropy of North Sea shale is a function of depth which is a quantitative agreement with the laboratory experiments of Jones and Wang (1981), Kaarsberg (1959), and the measurements on samples obtained in the Deep Sea Drilling project (Carlson and Christensen, 1977).

Lo et al. (1986) measured compressional and shear wave velocities for Chicopee shale to 100 MPa both parallel and perpendicular to bedding, as well as at 45^0 to bedding. They concluded that shale velocity anisotropy is due to preferred mineral orientation and cracks aligned parallel to bedding.

Johnston and Christensen (1995) combined measurements of velocity with X-ray diffraction measurements and SEM observations to relate velocity anisotropy to clay mineral orientation. ‘‘Orientation indices’’ were determined using an X-ray diffraction technique, and a positive correlation was found between the orientation of illite and chlorite mineral grains and velocity. Anisotropy at elevated pressures was, therefore, attributed to preferred mineral orientation rather than crack alignment (Figure 7). Velocity anisotropy in shale has also been related to thermal maturity as well as kerogen content and orientation (Vernik and Liu, 1997). For example Vernik and Nur (1992) found anisotropy values reaching 40 to 50 % for organic rich North Sea black shale.

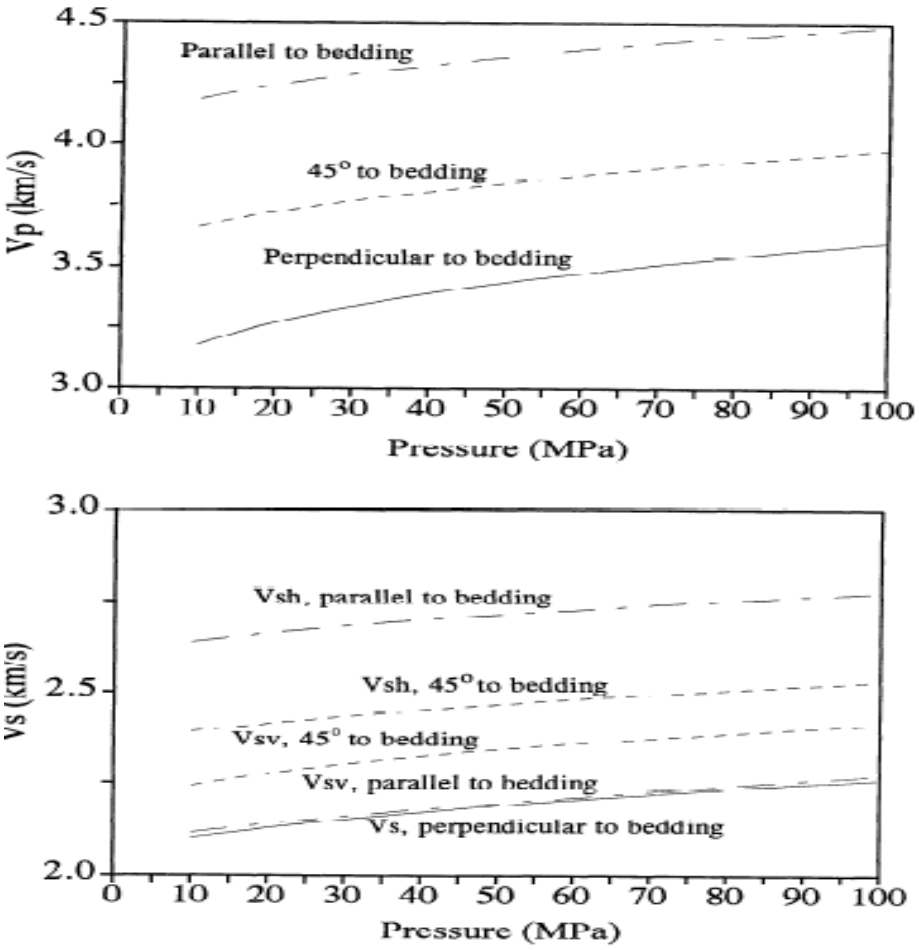

Figure 7: Compressional and shear wave velocities for selected propagation direction as a function of confining pressure for core sample analysed by Johnston and Christensen. (1993).

Hornby et al. (1994) uses an anisotropic effective-medium approach to model the elastic properties of shales. Comparison with the laboratory results of Jones and Wang (1981) demonstrates the validity of their model results.

More recently, the influence of pore fluid on elastic properties of shale has been investigated. Hornby (1998) measured compressional and shear wave velocities up to 80MPa on two fluid saturated shale samples under drained conditions. One sample was Jurassic outcrop shale that was recovered from under sea and stored in its natural fluid, and the other is Kimmeridge clay taken from a North Sea borehole. Measurements were made on cores parallel, perpendicular, and at 45^0 to bedding. Values of anisotropy were up to 26% for compressional and 48% for shear wave velocity, and were found to decrease with increasing pressure. The effect of reduced porosity was, therefore, concluded to be more influential on anisotropy than increased alignment of minerals at higher pressure.

Wang (2002) showed how to obtain elastic constants, velocities and anisotropies in shales from traditionally measured on multiple adjacent core plugs with different orientations. Wang used transversely isotropic (TI) rock, measured three plugs separately (one parallel, one perpendicular, and one $\pm 45^0$ to the symmetry axis) to derive the five independent elastic constants. Wang (2002) also suggested the advantage of this three-plug method is redundancy for calculations of the five independent elastic constants since each core plug measurement yields three velocities.

1.7 Anisotropy of Sandstone

Unlike the shale, clean sandstone is intrinsically isotropic. Sandstones are rarely clean; they often contain minerals other than quartz, such as clay minerals, which can affect their reservoir qualities as well as their elastic properties. The presence of clay mineral and clastic sheet silicates strongly influence the physical and chemical properties of both sandstones and shales (Bjørlykke, 1998). For example, in well sorted reservoir sandstones Jurassic age North Sea and Haltenbanken basin, nearly al the clay minerals are authigenic and the distribution of clay minerals then depends on the diagenetic processes. Clay can be located between the grain contacts as structural clay, in the pore space as dispersed clay, or as laminations as shown in Figure 8 (Sam and Andrea, 2001).

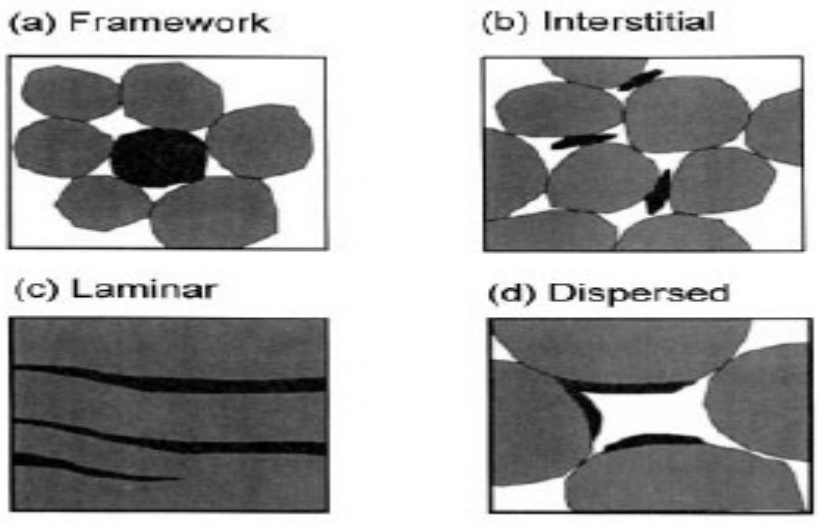

Figure 8: Shows Schematic diagrams showing the different distributions of clay in sandstone: (a) framework, (b) interstitial, (c) laminar and (d) dispersed. Grey represents quartz, black represents clay and white represents pore space (Sam and Andrea, 2001).

The distribution of the clay will depend on the conditions at deposition, on compaction, bioturbation and diagenesis. For example, diagenesis may result in the growth of clay minerals within the pore space and may also cause other minerals to be replaced by clay.

Compaction can lead to clay particles originally situated between grain contacts being squeezed out into the pore space and can also increase the alignment of clay particle orientations(Figure 9).

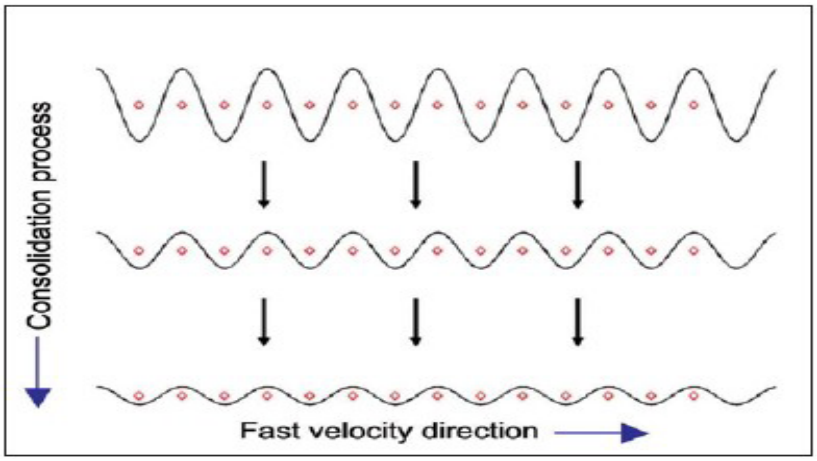

Figure 9.The consolidation process results in the alignment of clay minerals. Black lines represent platy clay minerals and red diamonds represent quartz sand grains. The degree of alignment is affected by the degree of compaction and the quantity of quartz grains in rocks. (Li, 2002).

Koesoemadinata and McMechan (2004), suggested that the correlation between compressional wave anisotropy and minerals that represent diagenetic processes of the Ferron sandstone. Anisotropy decreases with decreasing feldspar, increasing calcite content, and increasing with clay content. The value of horizontal velocity are higher than vertical (estimated 8.5%), which is attributed to laminated bedding or alignment of grain orientation.

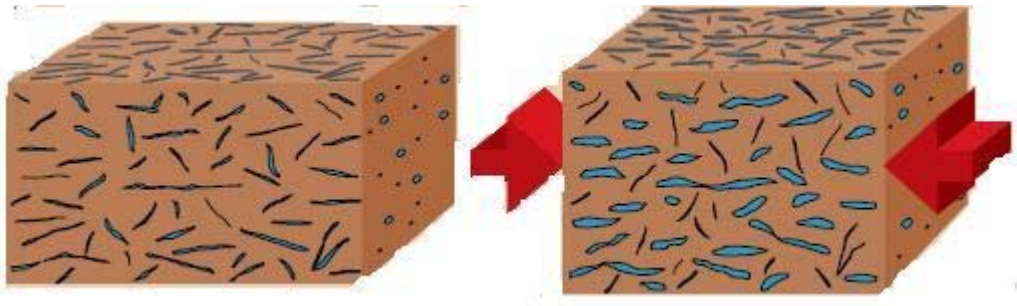

Figure 10: Non-uniform compressive stress operating on microcracks. In unstressed rocks with randomly oriented microcracks (a) the cracks may be open whatever their orientations. However, when stress is applied (b) cracks perpendicular to the direction of maximum compressional stress will close, while cracks parallel to it will remain open (Armstrong et al, 1994).

While most reservoirs are composed of relatively isotropic sandstones or carbonates, their properties may be modified by stress (Figure 10). Non-uniform compressive stress will have a major affect on randomly distributed microcracks in a reservoir. When the rock is unstressed all of the cracks may be open, however, compressional stresses will close cracks oriented perpendicular to the direction of maximum compressive stress, while cracks parallel to the stress direction will remain open. Elastic waves passing through the stressed rock will travel faster across the closed cracks (parallel to maximum stress) than across the open ones

In general, reservoir sands and sandstones are intrinsically isotropic unless they are fractured, finely layered, or clay bearing. Wang (2002) shows that the brine-saturated Africa reservoir sands, which are essentially clay free, have very little anisotropy (average $\approx 0.6\%$ P-anisotropy and $\approx 01.1\%$ S-anisotropy are probably within the measurement uncertainties). For the brine saturated tight sands, the anisotropy is 5.0% for the P-wave and 3.3% for the S-wave when averaged over all samples at all pressures. At the net reservoir pressure of 7500 psi (51.7 MPa), anisotropy is slightly lower, averaging 4.6% and 3.2% for P-and S-waves, respectively. Gas-saturated tight sands and shaly sands show some degree of anisotropy, ranging from 0% to 36% for P-waves and 0.3% to 19.5% for S-waves. When averaged at all pressures, the anisotropy is 9.9% for the P-wave and 5.5% for the S-wave.

1.9 Deviated well Anisotropy

A current trend in petroleum exploration and production is that more and more deviated wells are drilled, especially for deep water reservoirs. The issue of anisotropy is especially important for deviated wells penetrating deepwater reservoir sediment. Most of the geophysical formations exhibit anisotropy that is characterized by transversely isotropic (TI) symmetry. Deviated drilling through the overburden shale is often required to access horizontal wells in a reservoir and may help distinguish between intrinsic (or structural) and stress-induced shear slowness anisotropy. Where anisotropy is present, deviated well measurements differ from the expected vertical responses. (Furre and Brevika, 1998). Many acoustic anisotropy measurements using cross dipole tools have been made in deviated wells. However, interpreting the acoustic anisotropy data can be quite complicated due to the well deviation. Rowbotham et al. (2003) showed that correcting for velocity anisotropy significantly improves seismic inversion when data from deviated wells were the control data. Hornby et al. (2003) proposed to estimate anisotropy parameters from the sonic logs of differently deviated wells including a vertical well. This method, as well as a simplified version of the method of Rowbotham et al. (2003) is based on the assumption that a shale

layer is perfectly homogeneous around the wells so that the velocity variation depends only on the deviation angles of the wells.

Tsuneyama and Mavko, (2005) proposed an alternative method to estimate anisotropy parameters is necessary to correct the sonic log in heterogeneous geologic sequences and/or to perform an anisotropy correction with information from just a single well. For estimation of velocity anisotropy, they analyzed the laboratory measurements of Lo et al. (1986), Vernik and Liu (1997), and Wang (2002). Their method assumed that most subsurface rocks are horizontally transversely isotropic, and they analyzed the data for relationships between general well log information (Vp, Vs , density, porosity, effective pressure) and Thomsen's anisotropy parameters (ε, γ, δ).

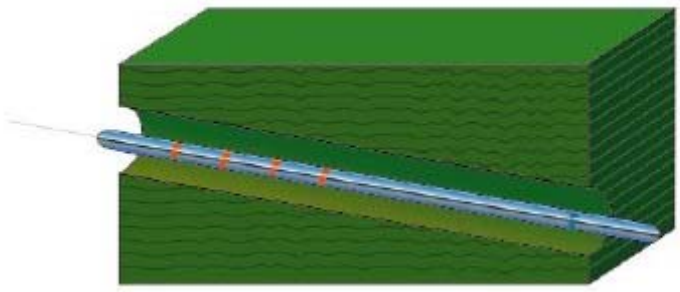

Figure 11: Illustration of a sonic tool in a deviated well penetrates a shale formation. For high angles (~> ± 40) anisotropy will cause the measured velocities to be faster than would be measured in a vertical well (Hornsby et al, 2003).

Chapter 2

2. Quantification of Velocity Anisotropy for Vertical Transverse Medium

Introduction

The elastic properties of a rock can be used to correlate with other properties such as lithology or porosity. Most geoscientists would say that when the density and P-wave and S-wave velocities have been established the rock is completely described; but this is correct only for isotropic rocks where velocities do not vary with direction.

Velocity anisotropy refers to that materials have different velocities (elastic moduli) properties in different directions. These velocity differences in sedimentary rocks are caused by typically a preferred alignment of anisotropic minerals such as clays, quartz, mica, etc., fractures or microfractures and stress induced layering, etc. One of the simplest and most ubiquitous symmetries displayed by these causes of anisotropy is vertically transverse isotropy (sometimes called hexagonal) media.

There are two basic approaches used to characterize vertically transverse isotropic (VTI) media: (1) the measurement on three plugs extracted along the vertical, horizontal and 45º to bedding and (2) acoustic tomography. In this section only the standard three plug method will be discussed only since it is commonly used in oil explorations.

Standard three plug method is by far the most common measurement approach. The method requires the extraction of three core plugs along prescribed orientations relative to the assumed symmetry axes. These orientations are parallel, perpendicular and typically 45^0 to the vertical symmetry axis. Either static or dynamic ultrasonic laboratory measurements can be performed on these plugs to provide the magnitude of tensor elements $C_{11}, C_{33}, C_{44}, C_{66},$ and C_{13} (Mavko, 1998). These five elastic constants can be recast into more geophysical meaningful parameter (Thomsen, 1986), Vp, Vs, epsilon (ε), gamma (γ) and delta (δ). Epsilon captures the difference between horizontally and vertically traveling P-waves. Gamma captures the same for S-waves. Delta is a nonintutive combination of elastic constants which controls the shape of the slowness surface at intermediate angles that it directly affects AVO and logging responses.

The three Thompsen parameters and vertical P-and S-wave velocities used to calculate the phase velocity surface as a function of angle to the bedding normal for anisotropic media. Determination of the three phase velocities is useful for visualizing three dimensional wave propagation in a VTI media

This chapter mainly deals about the quantification of velocity anisotropy in core sample and well log data. The quantification includes the basics of VTI media elastic parameters calculation and determination of Thompsen parameters and the concept of anisotropic wave propagation. In addition, other methods which used to predict and estimate the formation anisotropy are included. The final section summarizes the main points in the quantification of the velocity anisotropy and related concepts.

2.1 Elastic parameters of Transverse Isotropy

Transverse isotropy refers to the velocities being the same, or isotropic, in all directions transverse to the bedding-plane normal. A transversely isotropic medium is the simplest and most practical anisotropic model and is characterized by an axis of symmetry and a transversely isotropic plane perpendicular to this axis.

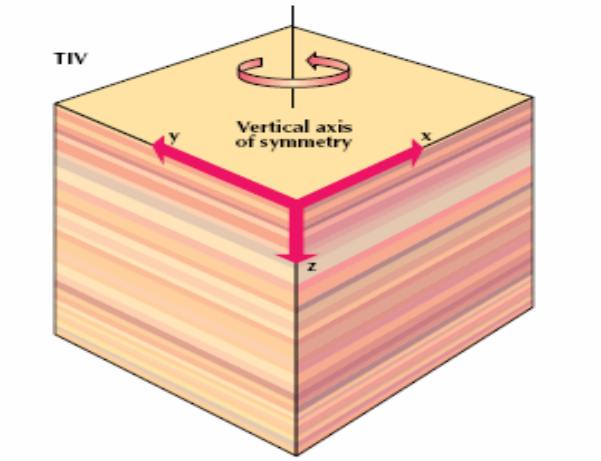

Figure 12: Simple geometries assumed for elastic anisotropy. In layered rocks, vertically transverse isotropic, elastic properties are uniform horizontally within a layer, but may vary vertically and from layer to layer (Armstrong et al, 1994).

The relation between stress (σ_{ij}) and strain (e_{kl}) in a VTI elastic medium is given by

$$\sigma_{ij} = C_{ijkl} e_{kl}, \qquad (1)$$

where and C is the Voigt matrix (Mavko et al,1998). From Figure 12 it is seen that if the axis is denoted Z, the other two principal axes (X and Y) are parallel to the transversely isotropic plane. In this coordinate system, the stiffness matrix C is expressed as

$$C = \begin{bmatrix} C_{11} & C_{12} & C_{13} & 0 & 0 & 0 \\ C_{12} & C_{11} & C_{13} & 0 & 0 & 0 \\ C_{13} & C_{13} & C_{33} & 0 & 0 & 0 \\ 0 & 0 & 0 & C_{44} & 0 & 0 \\ 0 & 0 & 0 & 0 & C_{44} & 0 \\ 0 & 0 & 0 & 0 & 0 & C_{66} \end{bmatrix} \qquad (2)$$

From the above matrix equation, Voigt matrix C, there are five non- zero independent elastic constants: $C_{11}, C_{33}, C_{13}, C_{44}$, and C_{66}. The six elastic constant is $C_{12} = C_{11} - 2C_{66}$. Here, C_{11} is the in-plane compressional modulus, C_{33}, is the out-of-plane compressional modulus, C_{44} is the out-of-plane shear modulus, and C_{66} is the in-plane shear modulus, C_{13} is an important constant that controls the shape of the wave surfaces.

The common way of estimating these five elastic constant is by measuring five different velocities on the three samples plugs cut from a single core sample in three different orientations as indicated on Figure 13.

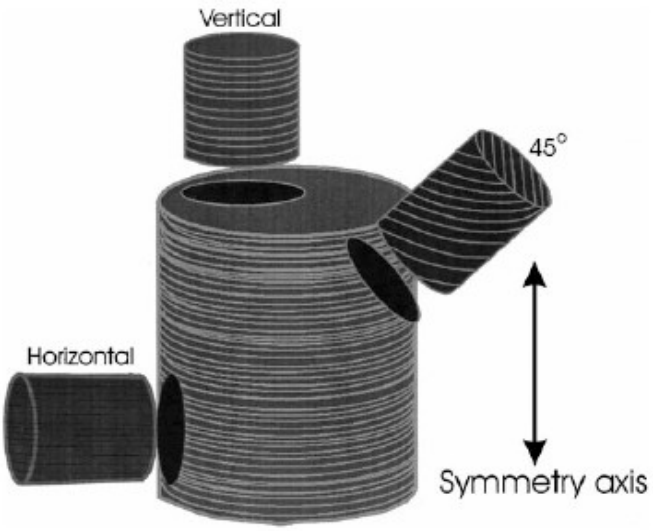

Figure 13: Traditional three-plug method for measuring transverse isotropy in laboratory core samples. Three adjacent core plugs (one parallel, one perpendicular, and one ±45 to symmetry axis) must be cut from whole cores and velocities measured to derive the five elastic constants (Wang, 2002).

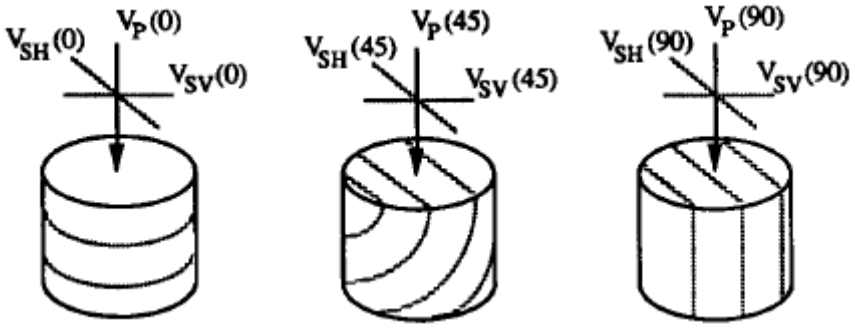

Figure 14: Scheme of sample preparation and velocity measurements in shales. Wave propagation and polarization with respect to bedding-parallel lamination is shown. Numbers in parentheses indicate the phase velocity angle with respect to the bedding-normal symmetry axis (Vernik and Nur, 1992).

As illustrated in Figure 14 the ultrasonic laboratory measurement will give five velocities and their descriptions are:

- $V_{po}(0) = V_{PV}$ is the P-wave velocity along the axis of rotational symmetry (usually the bedding normal),
- $V_{po}(90^0) = V_{PH}$ is the P-wave velocity parallel to the bedding,
- V_{SV} is the *S*-wave velocity normal to the bedding with polarization parallel to bedding,
- V_{SH} is the S-wave velocity parallel to the bedding with polarization parallel to the bedding,
- qV_{P45} is the quasi P-wave phase velocity and
- ρ is bulk density.

These five measured velocities taken from the core samples and the elastic constants are related through the following equations:

$c_{11} = \rho V_{p90}{}^2$,

$c_{33} = \rho V_{p0}{}^2$,

$c_{44} = \rho V_{Sv}^2$,

$C_{66} = \rho V_{SH}^2$, and

$$C_{13} = -C_{44} + \left[4\rho^2 V_{p45}^4 - 2\rho V_{P45}^2 \times (C_{11} + C_{33} + 2C_{44}) + (C_{11} + C_{44}) \times (C_{33} + C_{44})\right]^{1/2} \quad \textbf{(3)}$$

The anisotropy factors ε, γ and δ, are defined following the notation of Thomsen (1986), such that:

$$\varepsilon = \frac{C_{11} - C_{33}}{2C_{33}},$$

$$\gamma = \frac{C_{66} - C_{44}}{2C_{44}},$$

$$\delta = \frac{(C_{11} + C_{44})^2 - (C_{33} - C_{44})^2}{2C_{33}(C_{33} - C_{44})}, \quad \textit{(4)}$$

Since Thompsen (1986) used these three anisotropy parameters(ε, γ, δ) for the first time his paper has become the single most cited article in the history of Geophysics (Helbig and Thompsen, 2005), the parameters are know by the name Thompsen parameters. Alternatively in geophysics terminology as formation parameters.

Velocity measurement in the 45^0 direction is difficult especially on the core samples (since the core size is small and fractures and cracks are commonly developed). The best way around this is to use analytical relation, i.e. if V_{P45} is not measured then it is recommended to use the equation proposed by Hornby (2003). A solution for C_{13} is more complicated; however, for phase (plane-wave) propagation at 45^0, C_{13} can be expressed as:

$$C_{13} = -C_{44} + m\left[(C_{11} + C_{44} - 2\rho V_{P45}^2)(C_{33} + C_{44} - 2\rho V_{p45}^4)\right]^{1/2} \qquad (5)$$

where V_{P45}^2 is a compressional (*Vpv)* or shear (*Vsv*) wave velocity measurement taken at an angle of 45^0 relative to the axis of symmetry, m = -1 for *Vpv* velocity measurement, and m =1 for *Vsv* velocity measurement.

For practical use, it is convenient to express anisotropy using the parameters ε, δ and γ (Thomsen, 1986). For weak anisotropy, the Thomsen's parameters are a combination of elastic module C_{ij} as shown in equations (4) above and they are dimensionless. Alternatively the degree of the velocity anisotropy is quantified by the anisotropy coefficient ***A***, defines as

$$A = \frac{V^{\max} - V^{\min}}{V^{mean}} \times 100 \qquad (6)$$

where V^{max} is the maximum P-and S-wave velocity measured parallel to the lamination(bedding plane),V^{min} is the minimum P- and S-wave velocities measured normal to the lamination(bedding plane), and V^{mean} is the average of V^{max} and V^{min}.

Instead of V^{mean}, Vmax or V^{min} can be used in the denominator of A. Then the alternative method for quantification of the degree of anisotropy also can be expressed relative to the horizontal or vertical velocity also as:

$$A = \frac{V_{\max} - V_{\min}}{2V_{\min}} \quad \text{or} \quad A = \frac{V_{\max} - V_{\min}}{2V_{\max}} \qquad (7)$$

If $V^{\max} = V_{P,S}(90^0)$, $V^{\min} = V_{P,S}(0^0)$ and the media is represented by VTI shale, then for practical use, it is convenient to express anisotropy using the parameters ε, and γ (Thomsen, 1986). If the velocity measurements on a core sample are only on the vertical and horizontal direction, then for a practical purpose and weak anisotropy, the Thomsen's parameters ε and γ can be computed by the fractional difference of P-and S-wave velocities in the vertical and horizontal directions as:

$$\varepsilon \approx \frac{V_p(90^0) - V_P(0^0)}{2V_P(0^0)}, \qquad \gamma \approx \frac{V_S(90^0) - V_S(0^0)}{2V_S(0^0)}, \tag{8}$$

2.1 Phase velocities in a Transverse Isotropic Medium

Waves propagate in different manner in isotropic and anisotropic media. In homogenous anisotropic media, the ray velocity, that is the velocity of propagation of particle disturbance (or energy propagation), may differ from the phase velocity. Expressions for the phase velocity as a function of phase angle in transversely isotropic solids are found in many references (e.g., Thomsen, 1986; 1983; Banik, 1987).

$$\rho V_p^2(\theta) = \frac{1}{2}\left[C_{33} + C_{44} + (C_{11} - C_{33})\sin^2\theta + D(\theta)\right]$$

$$\rho V_{sv}^2(\theta) = \frac{1}{2}\left[C_{33} + C_{44} + (C_{11} - C_{33})\sin^2\theta - D(\theta)\right]$$

$$\rho V_{SH}^2(\theta) = \frac{1}{2}\left[C_{66}\sin^2\theta + C_{44}\cos^2\theta\right], \tag{12}$$

where ρ is density, and phase angle θ is the angle between the wave vector normal to the wave front and the symmetry axis along vertical direction. D (θ) is a compact notation for the quadratic combination (Daley and Hran, 1977):

$$D = \begin{cases} \{\ (C_{33} - C_{44})^2 + 2\left[2(C_{13} + C_{44})^2 - (C_{33} - C_{44}) \times (C_{11} + C_{33} - 2C_{44})\right]\sin^2 + \\ \left[(C_{11} + C_{33} - 2C_{44})^2 - 4(C_{13} + C_{44})^2\right]\sin^4\theta\ \}^{1/2} \end{cases} \tag{13}$$

Although equation (12 & 13) originally was designed for a weak anisotropic models, the parameters ***ε, γ,*** and ***δ***, are convenient to use in TI media with arbitrarily strong velocity anisotropy (Tsvankin and Thompsen, 1994). P–SV propagation is described by the parameters V_{P0}, V_{S0}, ***ε,*** and ***δ***, while the SH wave velocity depends on V_{S0} and γ (SH-wave anisotropy is elliptical). The simplified expression of the Phase velocities in terms of the Phase angle (θ), and the Thompsen parameters are given by:

$$V_p(\theta) = V_{po}(1 + \delta\sin^2\theta\cos^2\theta + \varepsilon\sin^4\theta)$$

$$V_{SH}(\theta) = V_{so}(1 + \gamma\sin^2\theta),$$

$$V_{SV}(\theta) = V_{so}(1 + \left[\frac{V_{Po}}{V_{so}}\right]^2 (\varepsilon - \delta)\sin^2\theta\cos^2\theta), \qquad (14)$$

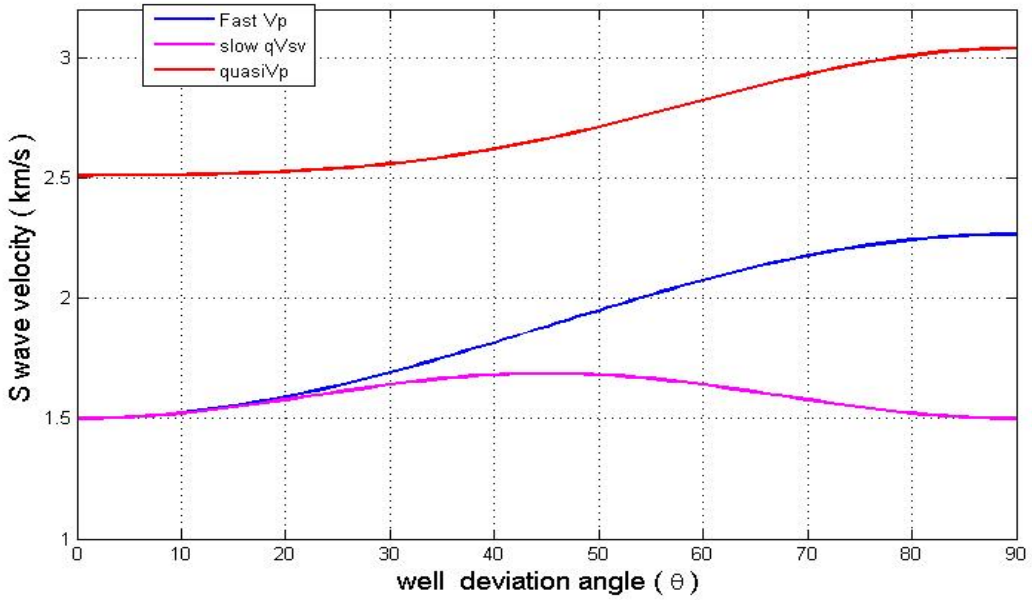

Figure 15: ***P wave Phase velocity surface for the pure shale sample (red curve), the fast (Vsh – blue) and slow (Vsv - pink) S wave Phase velocity surface for shale sample from North Sea. The formation anisotropy parameters used are*** $\varepsilon = 0.213$, $\gamma = 0.431$, ***and*** $\delta = 0.32$.

The calculation of phase velocity surface as a function of angle to the bedding normal for anisotropic media is useful for visualizing three dimensional wave propagation. Three velocity surfaces are found in rocks exhibiting transverse isotropy caused by mineral alignment parallel to bedding:

- a quasi-compressional wave surface **(qVp)**-the wave whose polarization vector is the closed to the propagation direction and is called the qP(quasi P) wave.
- a quasi-shear wave surface for shear waves vibrating in the plane perpendicular to bedding **(qVsv),** the slowest quasi shear wave
- a surface for shear waves vibrating parallel to bedding **(V_{SH}).**

The application of these velocity measurements for field data is illustrated in Figure 15 and 16.

Transition from isotropy to anisotropy (general elastic medium) can be detected, for instance, by appearance of two S-waves propagating with different velocities, a phenomenon called shear wave splitting. An incident shear wave propagates in an isotropic medium and is splitted into two orthogonally polarized shear waves when entering into an anisotropic region. The two shear waves propagate with different velocities inside the anisotropic region. When

re–entering the isotropic medium the two different waves propagate again with the same velocity. A good practical example of shear wave splitting is given in Figure 16.

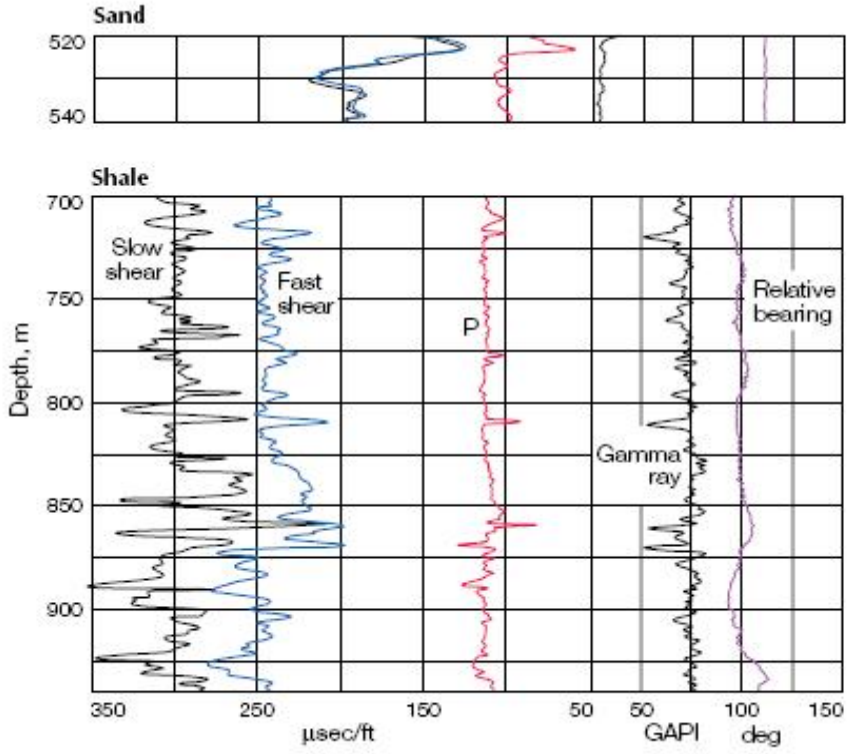

Figure 16: Sonic logs in a 60^0 deviated North Sea well. In isotropic sand (top), shear –wave slowness recorded in two azimuths show the same values (Black and Blue curves). In deeper anisotropic shale (bottom), two shear slownesses are recorded. Other curves indicated P–wave slowness, gamma ray and the receiver bearing relative to the vertical plane containing the borehole (Armstrong et al, 1994).

2.3 Phase, Group Velocity and Anisotropic Wave Propagation

The phase –velocity is associated with single phase-wave. A more general wave is composed by many plane-waves and can be considered as an energy disturbance, where the group (ray) velocity represents the velocity at which the energy travels. Waves behave differently in isotropic and anisotropic media as summarized below.

If seismic wave propagates in an isotropic media, then the Phase (V_{Phase}) and group (V_{Group}) velocities are the same, where the propagation media is anisotropic, say VTI, then V_{Phase} and V_{Group} will have different values. Due to the highly anisotropic nature of shales, group velocities are significantly lower than phase velocities**.** Sometimes the difference will

be more pronounced if the phase and group velocity exists in strongly anisotropic rocks such as black shales.

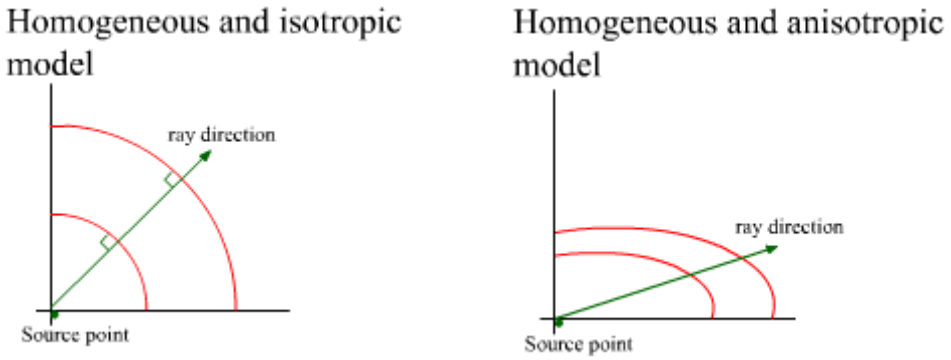

a b

Figure 17: a) Homogeneous and isotropic wave propagation model the wave fronts are spherical, V_{Phase} (Vp) is equal to V_{Group} (Vg), and ray is perpendicular to wave fronts. b) for anisotropic wave propagation model, wave fronts are not spherical, phase velocity is different from group velocity, and rays are not perpendicular to wave fronts.

For VTI media the relation between V_{Phase} and V_{Group} is expressed by the following method. Consider Figure 6, which shows the wave propagation in an anisotropic media. The energy follows the ray path (defined by the ray angle ϕ), and the travel time the energy takes from point a to point b is determined by the group velocity V_{Group}.

This relationship between phase and group velocity for a VTI medium can be written as:

$$V(\phi) = \sqrt{V^2(\theta) + \left(\frac{dV}{d\theta}\right)^2},$$

$$\tan(\phi) = \frac{\left(\tan(\theta) + \frac{1}{V}\left[\frac{dV}{d\theta}\right]\right)}{\left(1 - \frac{\tan(\theta)}{V}\left[\frac{dV}{d\theta}\right]\right)}, \qquad (15)$$

where θ is the angle between the group-velocity vector and the symmetry axis and ϕ is the angle between the phase-velocity vector and the symmetry axis as indicated in Figure 18. This relationship is shown equation (15) gives the relationship between the magnitudes of the

phase and group velocity vectors. The second equation gives the relationship between the angles of the two vectors relative to the symmetry axis (i.e., normal to bedding):

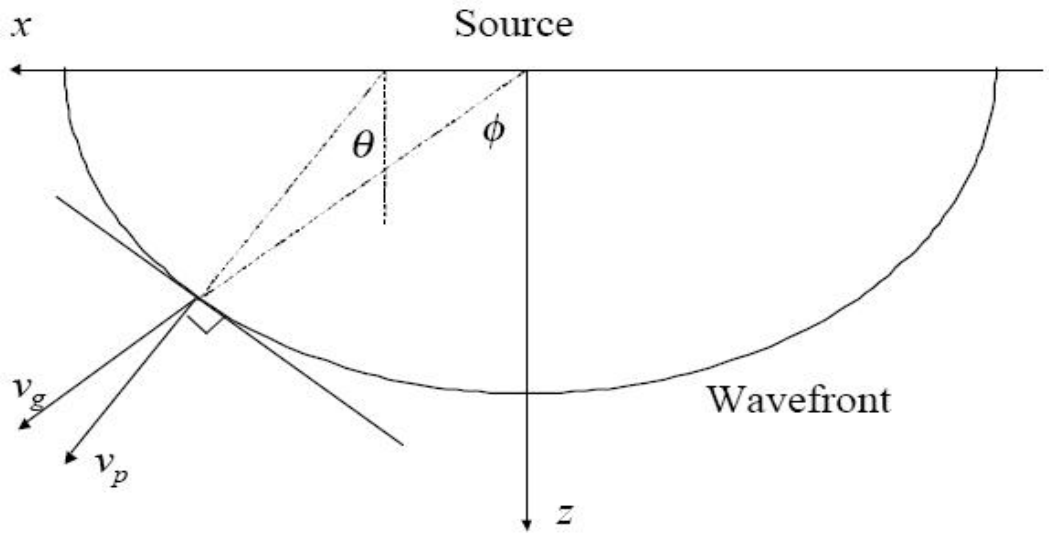

Figure 18: The definition of the phase angle θ, phase velocity V_{Phase}, ray angle ϕ, and ray (group) velocity V_{Group}. The direction of phase velocity V_{Phase} is orthogonal to the wave front (after Thomosen, 1986). Phase velocity is equal in magnitude and direction to ray velocity in directions parallel and perpendicular to the symmetry axis.

2.4 Elliptical anisotropy (Polar) anisotropy

From ultrasonic measurement of vertical and horizontal P-and S-wave velocities for TI media, all stiffness constants except C_{13} can be obtained by equation (3). The last term in equation (3) needs to measure the P-wave velocity along the direction at $\theta = 45^\circ$. However, the direct measurement of the phase velocity along an oblique direction is very complicated because the phase velocity is separated from the group velocity as shown in Figure 2.7 and 2.8, provided that most shales are very friable and fissured; it is often difficult to prepare the 45° core plug. Its edges break off easily (Wang, 2002).

Instead of directly measuring the P-wave velocity in the oblique direction, a non-spherical wave front is often assumed. Detail explanation about the elliptical assumption is given by Helbig (1983). But in this study the assumption is based on the actual wave surface of energy propagation from a point source which is an ellipsoid. This is illustrated graphically in Figure 19 (the concept and the figure taken from Song et al, 2004).

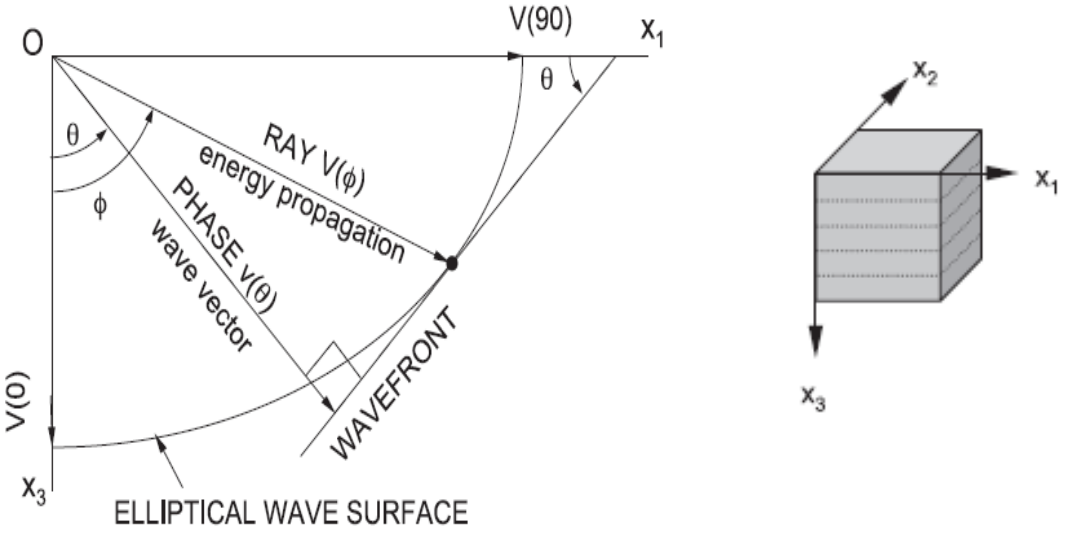

Figure 19: The relationship between ray velocity and phase velocity when the energy propagates in the shape of the elliptical wave surface. The wave surface is defined as the surface of particle disturbance at unit time. The symmetry axis is parallel to x_3 direction (Byun, 1984).

As explained in the previous section, the ray (V_{Group}) velocity, V (ϕ) as a function of ray angle ϕ is measured by the distance between the origin and the point on the wave surface divided by the time interval. The wave front is tangent to the wave surface, and the phase propagation is always perpendicular to the wave front. The phase velocity $V(\theta)$ which propagates with phase angle θ is obtained by (Byun, 1984):

$$V(\theta) = V(\phi)\cos(\phi - \theta), \qquad \text{for } \theta = 45^0$$

$$V(\phi) = \sqrt{\frac{V(90^0)^4 + V(0^0)^4}{V(90^0)^2 + V(0^0)^2}}, \qquad \text{where } \phi = \tan^{-1}\left(\frac{V(90^0)}{V(0^0)}\right) \qquad (16)$$

The relationship between $V(\theta)$ and $V(\phi)$ is also illustrated in Figure 2.8. The above equation (16) able to find $V(\phi)$ and $\phi = 45^0$ are obtained directly from the two orthogonal velocity measurements $V_p(90^0), V_{SH}(90^0)$, and $V_p(0^0), V_{SV}(0^0)$.

The standard practice for estimating anisotropic elastic constants using ultrasonic laboratory velocity measurements was found to be unsuitable as a result of the potentially large and unquantifiable errors in estimating the elastic parameters, especially the critical C_{13}

parameter. Then the polar anisotropy approach is used to quantify the observed anisotropy in the core sample. This method is recommended

1) When the velocity measurement from a core sample only on the vertical and horizontal directions.

2) When the velocity measurement at 45^0 was difficult to perform or had large uncertainties.

2.5 Anisotropy well log

Li (2002) presented an empirical relation ship which was established mainly based on physical understanding of the relationship between volume of clay, orientation of clay minerals, velocities, porosities and compaction. The method was applied on North Sea VSP measurement and it gave a good understanding for estimation of anisotropy. The method is *straightforward, easy to use and produces a continuous anisotropic profile*. Li (2002) proposed an estimation method of velocity, anisotropy ε and γ from V_P (0), Vs (0), and the clay volume in the equation

$$\varepsilon = 0.60\frac{V_{clay}\times\left(V_P - V_{Pwater}\right)}{V_{Quartz} - V_{Pwater} - 2.65\times V_{clay}}\ , \quad \gamma = 0.67\frac{V_{clay}\times V_S}{V_{SQuartz} - 2.29\times V_{clay}} \qquad (17)$$

where V_{clay} = volume of clay, V_P (or V_P *(0))* = P-wave velocity perpendicular to bedding, V_{Pwater} = an approximation of P-wave velocity at critical porosity, $V_{Pquartz}$ = P-wave velocity of quartz, V_S (or $V_S(0)$) = S-wave velocity perpendicular to bedding, and $V_{Squartz}$ = S-wave velocity of quartz. The constants used in equations 1 and 2 are: V_{Pwater} = 1.5 km/s, $V_{Pquartz}$ = 6.05 km/s, and $V_{Squartz}$ = 4.09 km/s. When velocity and clay volume logs are used, the estimated anisotropic parameters derived by using equation (17) are a form of well logs. They are called *anisotropic well logs*. Attempts to derive an equation using a similar approach for the anisotropic parameter δ were unsuccessful. Thus, the following equation is recommended. The third formation anisotropy parameter δ is estimated by using the best fit method as $\delta = 0.32\varepsilon$.

Another alternative to get the approximated formation anisotropy as a function of depth was suggested by the Hornby (2003). This method uses the volume of shale from the Gamma ray log and estimation anisotropy of the parameters ε and δ form 100 % shale content. The estimation values of ε and δ can be taken from core samples or well log derived parameters for a given formation. ε and δ for 100 % shale content may be zoned or say, input as a

gradient between shallow and deep intervals. For a particular depth the anisotropy parameter is calculated by the following expressions

$\varepsilon_c = V_{Sh}\varepsilon_{Sh,}$ and $\delta_c = V_{Sh}\delta_{Sh,}$

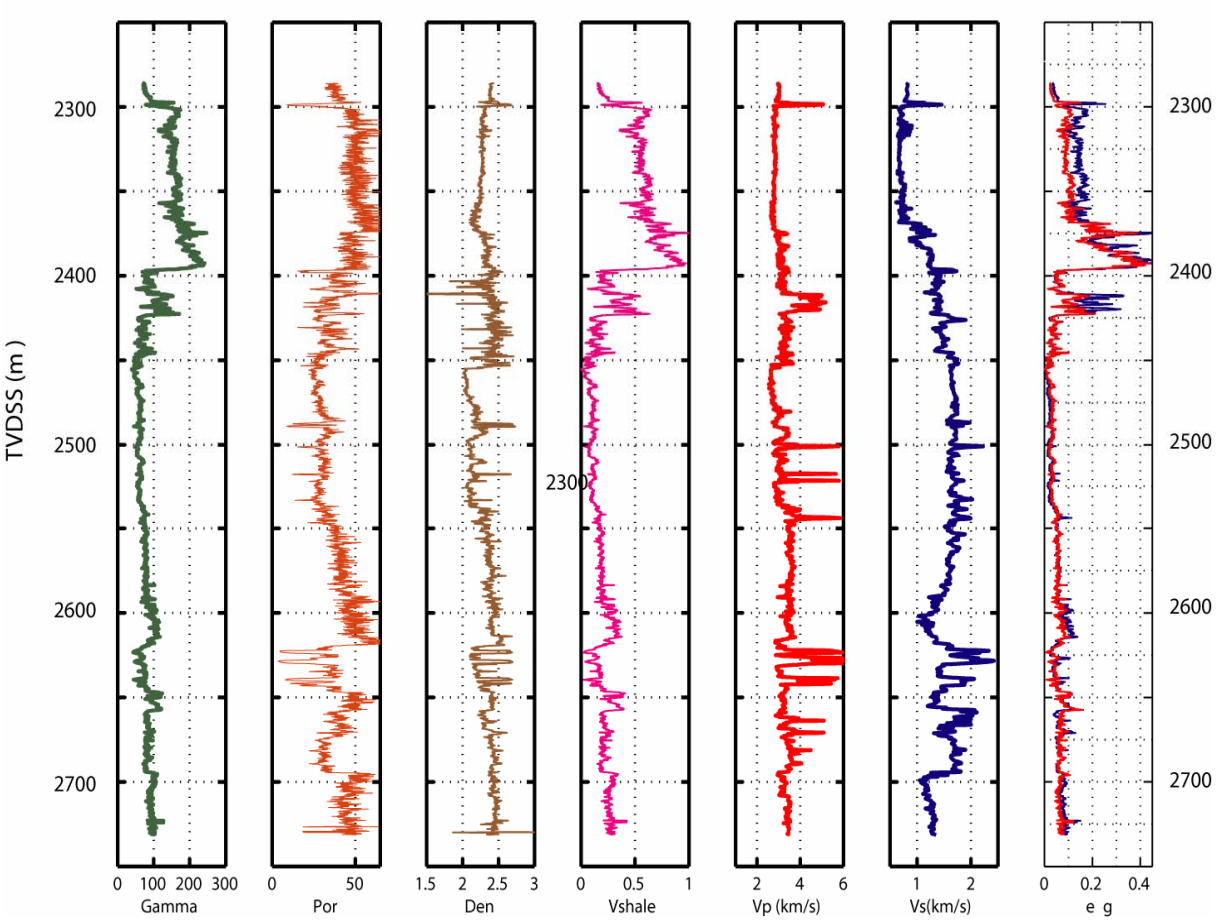

Figure 20: Well logs of a deviated well 33/9-A-16AT2. The seventh column from the left shows estimated epsilon (green) and gamma (red) by Li (2002) anisotropy well log method. The maximum formation anisotropy parameter, estimated was 0.45 for both P and S wave.

2.6 Backus Averaging for layer induced anisotropy

Consider a stacked section of horizontal elastic layers, each of which is much thinner than the seismic wavelength. Then for each stacked layer the elastic properties may vary arbitrarily. Backus (1962) has elegantly shown how to calculate the stiffness parameters that describe an equivalent elastic medium, under the assumptions outlined earlier. From the viewpoint of a long wave passing through the stack, the material appears to have less rapid varying properties in the vertical direction and to exhibit anisotropy, even if the entire stack is composed of isotropic layers. This has an important implication for seismic modeling and imaging.

Figure 21: an example of stacked horizontal elastic layers.

The relation between stress (σ_{ij}) and strain (e_{kl}) in a VTI elastic medium is given earlier in as $\sigma_{ij} = C_{ijkl} e_{kl}$, and C is the Voigt matrix

The five letter notations following associations to relate with the stiffness coefficients for a VTI medium given as:

$$\begin{aligned} a &= C_{11} = C_{22}, \\ b &= C_{33}, \\ f &= C_{13} = C_{23}, \\ l &= C_{44} = C_{55}, \\ m &= C_{66}, \end{aligned} \qquad (18)$$

Backus (1962) has shown how to calculate the stiffness parameters that describe an equivalent anisotropic medium for a stack of thin isotropic elastic layers. The response of this thin stacked isotropic section when a full sonic or long wave is passing through the stack is that the material will act as VTI anisotropic. In the final analysis, the theory yields a recipe for calculating layer induced anisotropic stiffness parameters from averaging properties of the isotropic elastic layers.

$$a = \left\langle \frac{\lambda}{\lambda + 2\mu} \right\rangle^2 \left\langle \frac{1}{\lambda + 2\mu} \right\rangle^{-1} + 4 \left\langle \frac{\mu(\lambda + \mu)}{(\lambda + 2\mu)} \right\rangle,$$

$$c = \left\langle \frac{1}{\lambda + 2\mu} \right\rangle^{-1},$$

$$f = \left\langle \frac{\lambda}{\lambda + 2\mu} \right\rangle \left\langle \frac{1}{\lambda + 2\mu} \right\rangle^{-1},$$

$$c = \left\langle \frac{1}{\lambda} \right\rangle^{-1},$$

$$m = \langle \mu \rangle, \qquad (19)$$

where μ and λ are the shear modulus and Lampe parameter respectively. The well know relation of these parameters with wave speeds are

$$V_p = \sqrt{\frac{\lambda + 2\mu}{\rho}}, \qquad \text{and} \qquad V_S = \sqrt{\frac{\mu}{\rho}} \qquad (20)$$

The degree of effective anisotropy depends on the details in parameter fluctuations between the layers (Berryman et al., 1999) and the length of the averaging window. The first effect is a fundamental connection to geology, certain rock formations being strongly layered structures while others are not. The second effect depends on the wave length of observed seismic waves, since this is the natural length scale of the averaging window.

Following Berryman (2005), the formula of the effective parameters (Thomsen, 1986) in terms of the five letter stiffness notation and averaged density is

$$V_{p0} = \sqrt{\frac{c}{\langle \rho \rangle}}, \quad V_{s0} = \sqrt{\frac{l}{\langle \rho \rangle}},$$

$$\varepsilon = \frac{a - c}{2c}, \qquad \gamma = \frac{(m - l)}{2l}, \qquad \delta = \frac{(f + l)^2 - (c - l)}{2c(c - l)}, \qquad (21)$$

The computation requires a model in which compressional (Vp) and shear (Vs) velocities and density (ρ) are know in each layer. This information is available from full sonic wave processing of sonic log data. The VTI medium can be completely characterized by (a, c, f, l, m, ρ) or the alternate parameter set mentioned earlier (V_{Po}, V_{So}, ε, δ, γ, ρ).

Liner and Fei (2007) suggested that these relationships are nonlinear, but they have the curious and useful property of being invertible. Specifically, if we know (V_{Po}, V_{So}, ε, δ, γ, ρ), then (a, c, f, l, m, ρ) can be calculated using the following equations

$$a = (1 + 2\varepsilon)\rho V_{Po}^2,$$

$$c = \rho V_{Po}^2$$

$$f = \rho[(V_{po}^2 - V_{So}^2)(V_{Po}^2(1+2\delta) - V_{So}^2)]^{1/2} - \rho V_{So}^2$$

$$l = \rho V_{so}^2$$

$$m = (1+2\gamma)\rho V_{so}^2 \quad , \qquad (22)$$

The mainly the application of Backus averaging is to calculate the effect of the intrinsic and layer induced VTI anisotropy. The intrinsic anisotropy is due to characteristics below sonic resolution (ex core measurement) and layer–induced anisotropy (computable from sonic logs). The observed velocity anisotropy will be the superposition between intrinsic and layer induced anisotropy. For this combined quantification of velocity anisotropy Backus averaging technique is useful. Detail use of Backus averaging techniques including some concept mention here can be obtained in article published by Liner and Fei (2007).

2. 7 Anisotropy relations

Different Authors described the linear relation between P-and S-wave anisotropy. Wang (2002) showed the general linear relationship between P-and S-wave anisotropies with a small deviation P-wave than S-wave anisotropy for most analyzed samples. The relation is also described for the best fit by a regression formula as:

$$\gamma = -0.01049 + 0.9560\varepsilon \qquad (23)$$

Tsuneyama and Mavko (2005) derived a slightly different regression formula from a compiled data set for brine-saturated sandstones and shales as follows.

$$\gamma = -0.0282 + 1.2006\varepsilon \qquad (24)$$

Li (2002) also derived the third formation anisotropy parameter δ from the best fit method $\delta = 0.32\varepsilon$

Wang (2002) suggested that these equations (22 & 23) shows that S-wave anisotropy may be estimated from P-wave anisotropy, or vice versa. Such estimations are independent of pressure, pore fluids, and lithology. This is particularly useful when S-wave anisotropy is available but P-wave anisotropy is not.

Wang (2002) also derive a formula which shows that the magnitude of anisotropy decrease exponentially in shales as porosity (ϕ) increases. The relation was given as:

$$\varepsilon = 0.35486e^{-7.417\phi} \quad , \; \gamma = 0.345461e^{-10.304\phi} \qquad (25)$$

For shales, anisotropy is affected by porosity because, with high porosity, young shales tend to be less laminated. As shales are compacted, porosity decreases and clay platelets are preferentially oriented. As a result, anisotropy increases.

Anisotropy in sands and carbonates is not directly affected by porosity. Instead, it is more affected by the texture (fractures, cracks, and lamination) and clay content. (Wang, 2002).

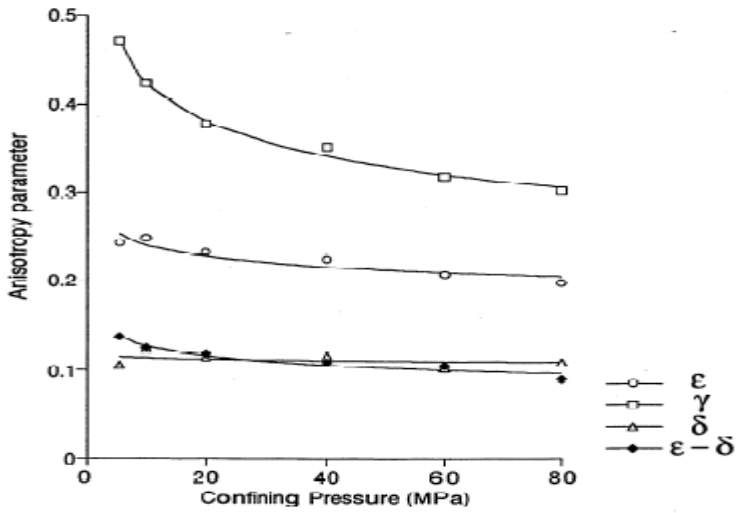

Figure 22: Anisotropy parameters for Jurassic shale. The anisotropy ($\varepsilon - \gamma$) of the shale decreases as a function of confining pressure. Here δ is positive and nearly constant for the entire interval, and the anellipticity factor ($\varepsilon - \delta$) is positive and decreases as a function of confining pressure (Hornby, 1998).

The relation between anisotropy parameters and confining pressure was discussed by Hornby (1998). From Figure 22 note that the anisotropy (ε, γ) of Jurassic shale decreases as function of confining pressure. The value of δ is positive and nearly constant for the entire interval, and anellipticity factor ($\varepsilon - \delta$) is positive and decrease as function of confining pressure. So shale basically becomes less anisotropic as a function of increasing confining pressure

Chapter 3

3. Geological Description of The Study Area

Introduction

This chapter will give short review of the Geological setting of the study area. The descriptions mainly focus on lithology and depositional environment of the Groups and Formation of the Hydrocarbon producing fields.

Core sample and well log data will be analyzed from two separate areas of the Norwegian Shelf: the Northern North Sea, and Haltenbanken. The data from northern North Sea came from two main hydrocarbon producing fields: Gullfaks and Statfjord Fields.

From Gullfaks Field only one cored sample, Brent Group, Broom Formation will be analyzed. On the Statfjord Field two cored sample and more than 10 well logs will be analyzed from three Groups and five formations. The geological setting of these two northern North Sea hydrocarbon producing fields is similar and to avoid repetition of concept, only the geological setting of Statfjord Filed will be given.

The data from Haltenbanken came from three well log cored samples. One from Haltenbanken South, Cromerknol Group Lange Formation. The other two cored sample came from Kristine Field, Faungs Group, Not Formation. The geological descriptions Haltenbanken will focus on the Lange and Not Formations in addition to the general geological setting of the area. The discussions are mostly based on the documents and texts taken from the Norwegian Petroleum Directory (NPD) bulletin and fact page.

3.1 Northern North Sea

The main structural features in this region are the Utsira high, the Horda platform, the East Shetland platform, the Viking Graben, and the East Shetland Basin. The Viking Graben is a north-south–trending linear trough in the northern North Sea, roughly following the Norwegian–United Kingdom sector boundary. These main structural elements are characterized by large normal fault blocks and were created during the Late Permian to Triassic rifting episodes, followed by reactivation during Jurassic stretching (e.g., Badley et al., 1988; Roberts et al., 1995). Normal basin subsidence and filling became the primary depositional mechanism by the Late Cretaceous (Glennie, 1990). Several areas in the North Sea close to the Norwegian mainland have experienced Cenozoic uplift and erosion. The sediments represented by our well data in the northern North Sea have not, however, been subjected to uplift because they are located too far west from the Norwegian coastline.

Detailed information of the lithostratigraphy from the Norwegian North Sea can be found in Deegan and Scull (1977) and Volleset and Dore (1984).

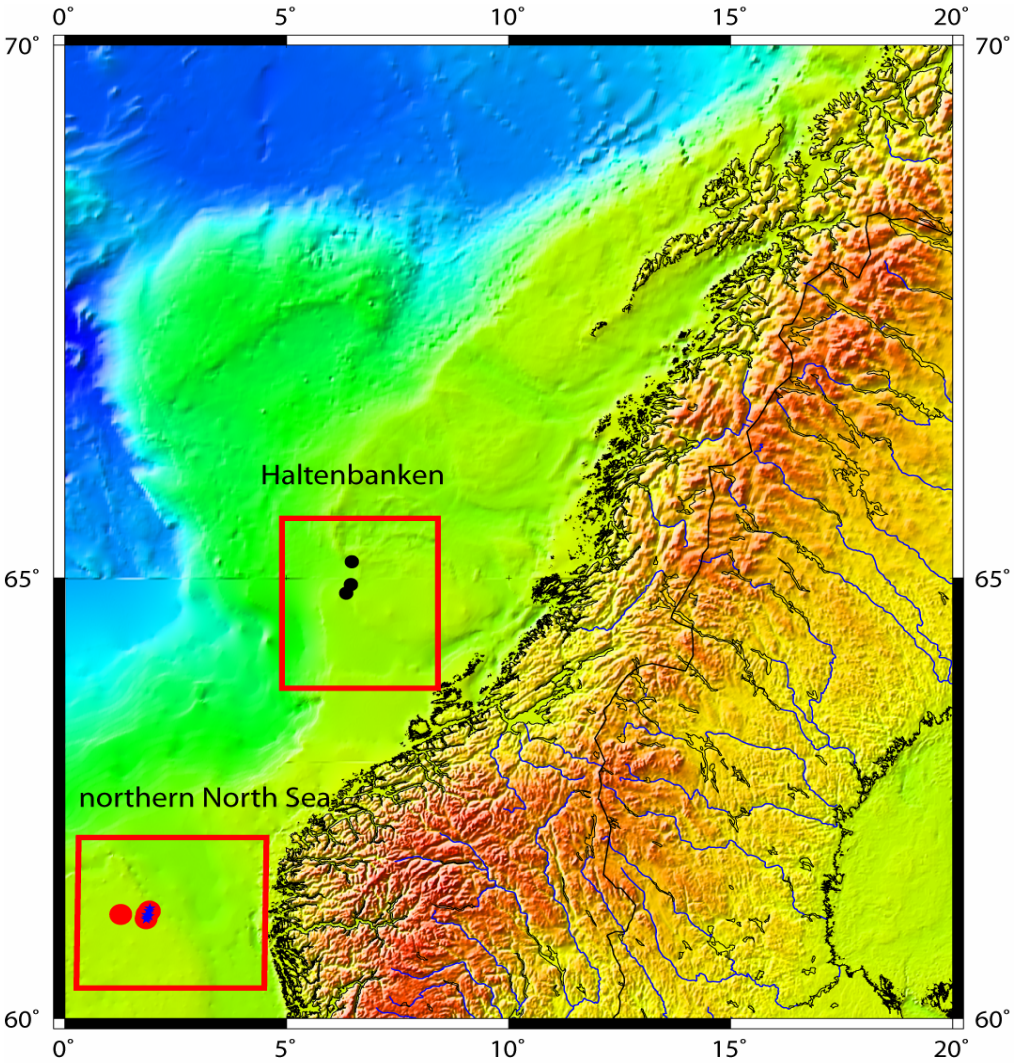

Figure 23: Map showing the location of two study areas on the Norwegian Shelf. The location of the well bores where the sample came indicate on dot circles

3.1.1 Gullfaks Field

The Gullfaks Field, situated in block 34/10 along the western flank of the Viking Graben (Figure 23), occupies the eastern half of a 10–25 km wide fault block and is bounded by large-scale faults with kilometre-scale offsets at the northern North Sea. The area has been affected by at least two major rift phases. The first phase occurred in the Permian and Early Triassic and affected the total width of the northern North Sea, whereas the second, late Jurassic, rift phase was more localised to the central portions of the northern North Sea (e.g. Færseth et al., 1995). The core sample was taken from Brent Group, Broom Formation. The short lithostratigraphic description will be given in the next section.

3.1.2 Statfjord Field

Location and structural setting

The Statfjord Field is located about 220 km northwest of Bergen on the western side of the North Sea RiftSystem (Figure 24a and 24b) within a sub-platform area according to the terminology proposed by Gabrielsen (1986). The sub-platform area represents the most prospective play type in the North Sea and several large oil fields are identified within this structural setting (e.g. the Gullfaks, Snorre, and Brent oil fields). The Statfjord Field structurally forms the eastern part of a major (first-order) fault block along the western margin of the Viking Graben (Figure 24a). Two other fault blocks, containing the Gullfaks, Tordis, Gullfaks South and Visund Fields, separate the Statfjord Field from the central part of the Viking Graben. Even though the Statfjord Field is located next to a major fault, most of the structure has undergone little deformation as compared to nearby fields located in a similar footwall position (e.g. the Gullfaks Field; Hesthammer and Fossen, 1999; Gullfaks South). The exception is the eastern flank of the Statfjord Field which is heavily affected by gravitational collapse structures.

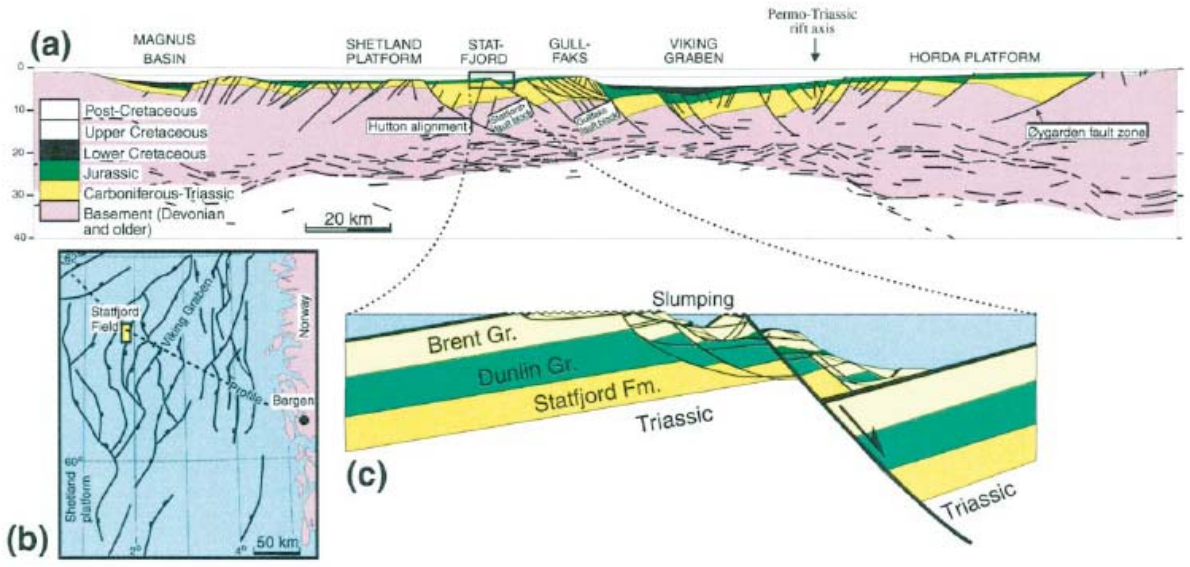

Figure 24: a) Regional profile across the northern North Sea and the Statfjord Field. b) For location and Fault map of the North Sea Rift System with location of the Statfjord Field. C) Detailed cross-section across the east flank of the Statfjord Field (Hesthammer and Fossen, 1999).

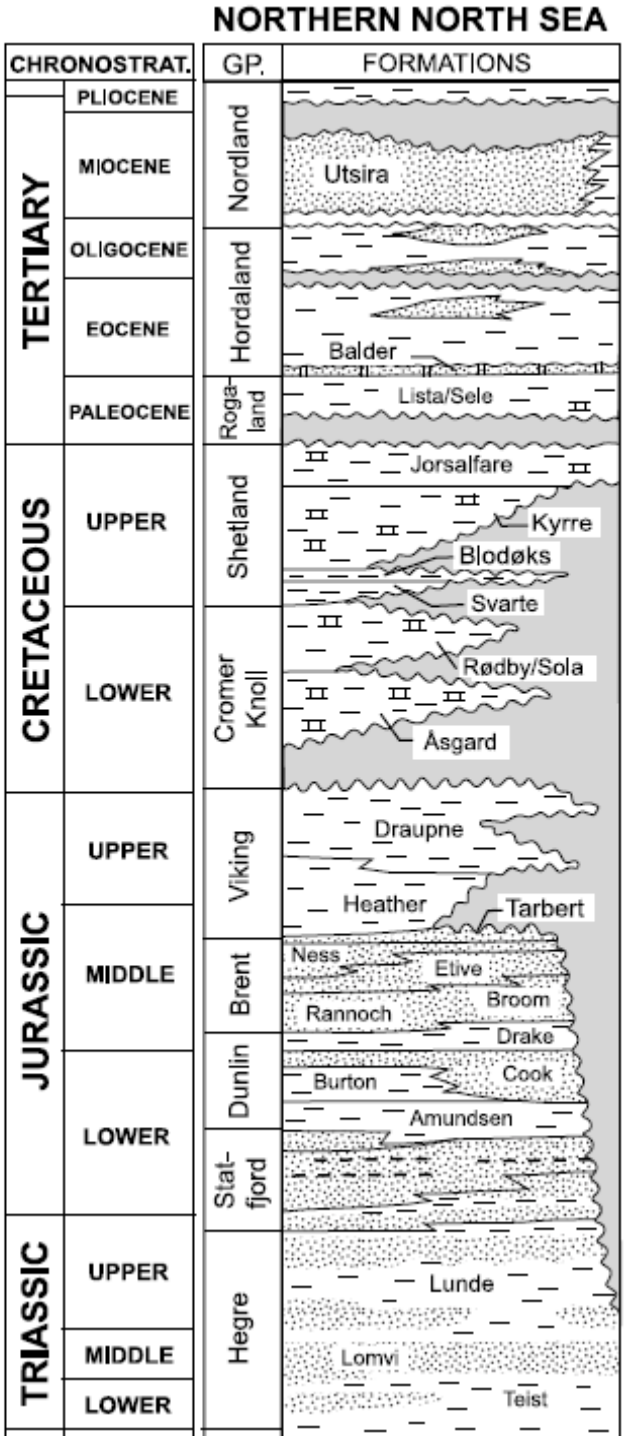

Figure 25: Generalized lithostratigraphic section of the northern North Sea, Haltenbanken, and the Norwegian Barents Sea region. Modified from Dalland et al. (1988).

Lithology and depositional environment description

Dunlin Group:

The Lower Jurassic Dunlin Group is recognized as an important and widely used developed unit in the northern North Sea and classified as: Amundsen (base), Burton, Cook and Drake (top) (Figure 25).

Burton Formation

Burton Formation is one of the four Formations of Lower Jurassic, (the latest Sinemurian to early Bajocian). Dunlin Group comprising four formations, the Amundsen (oldest), Burton, Cook and Drake (youngest) Formations. It has a thickness that ranges from 230-260m. On the Statfjord Field, these formations are informally referred to as DIII (Amundsen and Burton Formations), DII (Cook Formation) and DI (Drake Formation). The Amundsen and Burton Formations consist of shallow marine shale, claystone and siltstone. These are overlain by silt and sandstones of the Cook Formation. The Burton Formation lithology description obtained from type well log showed it consists of a uniform development of dark grey to reddish grey, soft noncalcareous claystone and shale which may be slightly carbonaceous in part.

Brent Group

The early Bajocian to mid-Bathonian Brent Group is 180-250m thick on the Statfjord Field and comprises sandstone, siltstone, shale and coal deposited in a northward prograding delta system. The unit is divided into five formations; the Broom, Rannoch, Etive, Ness and Tarbert Formations. On the Statfjord Field, the Brent Group is also informally subdivided into six zones (Bl- B6). Zones l-3 corresponds to the Ness and Tarbert Formations, whereas zones 4-6 correspond to the Etive, Rannoch and Broom Formations respectively. Their lithological descriptions of each formation from bottom to top given below.

Broom Formation

The Broom formation has consisted of variously medium to coarse grained, poorly sorted, frequently carbonate cemented sandstones, mudstones with floating coarse sand grains, pebbly sandstones and conglomerates. The facies varies from place to place as transgressive tidal flat, offshore sheet and fan delta system. The Broom formation ranges in thickness about 48 m from western margin of the basin and thins to the east and northeast. The formation layer of Broom is distinguished from the underlying Dunlin group and the overlying Rannoch Formation by its regular, but general gamma ray readings. The Formation also easily

identified in the Brent-Statfjord area. The depositional environment of the Broom Formation is interpreted as storm deposits and small distal bar build-ups on a shallow marine platform.

Rannoch Formation

The lithology of Rannoch Formation is light brown, fine grained, well sorted friable, very micaceous sandstone. Towards the top the formation tends to be coarser grained and less micaceous, often resulting in a distinctive gamma ray pattern suggesting a coarsening upward sequence. The depositional environment of Rannoch Formation is generally interpreted as delta front sheet sands/ or prograding shoreface sands.

Etive Formation

The Etive formation consists of massive grey brown to clear fine to coarse, occasionally pebbly and cross bedded sandstones. The mica content is generally low. The formation boundary is characterized by low gamma ray readings. This characteristics and the low mica content distinguishing it from the underlying Rannoch Formation. The depositional environment of the formation has been interpreted as upper shoreface, barrier bar, mouth bar and distributor channel deposits.

Ness Formation

The Ness Formation consists of an association of coals, shales, siltstones and very fine to medium grained sandstones. Small scale cross bedding and horizontal bedding is common. The shales are silty, fissile and frequently pyretic. Coarsening and fining upward sequences are common features. The varied lithology produces an irregular but distinctive gamma ray and sonic response. The lower boundary defines the top of Etive Formation and the upper contact is more similar with the sandstone of the overlying Tarbert Formation. The depositional environment of the formation is thought to represent delta plain or coastal plain deposit.

Tarbert Formation

The Tarbert Formation consists of grey to brown relatively massive fine to medium grained sandstone with subordinate thin siltstone and coal beds. The depositional environment is interpreted as a transgressive lag deposit. Overlying sandstones are occasionally fine grained and highly bioturbated with rare, planar, dipping lamina.

Viking Group

The lithology of the group consists of dark grey to back marine mudstones, claystones and shales. Local these argillaceous sediments are replaced by sandstones and conglomerates. There are two formations in this group that are widely distributed in the Norwegian sector. These are Draupne and Heather Formations.

Heather Formation

The formation consists of mainly grey silty claystones with thin streaks of lime stone. Two divisions are commonly recognized. The lower division is light to dark grey, hard silty claystone often micaceous and calcareous. The silty claystone of the Heather Formation were deposited in an open marine environment, brought about the marine transgression which intitially deposited the youngest formation of the Brent Group.

Draupne Formation

The formation consists of dark grey brown to black, usually noncalcareous carbonaceous occasionally fissile claystone. It usually characterized by a very high gamma ray response and anomalously low velocity. A gamma ray response of greater than 100 API units usually observed through out the formation. These properties ensure that the boundaries of formation are normally marked by strong log break. The Draupne Formation is considered to be deposited in a marine environment with high organic activity and restricted bottom circulation and often with an aerobic condition. On the average this shale is thicker on the WS than NE part of the Statfjord Field.

3.2 The General Geology of Halten Terrace

Haltenbanken is located on the Mid Norwegian Continental Margin (Figure 23 and 26). The structural framework in the area is the Trøndelag Platform to the east and the Vøring Basin to the west. The area is mainly formed in the same tectonically events as the North Sea with upper Triassic extension with faulting and subsidence followed by basin infilling, and lower Cretaceous rifting followed by subsidence and basin infill. The area has been subjected to late Cretaceous / early Tertiary rifting and uplift in the western Møre and Vøring basin with igneous activity. An almost compete 4-5 Km sequence from the Jurassic to the Quaternary if found in this area. Regarding the lithostratigraphy for the Haltenbanken, detailed information can be found in Dalland et al (1988).

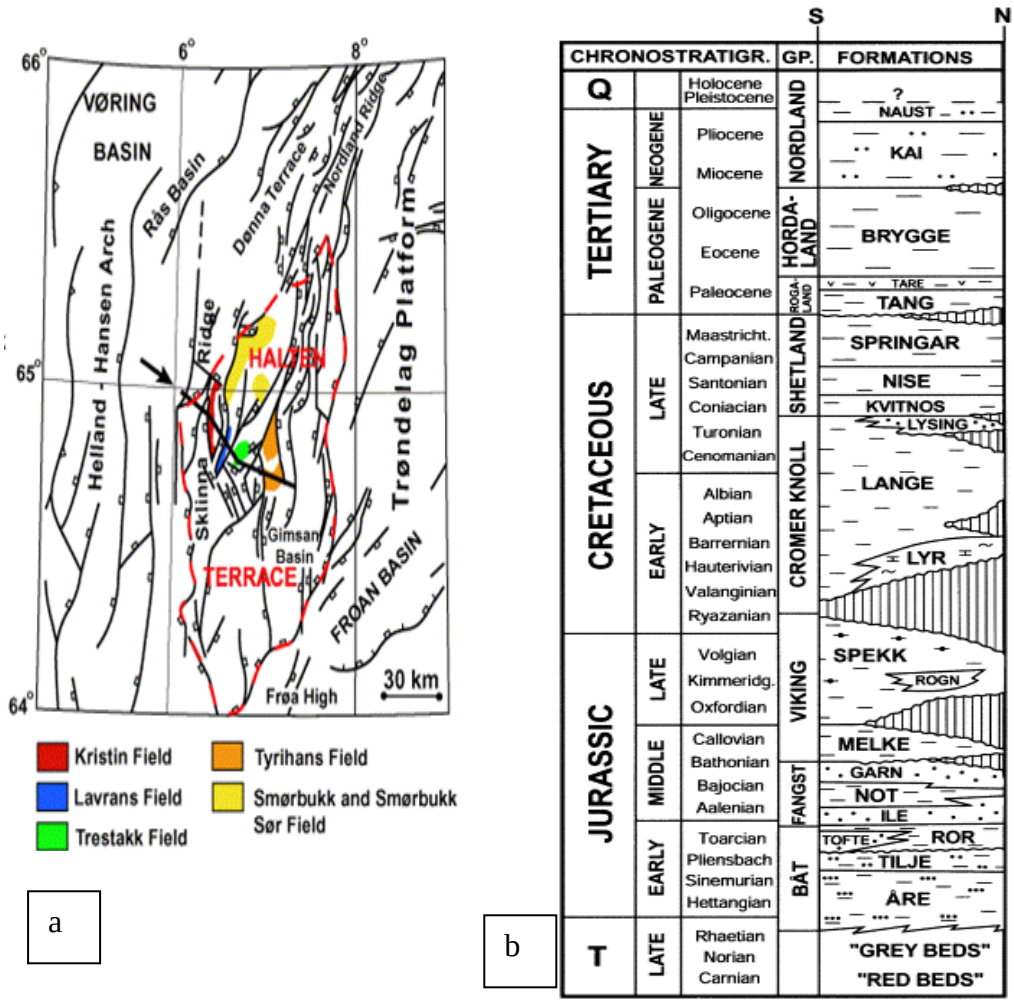

Figure 26: a) Location of Haltenbanken area, the regional tectonic frame work with the Halten South Fields, and well location in the Kristin and Lavrans Fields. b) Lithostratigraphic section from Haltenbanken (left) northwards to the Nordland Ridge area (right) (Modified from Storvoll, 2002).

Fangst Group

The Fangst Group typically comprises three lithological units: a lower fine to medium-grained sandstone with numerous shaly intrebeds, a middle mudstone, and an upper relatively massive fine to coarse-grained sandstone.

Not Formation

The lithology of Not Formation is clasystone with micronodular pyrite coarsen upwards into bioturbated fine grained sandstones which are locally mica rich and carbonate cemented. The lower boundary is defined by abrupt increase to steady high gamma ray response. The depositional part of the basal part (the lower boundary) reflects semi regional transgressions which lead to the development of lagoons or sheltered bays. The upward part of the unit

consists of prograding deltaic or costal front sediments. The Formation is recognized over the entire Haltenbanken area if not eroded.

Cromer Knoll Group

Cromer Knoll Group on Haltenbanken, the group consists of calcareous and non calcareous claystones interbedded with marls and stringers of carbonates and sandstones. Sandstones are more common in the upper part of the group. The group representatives are found throughout the Halten Terrace and in basinal areas to the west. Sediments were deposited in shallow deep marine environments. The Cromer Knoll Group comprises three formations: Lysing, Lange and Lyr.

Lange

The Lange Formation has lithology of dominant light/medium grey to green and brown claystones contain stringers of carbonates and sandstones. The base is generally marked by a distinct drop in gamma ray response and a decrease in interval time. The depositional environment of Lange Formation was marine, possibly shallow on the Halten Terrace area and deeper in the basin to the west.

Chapter 4

4. Velocity Anisotropy Analysis from Core Samples

Introduction

Ultrasonic velocity measurements were performed on dry and saturated samples/cores of shale and sandstone to investigate intrinsic velocity anisotropy. The samples/cores came from the Norwegian continental shelf (NCS) both from the northern North Sea and Haltenbanken Areas. The velocity measurement was performed by Norwegian Geotechnical Institute (NGI) over a period of several years from Statoil.

Triaxial tests were done on laminated shales, clayey siltstones, silty claystone and sandstones from five different wells (two from northern North Sea, three from Mid Norwegian Sea, Haltenbanken area). The samples were isotropically consolidated with stress varying from 2-40 MPa. The orientation of the sample where the compressional testes applied on specimens bored were: i) parallel with the lamination planes and are referred to as horizontal specimens ii) perpendicular (normal) to the lamination plane referred as vertical specimens iii) for some angle between the specimen axis and lamination plane (for some data set). The data set also contained other measured parameters like porosity, permeability, Total Organic Carbon (TOC) and water saturation for some samples. The selected core samples that is studied herein were taken from: Viking and Burton shale sample from the Statfjord Field area buried at shallow and intermediate depth, calcite cemented Broom sandstone from Gullfaks field at intermediate depth (~2.5 and ~2.8 km), the Haltenbanken Field (Lange and Not Formation) buried to ~ 4.4 - 4.9 km depth. All measurements on the different samples are given in relative to Kelly bushing (RKB). The detail geological description of the study area is given in chapter 3.

The laminated shales and sandstones were represented by vertically transverse isotropic (VTI) for the quantification of velocity anisotropy. The velocity anisotropy parameters ε and γ was estimated from the formulation describing the fractional difference between the P-and S-wave velocities in the vertical and horizontal directions and are given on the result section. The discussion part, explain the cause of the observed velocity anisotropy in each shale samples and some and general concept of the source of velocity anisotropy that was not observed in this study.

4.1 Core sample from northern North Sea

Sample taken from well 33/9-A-37B, Statfjord Field.

Well bore 33/9-A-37B was drilled in the central of the Statfjord Field near to the area affected by slumping close to platform A. The well is still producing hydrocarbons from two Jurassic reservoirs, the Brent and Dunlin reservoir sands. Two core sample from the Viking Group (Draupne Formation) and Dunlin Group (Burton Formation) taken at the depth of ***~2512*** and ***2869*** m MD RKB respectively(Figure 27)was analysed in this study.

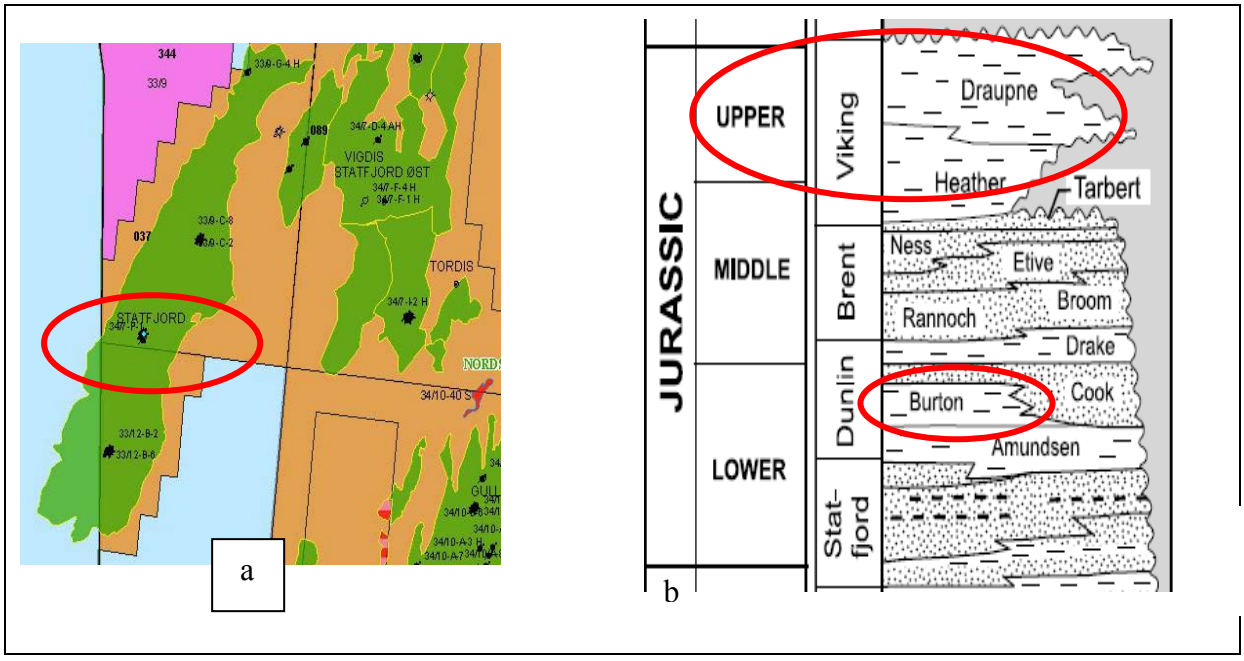

Figure 27: a) the location of well bore 33/9-A-37B on the Statfjord Field. b) Generalized lithostratigraphic section of the northern North Sea.

Database

Twenty- five triaxial test and eight permeability tests have been performed on shale material from well 33/9-A-37B in the North Sea. The following two shales were tested:

Viking shale from a depth of about ***~2512 m***

Burton shale from a depth of about ***~2869 m***

P and S wave velocities measured in connection with CIU triaxial tests at room temperature (~20^0) with back pressure 30 MPa are summarized in the table below:

Viking Shale

In this study of the Viking shale is assumed and modelled that the shale is on small scale a black organic rich, with transversely isotropic layers with illite / kerogen structure. The

sample contains mostly a type II organic matter and it is in an early maturation stage, with no hydrocarbons produced (Figure 28). P- and S-wave velocities measured in the vertical, horizontal and at angle of 32 ^{0} for this shale was collected on an isotropic effective stress of 5MPa and 30 MPa. The results are given in the Table 1.

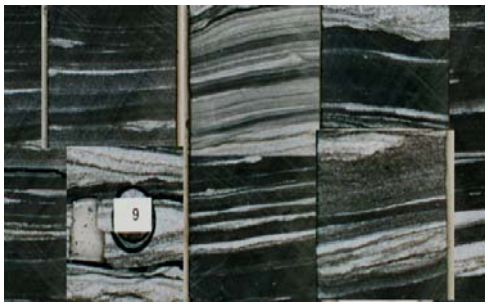

Figure 28: Core log picture of a level of the Viking shale, from the Statfjord Field, well 33/9-B-37B courtesy of the Norwegian Petroleum Directorate. The picture notices the fine lamination of illite and kerogen in the organic rich Draupne Formation black shale.

Table 1: Seven Isotropically consolidated undrained tests (CIU) on specimens bored in three directions with respect to the natural bedding of the shales (0, 32, 90 degree). The values set in parenthesis in the table are uncertain. The units of ConfPressure(MPa), velocity in m/s).

		Angle b/n specimen axis and lamination					
		Velocities at 90 ^{0}		Velocities at 0^0		Velocities at 32^0	
ConPressur	Velocity	Viking	Burton	Viking	Burton	Viking	Burton
5	Vp	2857	2953	3513	3812	3110	3346
5	Vs	(1521)	1352	1849	(1846)	(1664)	(1647)
30	Vp	3052	3117	-	-	-	-
30	Vs	1554	1526	-	-	-	-

<u>Burton Shale</u>

Velocity measurements from the Burton shale specimen from well 33/9-A-37B taken from intermediate measured depth of ~ 2869 m in the from Dunline Group P- and S-wave velocities measured in the vertical, horizontal and at angle of 32 ^{0} for this shale was collected on an isotropic effective stress of 5MPa and 30 MPa. The results are given in the Table 1.

Results

In the previous chapter the quantified anisotropy coefficient (A) was defined in terms of V_{max} and V_{min} which are velocities parallel and normal to the specimen bedding. The percentage degree of anisotropy coefficient for Viking shale at 5 MPa is computed as:

$$A = \frac{V_{\max} - V_{\min}}{0.5\left[V_{\max} + V_{\min}\right]} \times 100 = \frac{3513 - 2857}{0.5(3513 + 2857)} \times 100 \ = 21\%$$

If the Viking shale is assumed as a weak VTI media, then for practical use, it is convenient to express anisotropy using the parameters ε, and γ (Thomsen, 1986). For weak anisotropy, the Thomsen's parameters can be computed by:

$$\varepsilon = \frac{C_{11} - C_{33}}{2C_{33}} \approx \frac{V_p(90) - V_P(0)}{2V_P(0)},$$ which shows by how much VP (90) varies with VP (0)

$$\gamma = \frac{C_{66} - C_{44}}{2C_{44}} \approx \frac{V_S(90) - V_S(0)}{2V_S(0)},$$ which shows the shear wave splitting (fast and slow)

The corresponding Thomson parameters for P-wave velocity

$$\varepsilon = \frac{V^p_{\max} - V^P_{\min}}{2V^p_{\min}} = \frac{3513 - 2857}{2 \times 2857} \cong 0.11,$$

The corresponding S-wave quantified anisotropy coefficient (A) at 5 MPa

$$A = \frac{V_{\max} - V_{\min}}{0.5\left[V_{\max} + V_{\min}\right]} \times 100 = \frac{1849 - 1521}{0.5(1849 + 1521)} \times 100 \approx 19\%$$

$$\gamma = \frac{V^s_{\max} - V^s_{\min}}{2 \times V^s_{\min}} = \frac{1849 - 1521}{2 \times 1521} \approx 0.11$$

The P-wave velocity anisotropy parameter of Burton shale is

$$A = \frac{V_{\max} - V_{\min}}{0.5\left[V_{\max} + V_{\min}\right]} \times 100 = \frac{3812 - 2953}{0.5(3812 + 2953)} \times 100 \approx 25\%,$$

The corresponding Thomson parameters for Burton Formation shale

$$\varepsilon = \frac{V^p_{\max} - V^P_{\min}}{2V^p_{\min}} = \frac{3812 - 2953}{2 \times 2953} \approx 0.15,$$

$$\gamma = \frac{V^s_{\max} - V^s_{\min}}{2 \times V^s_{\min}} = \frac{1846 - 1352}{2 \times 1352} \approx 0.18 \quad ,$$

The S wave velocity measurement for Burton shale is uncertain, but approximately it is around $\gamma \sim 0.18$.

Sample taken from well 34/10-C-3, Gullfaks Field

Well 34/10-C-3 was drilled on the Eastern side of the Gullfaks Field. The well bore is still producing oil from two Jurassic reservoirs, Brent and Dunlin sands. As indicated by the red ellipse on the lithostratigraphic column (Figure 29), the core sample analyses was from a depth of around 2.5 km. This consists of Broom Formation, from the Middle Jurassic, Brent Group. Broom Fm is overlying by a hydrocarbon reservoir of progardational delta, with some calcite cemented units. The depositional environment of Broom was a prodelta setting.

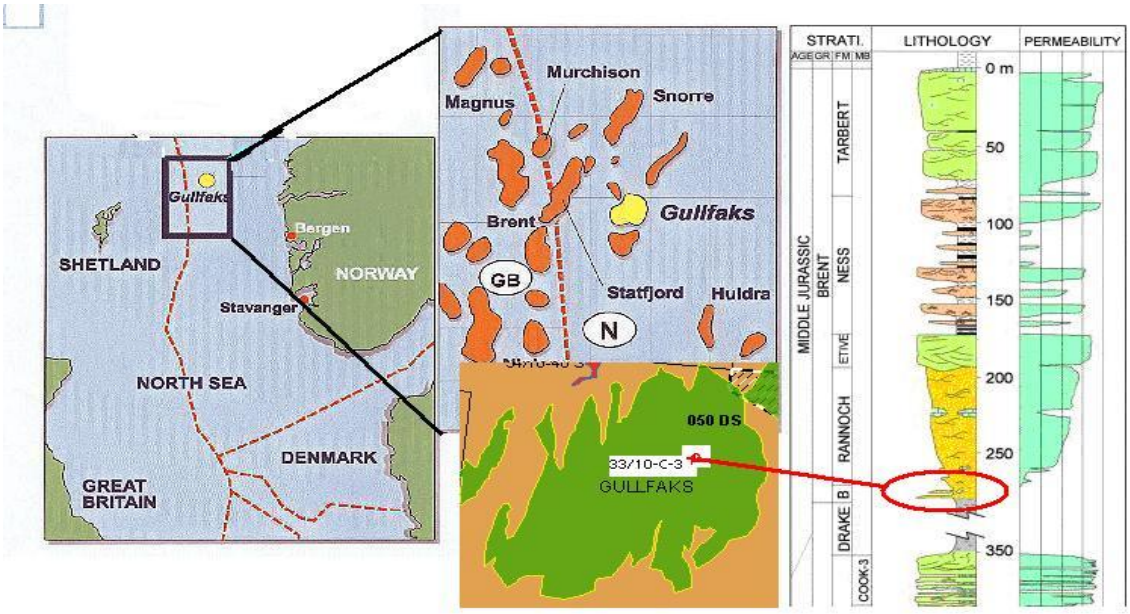

Figure 29: Figure shows the location of Gullfaks field at Northern North Sea, the Location of well 33/10-C-3 (indicated by red dot) where Core simples taken. The General lithostratigraphic column of the Gullfaks area for Middle Jurassic Brent Group.

Database

Three CID –triaxial tests have been performed on sandstone and mudstone from well 34/10-C-3 in the North Sea from the depth of ***2570 m***. The consolidation stress was 7 MPa for all tests. The following results were obtained:

For the two low porosity specimens of sandstone *cemented by calcite*

Porosity:…… 1.3-2.1 %

Bulk modulus at an isotropic

Stress equal to 7 MPa :…… 13-150GPa

Poisson's ratio halfway in shearing process:…… . 0.31 -0.33

P- Wave velocity at isotropic stress equal to 7MPa:…… 4990-5160 m/s

S- Wave velocity at isotropic stress equal to 7MPa:…… 2670-3050 m/s

One of the two specimens had bedding planes parallel to the axis of the plug. This specimen had the highest Poisson's ratio and the lowest acoustic velocity of these specimens. The specimens with much higher porosity consisted of mudstone with irregular beds of siltstone:

Porosity :…… 17.6 %

Bulk modulus at an isotropic

Stress equal to 7 MPa :…… 2.3 MPa

Poisson's ratio halfway to failure…….…… .0.17

P- Wave velocity at isotropic stress equal to 7MPa:……. .2870 m/s

S- Wave velocity at isotropic stress equal to 7MPa:……. .1485 m/s

Bulk Density …….. . 2.36 g/cm^3

Result

The Broom Fm calcite cemented sandstone can be assumed as VTI medium and the degree of anisotropy in this study is calculated as:

$$A = \frac{V_{\max} - V_{\min}}{0.5\left[V_{\max} + V_{\min}\right]} \times 100 = \frac{5160 - 4990}{0.5\left[5160 + 4990\right]} \times 100 \cong 3.3\%$$, for P wave velocity

$$A = \frac{V_{\max} - V_{\min}}{0.5\left[V_{\max} + V_{\min}\right]} \times 100 = \frac{3050 - 2670}{0.5\left[3050 + 2670\right]} \times 100 \cong 13.3\%$$, for S wave velocity

The corresponding Thomson parameters for sandstone specimens are

$$\varepsilon = \frac{V_{\max}^{p} - V_{\min}^{P}}{2V_{\min}^{p}} = \frac{5160 - 4990}{2 \times 4990} \cong 0.02,$$ for P-wave velocity

$$\gamma = \frac{V^s_{\max} - V^s_{\min}}{2 \times V^s_{\min}} = \frac{3050 - 2670}{2 \times 2670} \cong 0.07 \quad , \qquad \text{for S-wave velocity}$$

4.2 Core sample from Haltenbanken Area

Sample from Well 6506/11-7, Kristin Field

Well 6506/11-7 was drilled on a rotated and truncated fault block on the northern extension of the Kristin trend, west of the Åsgard Field (Smørbukk Discovery) or Haltenbanken South. The purpose of the well was to test the hydrocarbon potential of the M-prospect, which targets the Middle and Early Jurassic sandstones of the Fangst and Båt Groups. Information about the reservoir quality and the fluid properties were acquired. The well should also provide velocity information and establish a good seismic tie. Core sample is taken from this field at the depth of 4478 to 4482 m MD RKB from the Lange Formation.

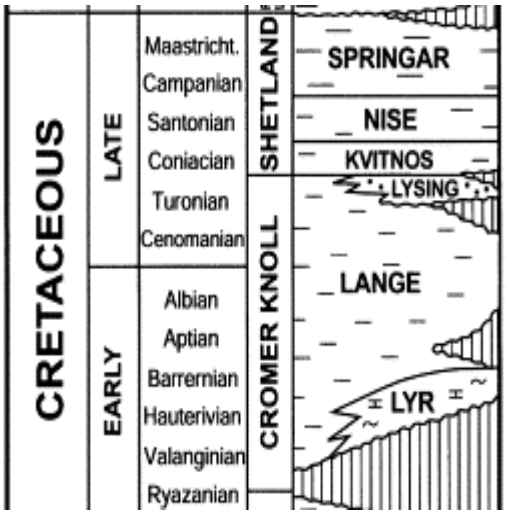

Figure 30: Lithostratigraphic sections from Haltenbanken. Lange Formation is Cromer knoll Group, early to late Cretaceous age.

From the lithostratigraphic column the Lange Formation shown in Figure 30, it is a thick shale layer fromation. It is recognised as compacted overburden shale buried down to ~ 4.5 to 4.6 km as seen also in the composite log in Figure 30. Below Lange Formation, there is a hydrocarbon reservoir unit of the Fangst Group sandstones. Therefore this thick shale may act as cap as well as seal rock.

Database

Twenty –one triaxial tests and four permeability tests have been performed on material from 4478 to 4482 m MD RKB in well 6506/11-7 from Lange formation at Haltenbanken South.

1 Index and classification test

Porosity, pycnometers method------- ---------- 7.9 -9.6 %

Water saturation, pycnometers---------- 97-103 %

TOC –value (total organic content):---------- 5.6-7.3.8%

2 Permeability test

Coefficients of permeability determined at an average effective isotropic stress of 5-11 MPa at an average pore pressure of 18-27 MPa and with gradients varying from 11300 to 48100:

Flow normal to the lamination ***0.80 - 1.8 x10^{-7} mD***

Flow parallel to the lamination ***11.2 – 23.70 x10^{-7} mD***

3 P and S- wave velocity

The acoustic velocities measured on specimens bored normal at 29 ^{0}, and parallel to the lamination at an isotropic effective stress of about 5 MPa and pores pressure of about 30 MPa (backpressure) given on Table 2.

Table 2: Selected velocity measurements from Fourteen CIU-tests on the specimens drilled at three directions with respect to lamination (0, 29, 90 degree).

Sample	Angle wrt lamination	Vp(0^0) m/s	Vp(90^0) m/s	Vs(0^0) m/s	Vs(90^0) m/s
1	90	3580	3700	1710	1930
2	29	4118	4118	2001	2001
3	0	4550	4650	2430	2620

For two specimen (8A1 and 8A2) bored beside each other from exactly the same depth normal to the lamination , with an isotropic effective stress equal to 10 MPa, velocities at two different temperature were measured. The results are given in Table 3 below.

Table 3: shows the temperature and velocity measurement for two specimens from the same depth, normal to the lamination. The isotropic effective stress was 10 MPa.

Specimen No	Temperature (^{0}C)	P-wave velocity (m/s)
A1	140	3349
8A2	21	3613

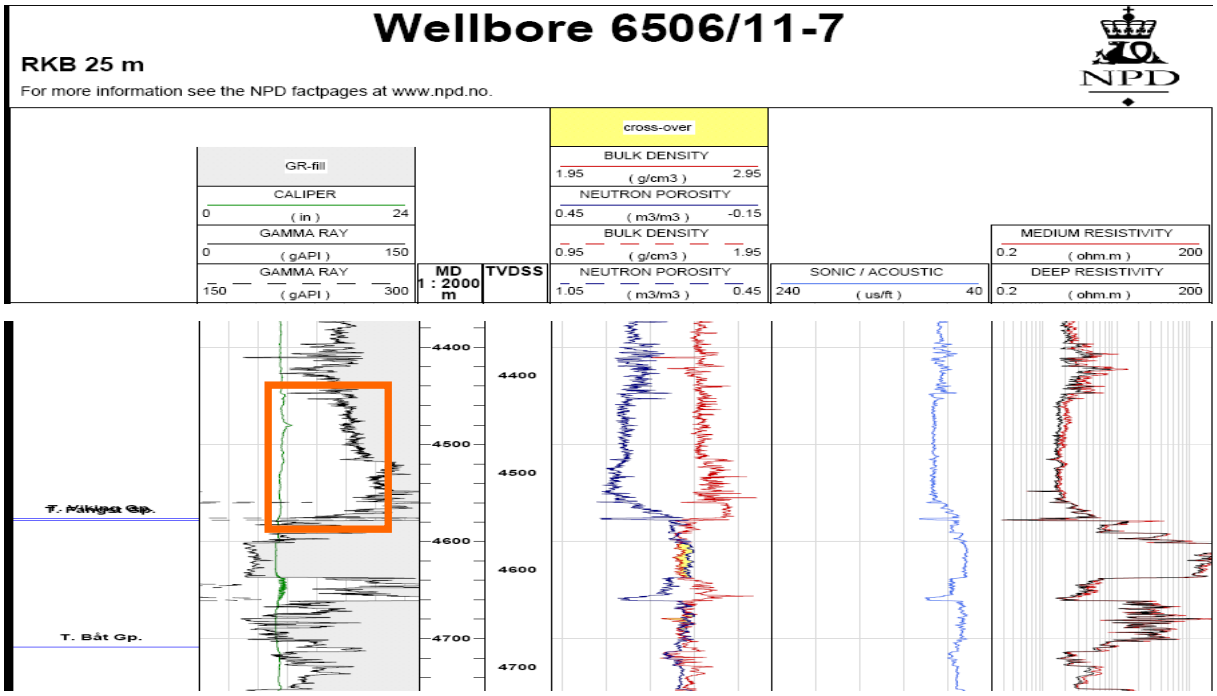

Figure 31: The composite logs of well 6506/11-7 notice the thick shale from Lange Formation at the depth 4.4 to 4.5 km as indicated by the rectangle on the gamma log.

Result

As shown in the composite log, approximately 100 m Lange Formation of Cretaceous age. From the P-and S-wave velocity measurement, the quantified velocity anisotropy coefficient (A) are calculated as:

$$A = \frac{V_{\max} - V_{\min}}{0.5[V_{\max} + V_{\min}]} \times 100 = \frac{4650 - 3580}{0.5[4650 + 3580]} \times 100 \approx 26\%, \text{ for P wave}$$

$$A = \frac{V_{\max} - V_{\min}}{0.5[V_{\max} + V_{\min}]} \times 100 = \frac{2620 - 1710}{0.5[2620 + 1710]} \times 100 \approx 42\%, \text{ for S wave}$$

In general based on the Table 2, the quantified velocity anisotropy coefficient for Lange Formation shale varies from 20 to 26 % to P-wave and 23 to 43 % to S wave velocity.

The corresponding Thomson parameters for Lange Formation are

$$\varepsilon = \frac{V^{p}_{\max} - V^{P}_{\min}}{2V^{p}_{\min}} = \frac{4650 - 3580}{2 \times 3580} \cong 0.15, \qquad \text{for P-velocity}$$

$$\gamma = \frac{V^{s}_{\max} - V^{s}_{\min}}{2 \times V^{s}_{\min}} = \frac{2620 - 1710}{2 \times 1710} \cong 0.27 \qquad \text{for S velocity}$$

From Table 3, the test result shows that acoustic velocity is higher at room temperature (21-25 ^{0} C) than at 140 ^{0}C. In addition to that the Lange shale has a TOC content of 5.6-7.3.8 %,(with porosity ~ 7.9 -9.6 %), and will at high temperature (140 ^{0}C) liquefied, and this may decrease the velocity measurement.

Sample from Well 6406/2-7, Kristine Field

Well 6406/2-7 was the fourth wildcat drilled in the PL 199 license. The well was drilled on the eastern part of the Erlend structure in the western part of block 6406/2, southwest of the Kristin Field and northwest of the 6406/2-6 Ragnfrid discovery on Haltenbanken (Figure 32 left). The Erlend structure is an easterly dipping segmented horst. Well 6406/2-7 was drilled high on the Erlend structure's south-eastern high. The main objective of well 6406/2-7 was to test the hydrocarbon potential of the Erlend structure within the Early to Middle Jurassic Fangst and Båt Group sandstones.

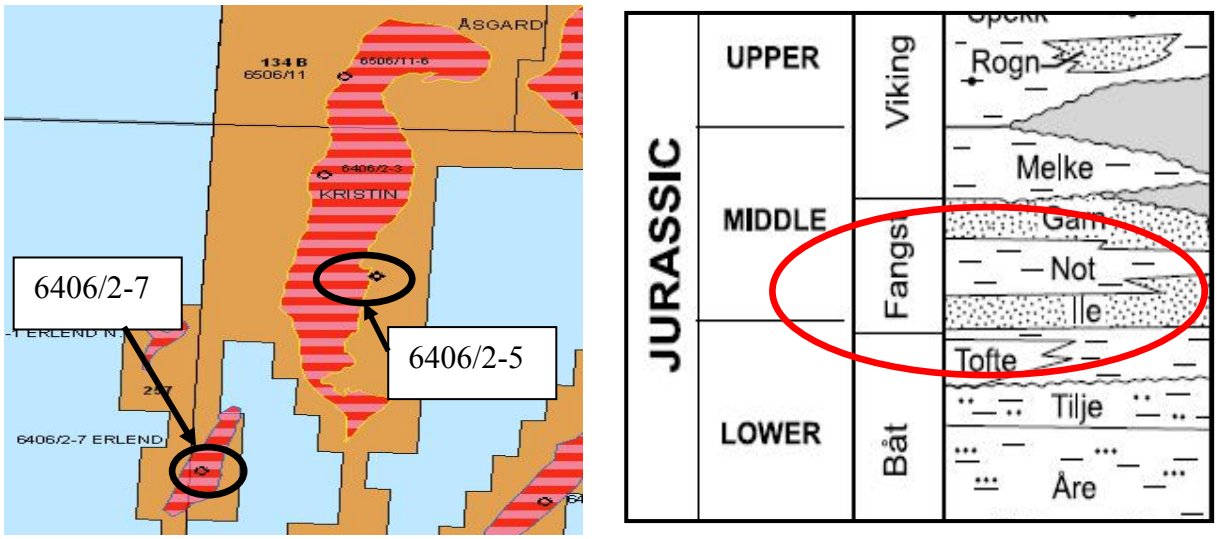

Figure 32: location of exploration well bores 6406/2-7 and 6406/2-5(left). Lithostratigraphic column from the Haltenbanken area. The Middle Jurassic, Fangst Group, Not Formation is indicated by ellipse (right).

Core samples were taken from well bore 6406/2-7 from the Middle Jurassic (Bajocian-Bathonian) Fangst Group, Not Formation at the depth of 4573 to 4591 m MD RKB. The lithology of Not Formation is clasystone with micronodular pyrite coarsening upwards into bioturbated fine grained sandstones which are locally mica rich and carbonate cemented. The lower boundary is defined by abrupt increase to a steady high gamma ray response (on Figure 33). The depositional environment of the basal part (the lower boundary) reflects semi

regional transgressions which lead to the development of lagoons or sheltered bays. The upward part of the unit consists of prograding deltaic or costal front sediments.

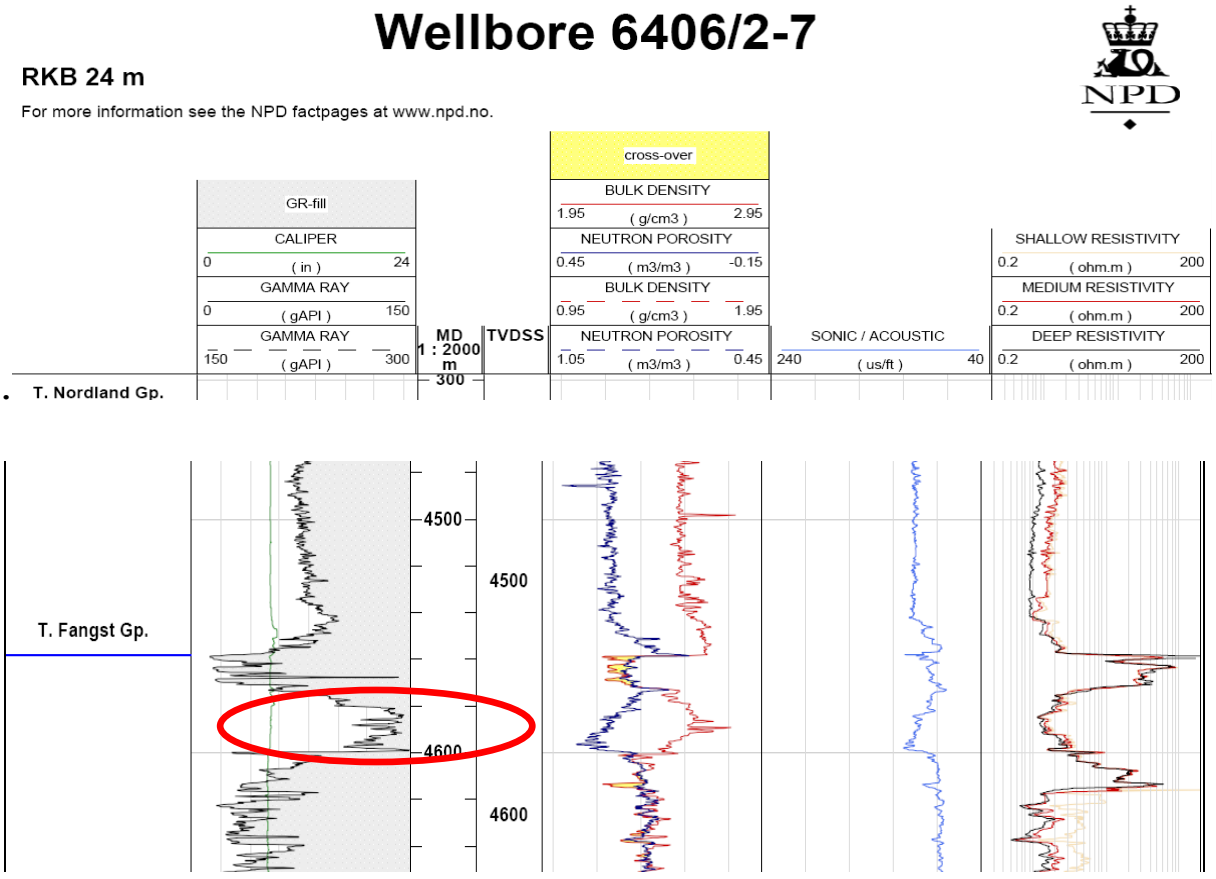

Figure 33: The composite log of well 6406/2-7 for a section of the Fangst Group. The Not Formation which is indicated by the ellipse has high gamma ray values, high bulk density, low sonic (acoustic) and low deep resistivity well logs values.

Database

Thirty one triaxial tests, six permeability tests and three series of Brazil tension tests have been carried out on laminated shales from four different locations. Of these twenty eight triaxial tests, six permeability tests and two series of Brazil tension tests were carried out on material from the Not Formation in well 6406/2-7 from 4573 to 4591 mMD RKB. These triaxial tests were as follows.

Test result for the Not Formation in Well 6406/2-7

1. ***Index and classification test***

Porosity, pycnometers method------- ---------- 7.5 -10.9 %

Porosity, helium method ---------- ---- 7.8 -11.3 %

Water saturation, pycnometers---------- 61-108 %

Water saturation, helium ---------- 60-101 %

TOC –value (total organic content):---------- 4.3-8.8%

2 ***Permeability test***

Coefficient of permeability determined at an average effective isotropic stress of 6-12 MPa at an angle pore pressure of 18-27 MPa and with gradients varying from 14600 to 72300:

Flow normal to the lamination ***1.0 - 4.2 x10^{-7} mD***

Flow parallel to the lamination ***7.6 - 27.12 x10^{-7} mD***

3 ***P- and S- wave velocity***

The acoustic velocities measured on specimens bored normal, 34 ^{0}, and parallel to the lamination at an isotropic effective stress of about 5 MPa (and around 5MPa for parallel and 34 ^{0} bored samples) and a pore pressure of about 30 MPa were as follows:

Table 4: Selected velocity measurements from Fourteen CIU-tests on the specimens drilled at three directions with respect to lamination (0, 29, 90 degree).

Sample	Angle wrt lamination	Vp(min) m/s	Vp(max) m/s	Vs(min) m/s	Vs(max) m/s
	90	3200	3700	1620	2020
	34	4040	4065	2200	2390
	0	4270	4470	2300	2475

For one specimen (11B) bored normal to the lamination, isotropic effective stress 5 MPa and pore pressure 1 MPa, the following velocities at two different temperatures were measured.

Table5: shows the temperature and velocity measurement for a specimen. The isotropic effective stress was 5 MPa.

Temperature (0 C)	Vp(m/s)	Vs(m/s)
20	3315	1695
137	2917	1499

Result

The quantified anisotropy coefficient (A) for Not shale at ~ 5 MPa isotropic effective stresses is calculated by comparing parallel and normal velocity measurements. The value of A was varies 14% to 33 % for the different combination of P-wave velocity and 20 to 41 % for the different combination of S-wave velocity as given in Table 4.

The corresponding Thomson parameters for P velocity

$$\varepsilon = \frac{V^{p}_{\max} - V^{P}_{\min}}{2V^{p}_{\min}} = \frac{4470 - 3200}{2 \times 3200} \cong 0.19, \qquad \text{for P-velocity}$$

The corresponding S wave velocity anisotropy at 5 MPa

$$\gamma = \frac{V^{s}_{\max} - V^{s}_{\min}}{2 \times V^{s}_{\min}} = \frac{2475 - 1620}{2 \times 1630} \approx 0.26 \qquad \text{for S velocity}$$

Samples from well 6406/2-5, Kristin Field

Well 6406/2-5 was the second well drilled on the Kristin structure in the north-western part of block 6406/2, south-west of the Smørbukk Field and north-west of the Lavrans Field on Haltenbanken (Figure 32 left). The discovery well 6406/2-3 was drilled high on the structure; it tested gas and condensate in a down-to situation in both the Garn and the Ile Formations. The main objective of well 6406/2-5 was to test the hydrocarbon potential of the Garn and Ile Formations in a down flank position. The location of Kristin Field on Mid Norwegian Shelf (Halten Terrace) is indicated on Figure 32.

Database

Twenty three triaxial tests have been performed on laminated clayey siltstone and on laminated silty claystone from well 6406/2-5 situated in Haltenbanken area. The samples came from the depth interval 4923 to 4944 m and the test result for the materials at this depth interval are summarized and given in Table 6.

Table 6: The test result for the material in the depth interval 4923 to 4939 meters which is described as ''clayey siltstone'' and the test result for the material in the depth interval 4943 to 4944 meters which is described as ''silty claystone'' are summarized as follows.

Sample	MD(m)	Test	Angle	Vp(min)	Vp(max)	Vs(min)	Vs(max)
Clayey-siltstones	4923-39	U	90	3800	4080	1900	1980
	,,	D	90	3940	4230	2200	2330
	,,	U	0	4670	4830	2570	2730
Silty - claystone	4943-44	U	90	3520	3860	1980	2030
	,,	D	90	3200	3420	1800	1880
	,,	U	0	4290	4610	2310	2610

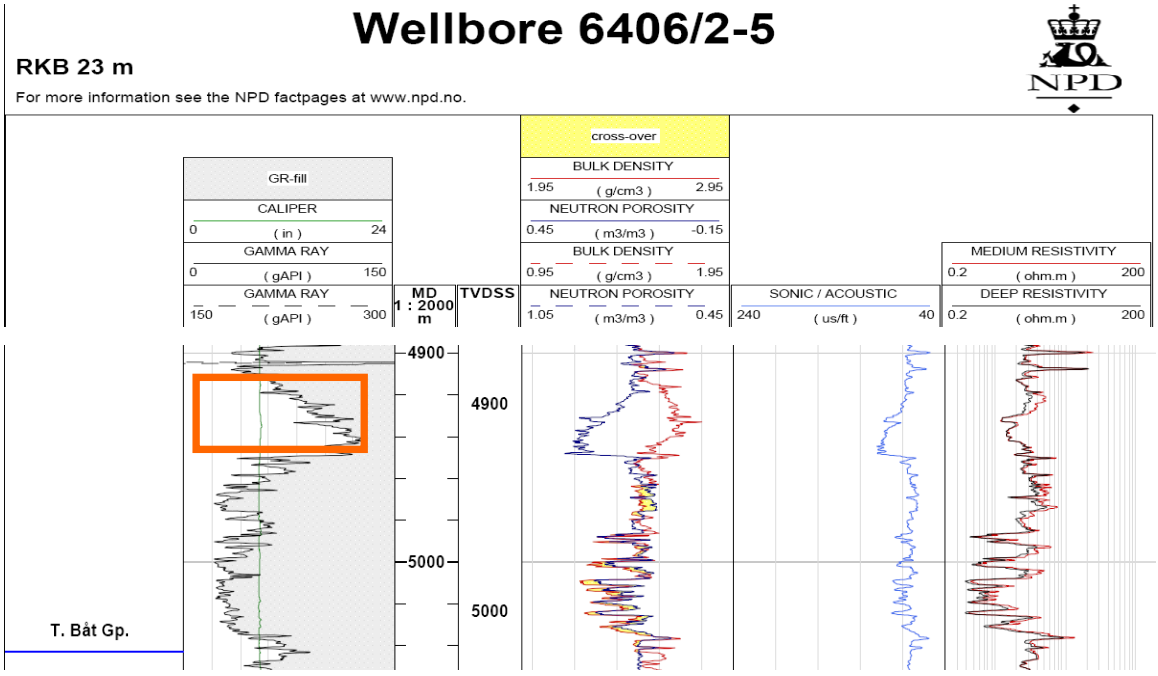

Figure 34: the composite log of from the exploration well bore 6406/2-5 around the deepest part well (displayed between 4900 to 5500 m). The gamma log showed remarked increase from upper unit of Not Formation (clay siltstone) to the lower unit (silty claystone).Hydrocarbon reservoir is Ile Formation is located Below Not Formation.

Result

The quantified anisotropic coefficient of the Not shale at the Kristin Field is calculated from the test result displayed in Table 6 for undrained isotropic compressional (CIU) tests.

Clay siltstones: the P wave degree of velocity anisotropy coefficient (A) varies from 17% to 23 %, and S wave varies 30% to 33 %. The corresponding Thompsen parameters have a value of the order of $\varepsilon \approx 0.09$, and $\gamma \approx 0.19$.

Silty Claystone: the P wave velocity anisotropy coefficient (A) varies from 17% to 27 %, and S wave varies 25% to 28 %. The corresponding Thompson parameters have a value of the order of $\varepsilon \approx 0.15$, and $\gamma \approx 0.16$.

4.3 Discussion

4.3.1 Northern North Sea Area

Statfjord Sample

The result of from the ultrasonic velocity measurements of the Viking shale (Draupne Formation) specimens showed that the samples to be are intrinsically anisotropic due to the alignment of clay (Illite and kerogen) minerals. The P-and S-wave velocity anisotropy found the specimens were approximately similar in value (~0.11) at the measure depth of 2512 m, on 5 MPa isotropic stresses.

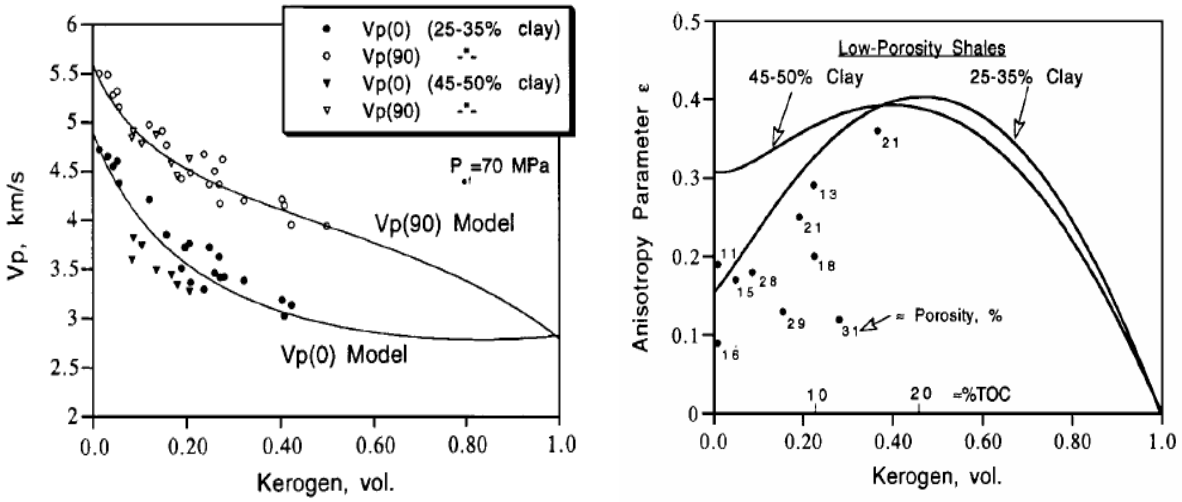

Figure 35: Left) velocity anisotropy versus kerogen content for two groups of black shales with different clay content. Dry measurements at 70 MPa are shown on the background of modified Backus model predictions. Right) The P wave anisotropy parameter ε as a function of kerogen content in low-porosity shales compared to the data on high-porosity source rocks obtained at 70 MPa and dry conditions (Vernik and Nur, 1992)

The Viking shale sample is organic rich black shale, containing type II kerogen. At this depth (2512 m) it was not matured. The same formation as Viking shale (Draupne Formation) buried at greater depth in the central part of the Viking Graben showed substantial velocity anisotropy (Vernik and Nur, 1992).

Figure 35 (right) shows the anisotropy parameter ε as a function of the kerogen content · for the low porosity black shales of both shale groups using their model predictions from Figure 35(left), i.e., again for dry data at 70 MPa confining pressure. Both shale groups suggest that the anisotropy increases with kerogen present reaching a maximum of about $\varepsilon = 0.40$ to .50 at a kerogen content of K= 40 - 45 % or 15–20% TOC. Note that the increase is especially strong for the black shales with moderate clay contents

One might speculate that the effect of kerogen on velocity anisotropy is strongly related to the texture of black shales, notably to their compaction and associated flattening of clay particles, as suggested by Kaarsberg (1959). Additionally, this compaction process results in rearrangement of ductile organic matter to create a finely laminated lenticular texture parallel to the bedding (Johnson, 1987).

The degree of the Burton Formation (Dunlin Group) P-and S-wave velocity anisotropy is higher than in the Viking shale, since the Burton shale was buried down to greater depth than Viking shale. The Burton shale would have been subjected a greater amount of overburden stress, and this will often give rise to tendency of more preferential alignment of grains and pores parallel with the bedding plane. The degrees of anisotropy also increase with increase of burial depth.

Layer induced P-and S-wave velocity anisotropy predicated from the well bore 33/9-A-37B using the concept of anisotropic well log (Li, 2002) can be compared with observed intrinsic anisotropy form the core measurement (Figure 36). As shown in the blue ellipse on Figure 10, the value of ε varies between 0.15 to 0.25 and γ varies between 0.19 to 0.3 at depth around the location of Viking shale. But from core sample measurement the Viking shale has P- wave velocity anisotropy of ε= 0.11 and γ=0.11.

These results may also give direct comparison between laboratory and well log derived velocity anisotropy, such as the intrinsic from the core sample and layer induced one from the well log. The observed anisotropy on Viking and Burton shale may be the superposition between induced and intrinsic velocity anisotropy

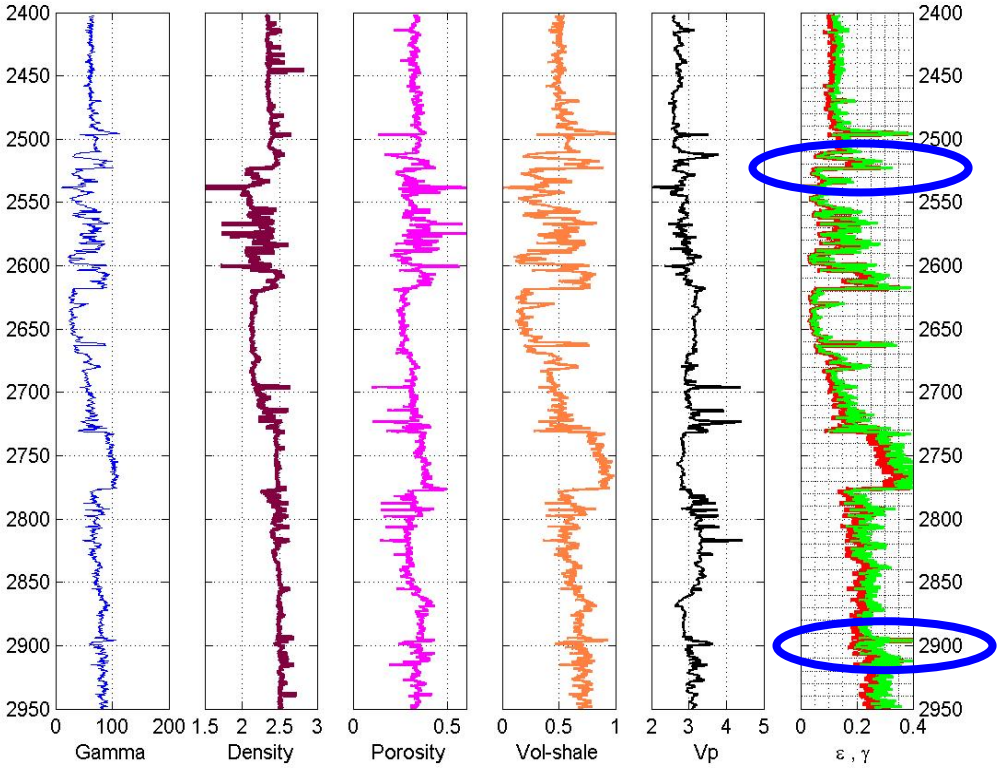

Figure 36: Predicated P-and S-wave anisotropy well log shown in the sixth column for well bore 33/9-A-37B. In the anisotropic well, the two blue ellipses show the location where the Viking and Burton specimens taken, the red curve-P-wave and green curve-S-wave anisotropy. The estimated anisotropy on is the order of $\varepsilon \approx 0.15, \gamma = 0.25$ ***at location of the Viking shale and*** $\varepsilon \approx 19, \gamma \approx 0.27$ ***at the location the location of Burton shale. Generally the degrees of anisotropy depend on the clay mineral content and depth.***

Gullfaks Field Sample

The calcite cemented Broom Formation sandstone has low porosity. The sandstone cemented by calcite will have fewer tendencies for rearrangement of grains and alignment of pores during burial. The overall structure of the sand body will be stiffened by the cementation and decrease development of lamination.

The velocity of the Broom shale varies between 4990 and 5160 m/s for P-wave and 2670-3050 m/s for S-wave. The corresponding velocity anisotropies were to the order of 0.02 % for P-wave, and 0.07% S-wave, which is very small as compared to the calculated anisotropy for shale specimens analysed in this study, taken from nearby Statfjord Field. A likely explanation for why velocity anisotropy decreases with the presence of (increasing) calcite cementation, may be as the result calcite cement reduce of the overall grain alignment and also reduction of preferred pore orientations. Because calcite cementation happens before

compaction, calcite cementation generally happens early at shallow depth before much compaction.

Koesoemadinata and McMechan (2004) described a model which analysis the effect of calcite cementation and clay content on velocity anisotropy in sandstone samples.

$A = -0.595 xCalcite + 14.472,$

this shows the inverse relation between anisotropic coefficient and calcite content of the sample. Anisotropy decreases as the calcite increases.

In general, reservoir sands and sandstones are intrinsically isotropic unless they are fractured, finely layered, or clay bearing. Wang (2002) shows that the brine-saturated Africa reservoir sands, which are essentially clay free, have very little anisotropy. The average values around 0.6 % P-anisotropy and 1.1% S-anisotropy are probably within the measurement uncertainties. The same is true for the specimens analysed in this study with isotropic triaxial undrained test, since isotropic consolidation will mainly promote reduction in the pore volume without significant changes in grain orientation. This is also the case for Brent Group, Broom Formation.

4.3.2 Haltenbanken Area

Lange Formation

The Lange Formation shale is intrinsically anisotropic with $\varepsilon \approx 0.15$ for P-wave and $\gamma \approx 0.27$ for S-wave. These values of the Thompson parameters indicate that the Lange shale has weak P-wave and strong S-wave velocity anisotropy. The explanation for the observed anisotropy is that, the shale was buried to a deeper level than the other shales studied.

Figure 37: The core photographs taken from well 6406/2-7 Core log picture a level of the Not Formation, from the Kristine field, well 6406/2-7 courtesy of the Norwegian Petroleum Directorate. a) At the depth of 4588-4593 m, b) at the depth of 4573- 4578 m.The picture notices the fine lamination between shale and some lighter sands layer.

Chemical compaction is more dominant where at deeper depths (Lange Formation ~ 4478 to 4482 m MD RKB). Compaction in general alters the nature of shales; enhance the alignment of clay minerals parallel to the bedding plane. The low porosity (~ 7 to 9%) found in the Lange Formation may be a combined effect of the overburden pressure and chemical compaction which may also resulted in the complete transformation of smectite to illite in the clay mineral compositions. These compaction and dewatering processes may be the likely explanation of the pronounced S-wave anisotropy ($\gamma \approx 0.27$) than the P-wave anisotropy. Since small pores will be empty, and the shale layer may be very stiff for S-wave polarization. All in all the Lange Formation was found to be intrinsically anisotropic.

Not Formation

Not shale from well bore 6406/2-7

The Not shale which was taken from the lower basal part of the Not Formation is intrinsically anisotropic due to the clay mineral preferential alignment. The velocity anisotropy was estimated to be in the order of $\varepsilon \approx 0.19$ for P-wave and $\gamma \approx 0.26$ for S-wave. From the index and classification test data, the shale documented low porosity which varies 7 and 11 %, and a permeability of around 1 nano Darcy at 6-12 MPa isotropic consolidation stress.

The Jurassic shale Not Formation contains significant amounts of silt and sand stringers (Dalland et al, 1988). As discussed by Storvoll, et al (2005), quartz cement may also precipitate more easily in Jurassic shale because the sand and silt content increases potential nucleation positions when the sediments are buried deeper at higher temperatur*es*. As seen in the core picture (Figure 38), the Not Formation shale is finely laminated sand and silt containing shale buried around 4.5 km depth where chemical compaction is dominating. It is also sandwich between two well compacted sandstone reservoir units (the Gran Formation and the Ile Formation) which may cause rigidity in the Not shale.

Not shale from well bore 6406/2-5

From the composite log the Not Formation showed an increasing in gamma log from the upper part of clay siltstone to the lower unit of silty claystone accompanied by high value in neutron porosity and bulk density. The estimated P- and S-wave anisotropy was in the order of $\varepsilon \approx 0.09$, and $\gamma \approx 0.19$. The explanation for the observed small anisotropy found in the depth interval 4923 - 4939 m is its poor lamination and the less preferential alignment of clay mineral which influenced by the presence of silt and sandstone.

.

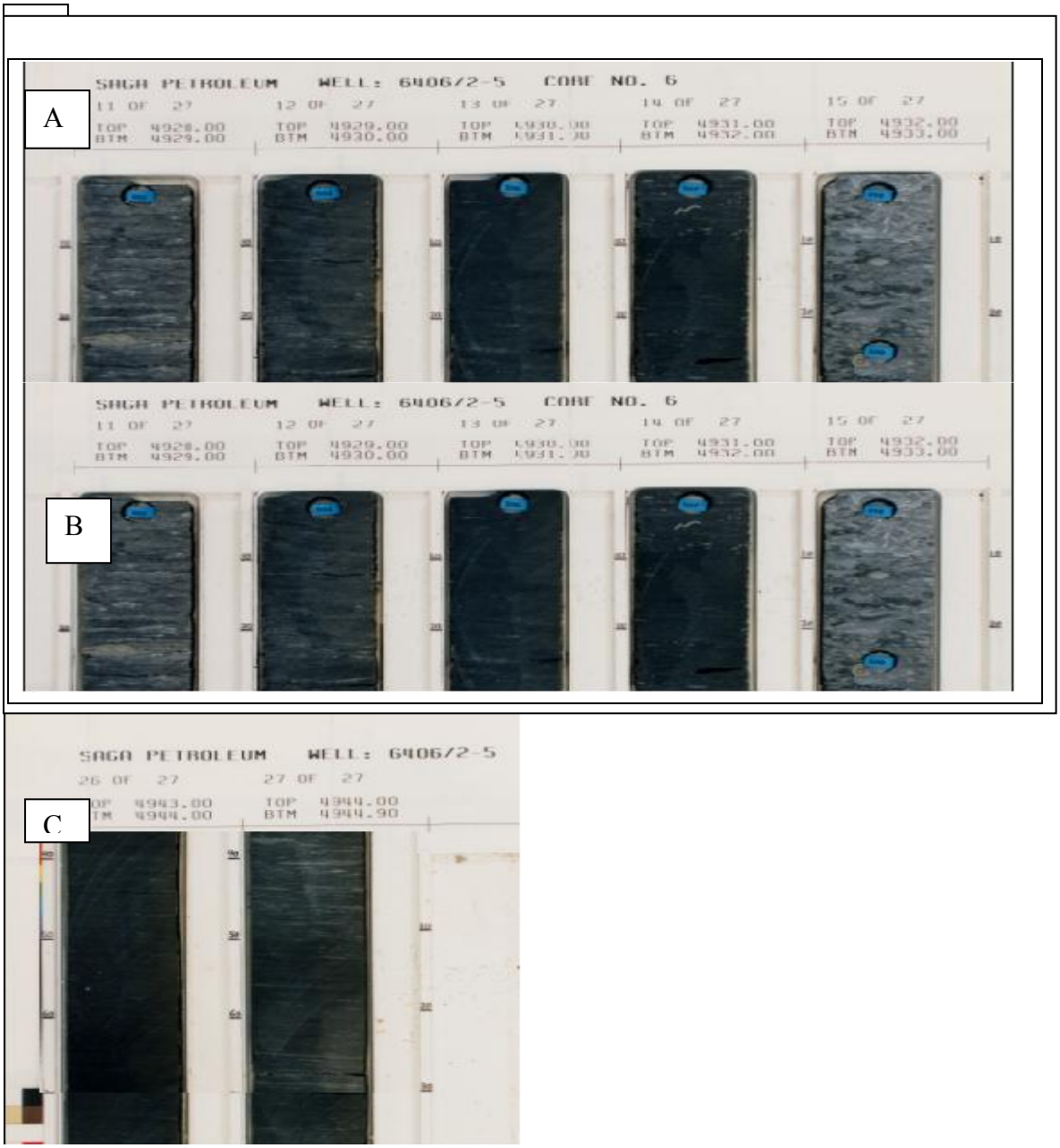

Figure 38: A, B, C: Core log picture of a level of the Not Formation, from the Kristine Field, well 6406/2-5 courtesy of the Norwegian Petroleum Directorate. The picture is taken from core A) clayey siltstone at depth 4923-4928 m, it has lithological difference within small later change, and it is the upper part of the prograding deltaic sediments. B) Clayely siltstone from depth 4929-4933m C) silty claystone depth 4943-4944 m dark shale and some lighter silty sands layer in the second column which is the lower basal part and deposited during a semi regional transgression.

The lower unit of the specimens taken from the depth 4944 m has a lithology of silty claystone, is grey, has lenticular lamination and contains thin lenses of silt as shown in the core picture (Figure 38). The depositional environment reflects a semi regional transgression. The velocity anisotropy was estimated to the order of $\varepsilon \approx 0.15$, and $\gamma \approx 0.16$, which is in the

range of weak anisotropy (Thompsen, 1986). As compared to the upper unit claysiltstone the lower unit siltyclaystone of Not Formation has higher velocity anisotropy since it contains more clay, which could explain the observed velocity anisotropy.

Table 7: summarized velocity anisotropy of shale and sandstones analysed on this study.

Well bore	Field	Formation	Depth(m)	ε	γ
33/9-B-37B	Statfjord	Viking shale (Draupne)	2512	0.11	0.11
33/9-B-37B	Statfjord	Burton	2869	0.15	0.18
34/10-C-3	Gullfaks	Broom	2570	0.02	0.07
6506/11-7	Haltenbanken	Lange	4478-4482	0.15	0.27
6406/2-5	Haltenbanken	Not	4573-4591	0.19	0.26
6406/2-7	Haltenbanken	Not(claysiltstone)	4923- 4939	0.09	0.19
6406/2-7	Haltenbanken	Not (siltyclaystone)	4943-4944	0.15	0.16

Numerical -Haltenbanken Area core sample velocity Anisotropy

The Elliptical method discussed in the chapter 3 has been applied for 7 shale samples taken from the Haltenbanken area. The input that is used here to calculate the stiffness constants are Vp, Vs at parallel and perpendicular to the lamination axis and the measured density given in Table 8.

Table 8: measured velocity (m/s), density (gm/cm^3) and porosity with applied confining pressure (MPa) for selected laminated shale samples from Haltenbanken Area.

Sample	**Pres**	**Density**	**Porosity**	**Vp(0)**	**Vp(90)**	**Vs(0)**	**Vs(90)**
1	10.00	2.59	60.00	4080	4830	1980	**2730**
2	8.60	2.57	30.00	3860	4610	2030	**2610**
3	1.25	2.64	7.00	4990	5160	2670	**3050**
4	7.87	2.10	5.00	3700	4470	2020	**2475**
5	7.90	2.20	10.00	3700	4650	1930	**2620**
6	5.00	2.37	22.00	2857	3513	1521	**1849**
7	**5.00**	**2.47**	**15.00**	**2953**	**3812**	**1352**	**1866**

Table 9: the five independent elastic constants (GPa) and Thompsen parameters derived from Table 8 data of velocities and density measurements using equation.

Sample	C_{11}	C_{33}	C_{44}	C_{66}	C_{13}	ε	γ	δ
1	60.42	43.11	10.15	19.30	27.74	0.20	0.45	**0.12**
2	54.62	28.29	10.59	17.50	22.06	0.20	0.33	**0.14**
3	70.29	65.74	18.82	24.56	23.25	0.21	0.15	**0.07**
4	41.96	2.75	8.17	12.86	15.93	0.03	0.25	**0.17**
5	47.57	30.12	8.20	15.10	20.76	0.23	0.42	**0.27**
6	29.25	19.35	5.48	8.10	11.98	0.29	0.24	**0.21**
7	**35.89**	**21.52**	**4.52**	**8.60**	**18.97**	**0.26**	**0.45**	**0.36**

This sample sets taken from the Haltenbanken Area is clearly anisotropic because it can be seen from Table 8 that $C_{11} > C_{33}, C_{66} > C_{44}$, and $C_{12} = C_{11} - 2C_{66} > C_{13}$. For anisotropic rocks, $C_{11} = C_{33}$, $C_{12} = C_{13}$, and $C_{44} = C_{66}$, (Wang, 2002). The five independent elastic constants and the bulk density can be used to calculate the three (one compressional and two shear) velocities as a function of the incidence angle θ as shown below.

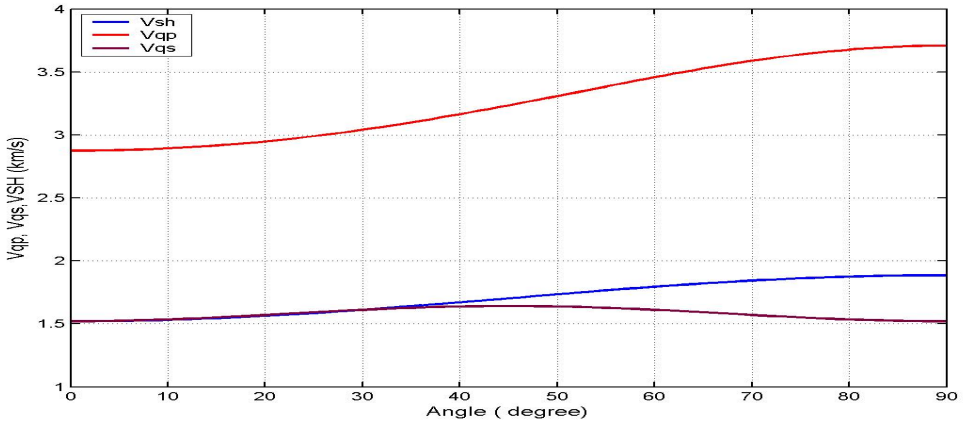

Figure 39: Quasi- P wave (red), quasi –S wave(blue), and Horizontal fast S wave(blue) for sample 6 (from Table 7 and 8). (ε- δ> 0).

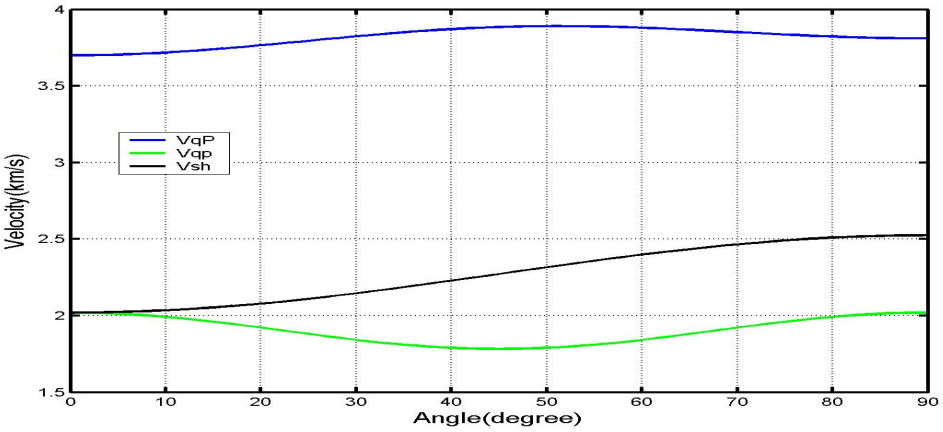

Figure 40: Quasi- P wave (Blue), quasi –S wave (green), and Horizontal fast S wave (black) for sample 4 (from Table 7 and 8). Here the S wave splitting started at 10 degree (ε-δ = -0.14).

Chapter 5

5. Velocity Anisotropy from Well Logs

Introduction

Sonic logs provide ground truth data on formation velocities for seismic imaging and inversion and for generating synthetic seismograms that are used in seismic ties. Where anisotropy is present, deviated well log measurements differ from the expected vertical well log responses. According to Hornby et al (2003) direct or indirect measurement of in-situ shale velocity anisotropy has been difficult to estimate using surface seismic methods, their reasoning is that the sonic tool measures the velocity parallel to the well bore; the measured sonic velocity in deviated wells records the compressional velocity anisotropy present within the shales.

Ultrasonic laboratory core measurement on shale specimens taken from the northern North Sea revealed that the shale exhibit intrinsic and layered anisotropy as explained in the previous chapters. But there many uncertainties and difficulties in ultrasonic laboratory measurement analysis and quantification of shale anisotropy. A valuable and natural alternative to core sample analysis is applied on sonic logs in wells drilled in various deviation angles with respect to the shale layering.

Deviated wells are commonly drilled in producing fields in order to reach distant locations for production or for injection of one fluid to produce another. This common and widely is used technology is used in the North Sea oil fields including the Statfjord Field. For deviated wells in offshore fields velocity anisotropy effects should be corrected for in order to obtain a realistic sonic log response equivalent to seismic data for small incident angles. Rowbotham et al. (2003) showed that correcting for velocity anisotropy significantly improves seismic inversion when data from deviated wells were the control data. Well control is often distorted when the correction for sonic log is not applied, especially for geologic sequences with interbedded shaley layers, highly anisotropic shale layers overlaying either an isotropic reservoir sand layer and dipping strata (large angle bedding dip) where the expected anisotropy effect is large. Hornby et al. (2003) proposed to estimate anisotropy parameters from the sonic logs of differently deviated wells including a vertical well. This method, as well as a simplified version of the method of Rowbotham et al (2003), is based on the assumption that a shale layer is perfectly homogeneous around the wells so that the velocity variation depends only on the deviation angles of the wells.

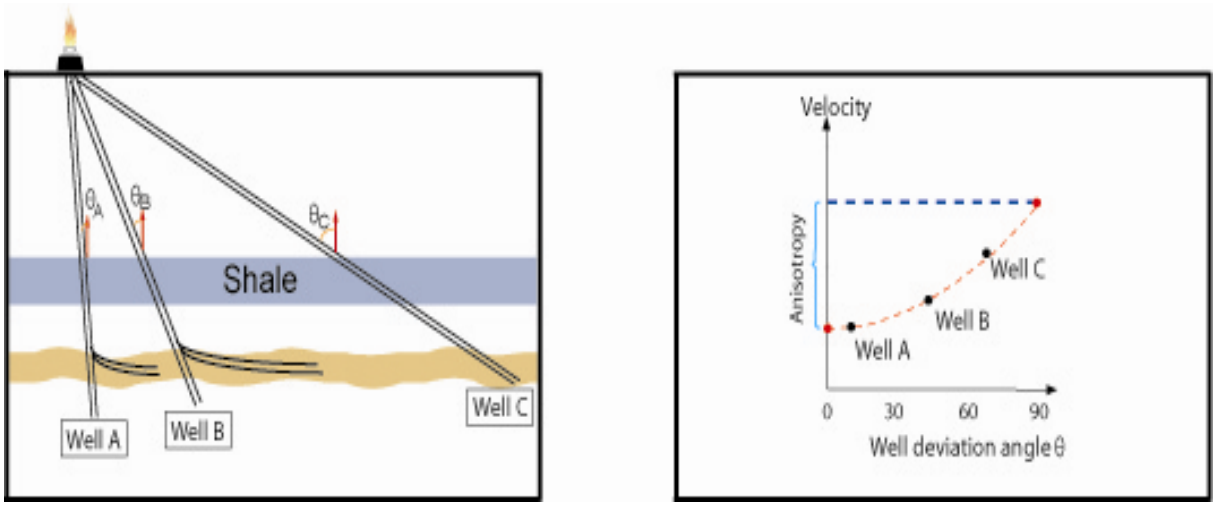

Figure 41: The method for quantification of VTI type seismic and anisotropy in a shale layer illustrated by using wireline velocity logs in three wells A, B, and C drilled at various deviation angles θA, θB, and θC. The velocities in the shale layer as sampled in the three wells (black circles) are plotted versus their respective well deviation angle. To define the shape of the velocity-angle curve (broken red line), wells at several different angles are needed. To estimate the degree of anisotropy, one needs in principle only a vertical and a horizontal well (red circles). (Modified from Brevik et al, 2007).

This chapter consists of two sections: Vertical and deviated well P-wave comparison and Velocity Anisotropy and Velocity versus well deviation angle. The study focus on a simple method for documentation and quantification of layer induced anisotropy in shales based on observation from a set of composite -wire line logs (sonic) acquired in vertical and deviated wells from the Statfjord Field in the northern North Sea. In the first section four well logs (one vertical and three deviated well bores) is used for the comparison of velocity anisotropy. In the second section, two vertical and ten deviated well bores is used to investigate the variation of velocity with well deviation angle.

5.1 Database

More than 160 wells have been drilled on the Statfjord Field. Many of these are within the area affected by gravity failure. According to Hesthammer et al (1999) the area affected by slumping is characterized by anomalous log signatures which can only be explained by extensive and complex deformation. Most of the wells selected for studying velocity anisotropy in the Statfjord Field are far form the deformed area to reduce uncertainties created by the slumping and gravity failures.

The database that has been used in this study consists of wireline logs containing information about compressional and shear velocity, caliper, bulk density, and deep resistivity from both deviated and vertical wells. The wells penetrate three stratigraphic formations. For the precise interpretation the entire well log data set for velocity changes as a function of depth and angle of deviation is used instead of the average values. The deviation angles of the well bores varies from 0 to 85^0. For quality control, log data that were obviously influenced by the logging operation by showing significant deviation from the overall trends, especially at the beginning of the individual logging runs were also removed. This also minimizes problems related to depth measurements. Vertical wells are drilled close to the vertical, and the measured depth is therefore assumed to correspond to the true vertical depth. For the deviated wells measured depth wad related to true vertical depth by the well bore inclination with respect to the vertical axis. Note that complete log data were not always available for all the drilled formations and/or wells especially for the deviated wells.

The compressional and shear wave velocities are assumed to be measured along the well path and represent the effective value at the given well deviation. Sonic velocities together with neutron porosity and gamma ray plots are used repeatedly for lithology identification and selection of shale (pure shale).

5.2 Model Description

Let us consider the simplest and probably most practical anisotropic model a transversely isotropic (VTI) medium with a vertical symmetry axis (Thmopsen, 1986). VTI (also referred to as polar anisotropy) is typically encountered where layer-induced anisotropy is present and where structural dip is small. This often occurs in geological environments with an extensional structural style (rifts for example) and near the crest of structures. The layered VTI equivalent model representation of the Statfjord Field for five formations is illustrated in Figure 42.

The Lower Cretaceous is a strong seismic reflector layer in most of the North Sea area. The Lower Cretaceous has a higher velocity and a lower radioactive signal than the underlying Kimmeridge clay formation, and there are normally strong log break at this boundary as observed in this analysis and published data (Vollset and Dore, 1984). A reduced amount of smectite and/or the transformation of smectite to illite-chlorite in the upper Cretaceous shale layers may also contribute this velocity increase (Storvoll, 2005).

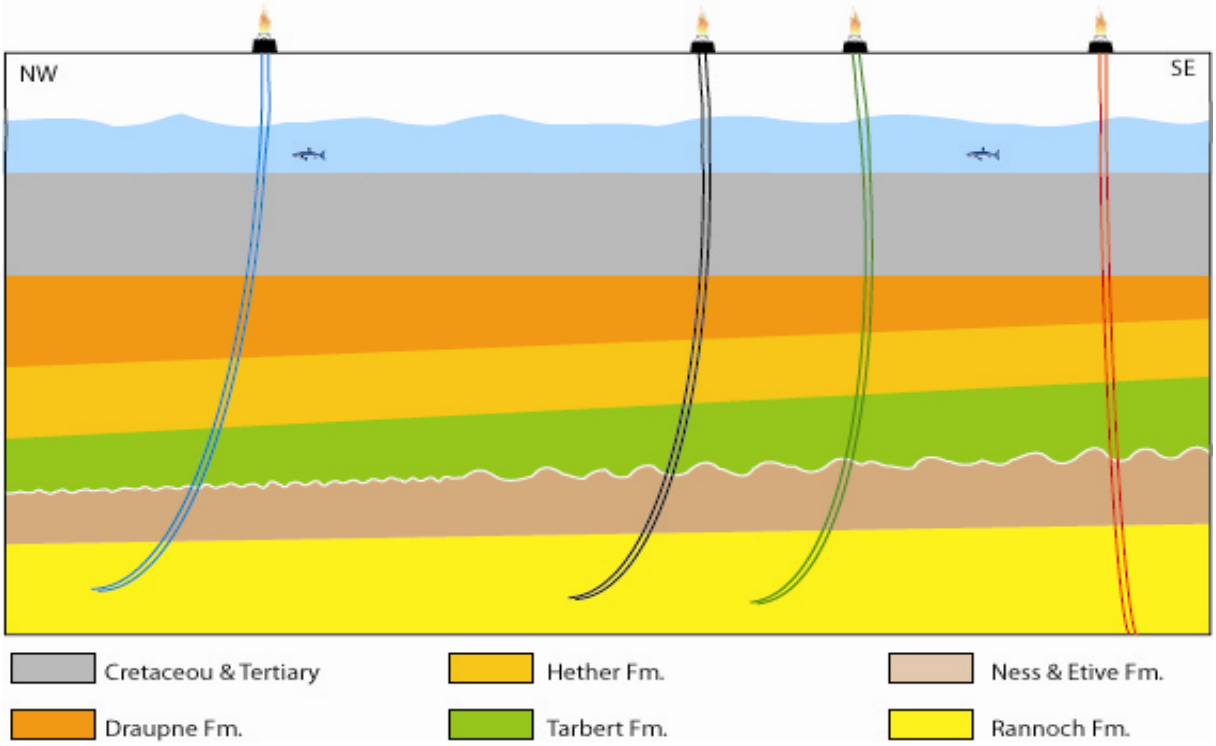

Figure 42: A model figure which represent the equivalent vertically transverse isotropic (VTI) media for Statfjord Field.

The Draupne shale (the hot Kimmeridge clay formation) is defined as having a very high gamma ray response and anomalously low velocity. A gamma ray response of greater than 120 API units is taken to be indicative of the formation. These properties ensure that the boundaries of the formation are normally marked by strong log breaks. The Draupne Formation is considered to be deposited in a marine environment with high organic activity and restricted bottom circulation. On the average this shale is thicker in the SW than NE part of the area. The Heather shale includes about 70 m of shale directly below the Draupne shale.

The recorded P-and S-wave velocities from well logs measurements which penetrates the shale formations are assumed to represent the group velocities as recorded at the group angles (measured along the well path). The dip of the formations (bedding angle with the horizontal plane) on Statfjord area is about 3^0 to 4^0; this is rather small deviation and assumed not affect the result at a seismic scale. If both the bedding (layer) dip and the large well deviation angle add up, this will be a source of error. Due to the dipping beds burial depth of the individual formations will vary across the area and the degree of diagensis and compaction will be as a result also varying in the same formations. Correcting for the effects of dips goes beyond the

purpose of this study and requires information about the 3D seismic volume. Therefore approximate depth (not bedding dip) adjustment is applied during the data analysis to minimize uncertainties when velocity data from vertical and deviated well are compared (Mancini, 2004)

5.3 Results

5.3.1 Velocity Anisotropy from comparison of Vertical and deviated well bores

The data and TIV model of described above applied on four well bores. One vertical and three deviated well bores which penetrates three lithostratigraphic formations in the Statfjord field. The wells names and their location are shown in Figure 43.

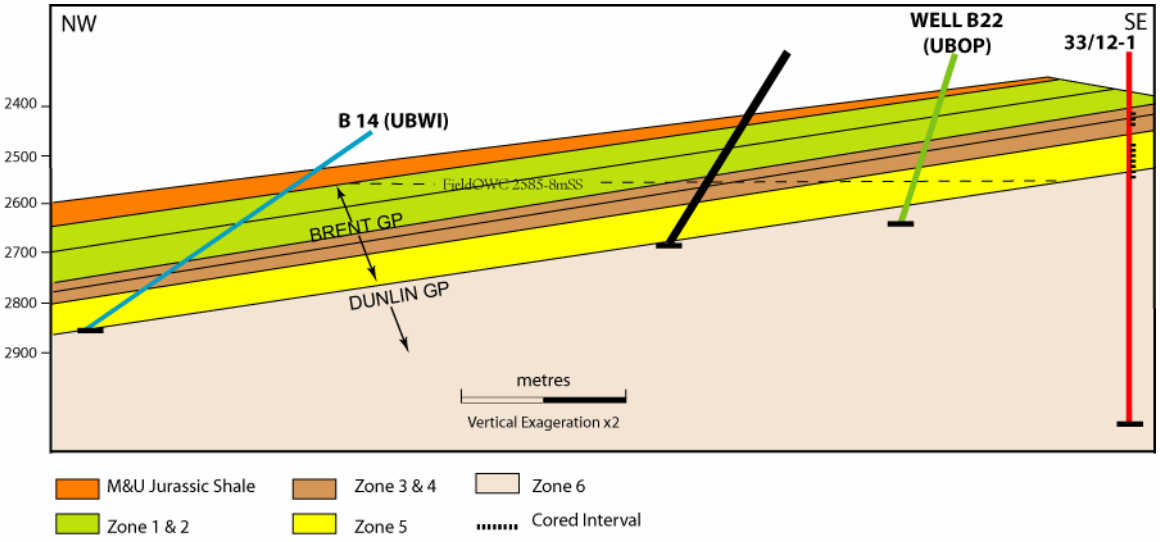

Figure 43: Four wells bore on Statfjord Field Platform B. Well 33/12-1- vertical which penetrated three formations, the other three are deviated wells penetrated two formations. The structural view of the figure is vertically exaggerated two times.

The velocity variation between vertical and deviated well bores is shown on Figure 44 and 45. The observed velocity variation on Lower Cretaceous shales was from 2.5 to 3.4 km/s on the average around 2365 m TVDSS and this velocity increment is accompanied by a dramatic velocity decrement in an underlying Draupne shale in all four well log data sets. When the vertical and deviated well log velocity of the Draupne Formation is compared, the sonic velocity in deviated well documented higher than the vertical (Figure 44). The average velocity is 2.3 km/s on the vertical and 3 km/s on the deviated wells around 2378 m TVDSS. The degree of anisotropy for Heather shale is less than the overly Draupne shale. For Brent Group, the Tarbert Formation gamma ray and velocity logs trends shows a very small

deviation with all wells, this is due to intrinsic isotropic behaviour of the formation. The fluvial dominated but the overall heterogeneity of the Ness Formation in Figure 44 is has a variable gamma ray and velocity profiles observed. The gamma ray response are both complex and characteristically represented by upwards – diminishing patterns over the major sand bodies.

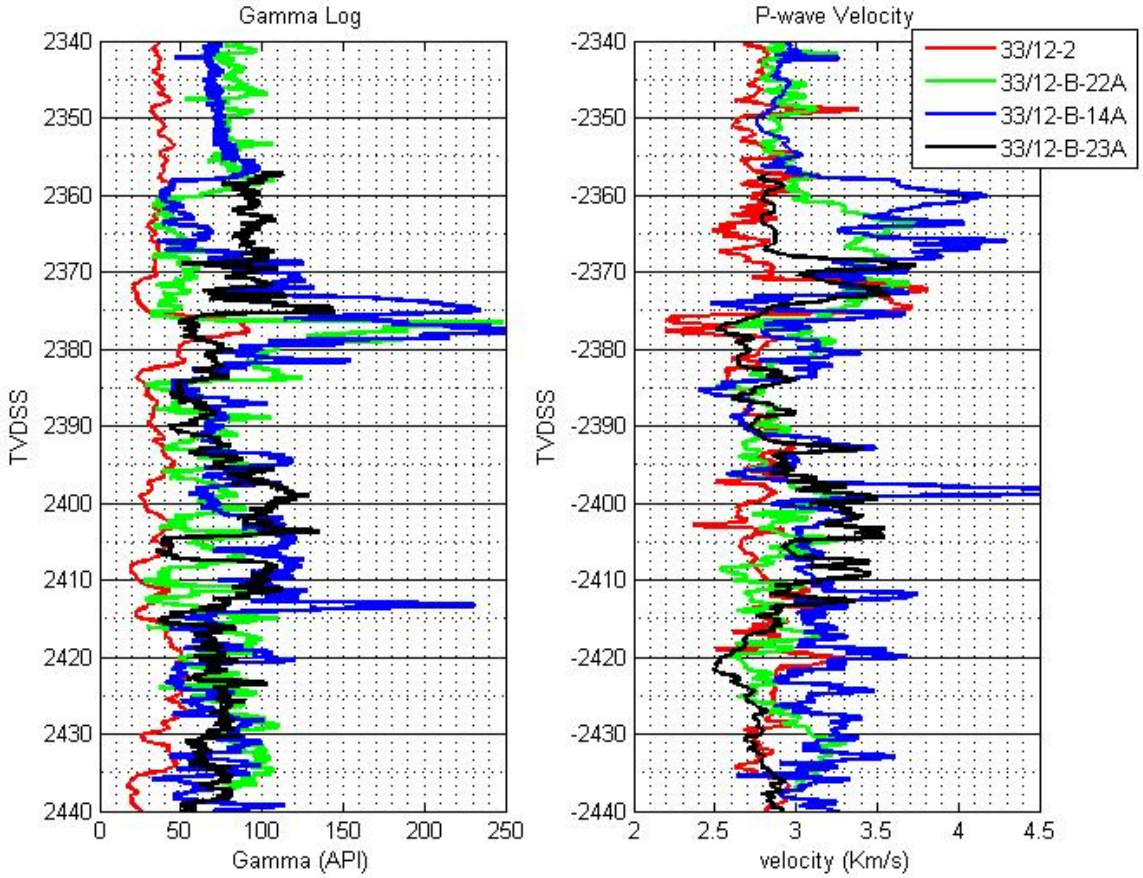

Figure 44: shows four well log gamma and velocity plot. One is vertical (red curve) the other three are deviated (green33/12 - B-22A (~ 53^0), blue33/12 - B-14A (~ 83^0), black33/12 - B-23A (~ 75^0). The results show systematic increase with velocity (decrease in average slowness) with increasing deviation angle for shale Formations.

5.3.2 Velocity versus well deviation angle

In well logs the dependency of the velocity on the angle of deviation has been noted in anisotropic media (Brandsberg-Dahl and Berkved, 2002). In this study a similar approach is used to verify the presence of polar anisotropy in the Statfjord field. In this study pure shale is collected from many well bores from the Statfjord Field. Both vertical and deviated wells are used. The criterion used for selection of shales was their corresponding gamma ray reading (≥ 180 API was considered a shale). The distribution of well log parameters for the selected shale is shown in Figure 45 below.

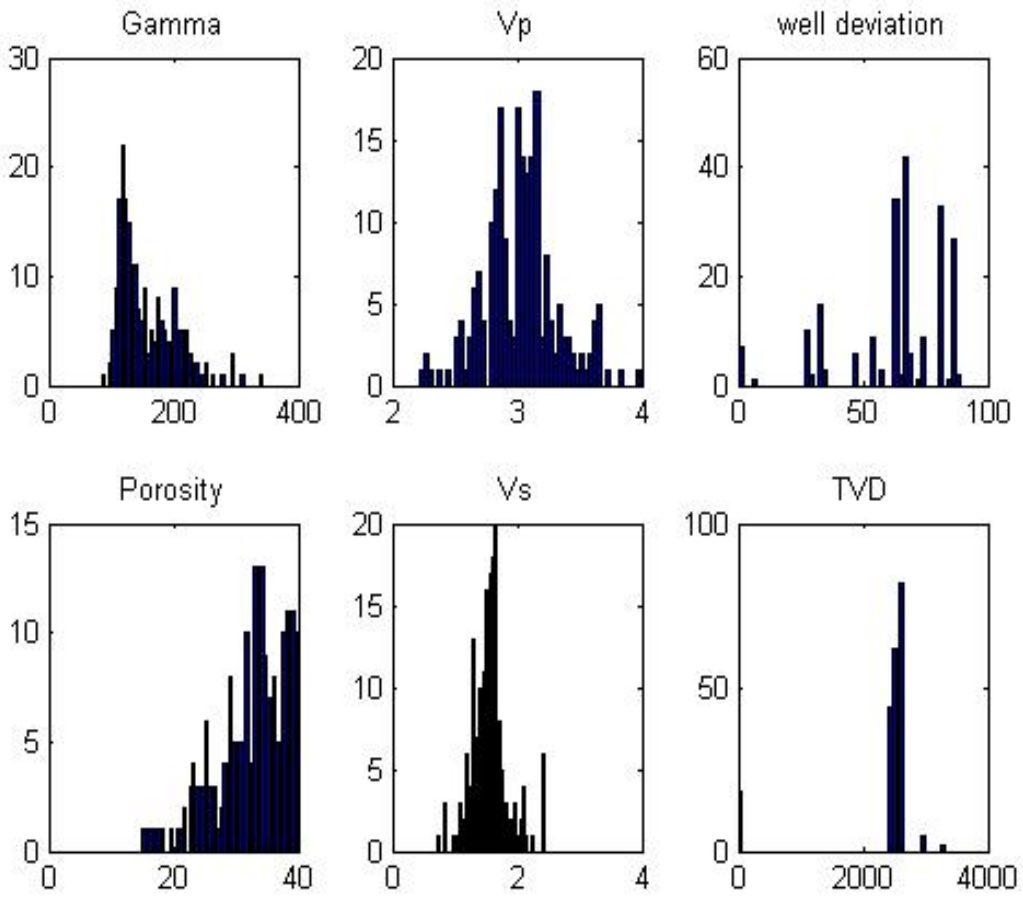

Figure 45: show the distribution of the well log parameters use to select shale from the vertical and deviated wells.

The plot of P-and S-velocity against the angle of deviation from two vertical and eight deviated wells for shale samples are shown in Figure 46. The solid curves (read for P-wave and green s-wave) are the second degree best fit for the velocity versus well deviation angle.

Shales are consisting of clay minerals and the distributions of clay minerals are dependent on factors such as provenance, depositional environment, climate and diagenesis. Smectite, illite, kaolinite and chlorite are the most common clay minerals present in the North Sea area (Pearson, 1990).

Figure 46 shows the P- and S-wave velocity versus with well deviation angle for shale sample taken from different locations in the Statfjord Field area. The general trend is that the velocities increase with an increase in the deviation angle. There is, especially good relation observed between P- and S-wave velocities which appear to increase with the well deviation angle up to 75^{o}. This general trend could be due to that pure shale has a sheet-like structure consisting of clay platelets; this is a natural anisotropy type as long as compaction processes

are acting. Processes of this kind probably lead to a stack of platelets oriented orthogonally to the vertical axis, thereby creating a TIV property (Brevik et al, 2007). On the other hand the velocity versus angle of deviation has showed a slight decrement between 80 and 90^0. The overall velocity anisotropy decrement at these angles may be due to the mineralogical complexity of the Brent Group sands.

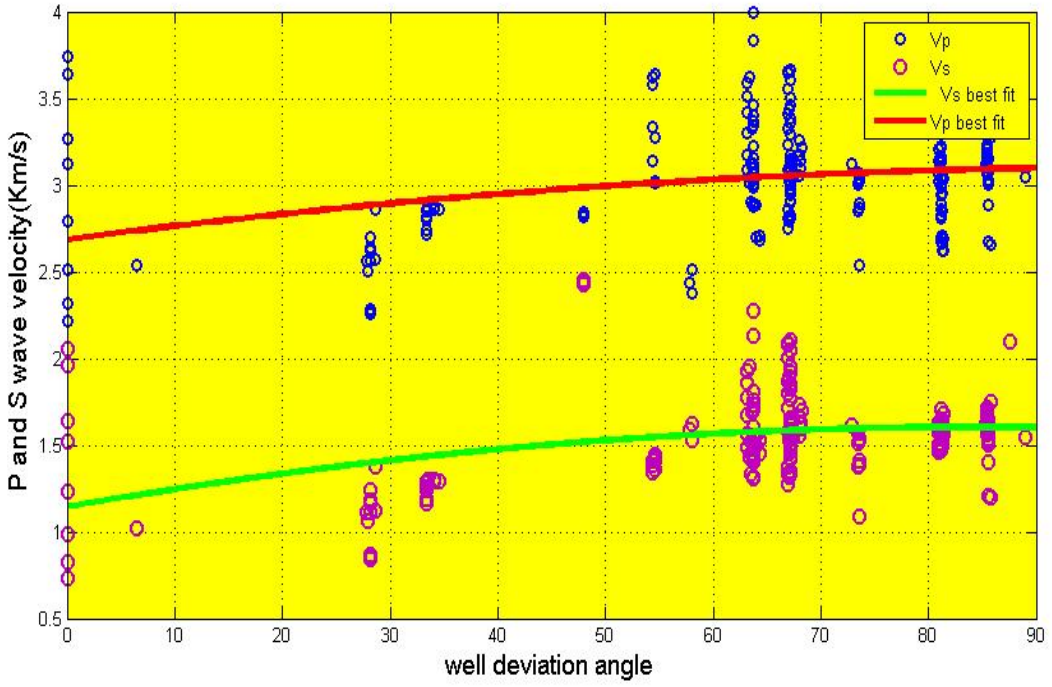

Figure 46: P- and S--wave velocity versus well deviation angle for shale samples taken from different location on the Statfjord Field. Blue dotes stands for Vp and pink for Vs. The data clearly show that the velocity of shales increases with increase of well deviation angle up to ~65-70^0 and after this angle velocity decrease slightly.

5.3.3 Pure shale sample and Anisotropy parameters relation

In this subsection pure shale samples is selected to refine the estimation of formation parameters, to derive a relation between them and porosity and volume of shale. The selection criteria for pure shales were an extension of the first subsection. Here the gamma ray reading of the shale is ≥ 200 API. This step may help to reduce estimation error which could be created from logging tool data selection. The result is displayed in Figure 47.

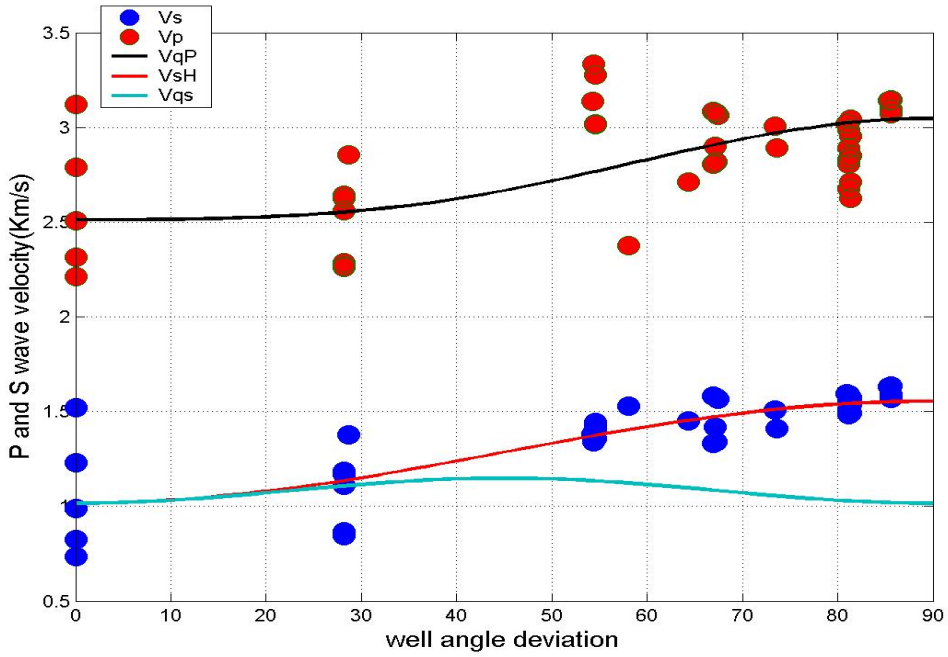

Figure 47: Phase velocity surface for the pure shale sample ($API \geq 200$). Well log shale velocities are shown as dot symbols, calculated velocities are shown as black (Vp), light blue (Vs) and red (Vsh). Note good agreement between calculated fast shear velocity (Vsh) and shear wave well log velocities. The estimated value of anisotropy parameters are ε=0.15, $\gamma = 0.52$ and δ = 0.032.

The formation anisotropy for pure shale sample plotted in Figure 48 estimated for the best fit calculated velocities gives the following parameter values; ε=0.15, γ=0.52 and δ= 0.032. The velocities at a vertical are V_{po}=2.51 km/s, V_{so}=1.006 km/s and the density used was $\rho = 2.4 g/cm^3$. The corresponding stiffness components calculated from these elastic parameters are: $C_{11} = 21.56, C_{33} = 15.12, C_{13} = 10.44, C_{44} = 2.43, C_{66} = 4.52$, all units are in GPa.

5.4 Discussion

5.4.1 Velocity anisotropy from vertical and deviated well bores

Cretaceous shale

A reduced amount of smectite and/or transformation of smectite to illite-chlorite in the lower Cretaceous shales may also contribute to the velocity increase from 2.5 to 3.4 km/s on the average around 2365 m TVDSS. This velocity increment is accompanied by dramatic velocity decrement in an underlying Draupne Formation. The observed velocity contrast between the Cretaceous shale and Upper Jurassic Draupne shale makes the both shale formations easily identifiable seismic units in most of North Sea field (Vollset and Dore, 1984). The likely explanation for the high velocity value of the Cretaceous shale may be that the bound water in smectites is released when smectite is transformed to illite and/or chlorite (Storvoll, 2005).

$$Smektite + K^{+} \rightarrow Illite + Chlorite + quartz + H^{+}$$

$$Koalinite + K - feldspar = Illite + Silica + quartz + H^{+}$$

In the northern North Sea area the transition from smectite to mixed-layer clays and illite-chlorite starts at around 80 ^{0} C, and this temperature corresponds to a depth of between 2 and 2.5 km (Storvoll, 2005). The Cretaceous shales are found at different depths, and show the velocity close to 4 km/s for the highly deviated well (blue curve) and 3.7 km /s for vertical well (Figure 44 and 48).The first and most likely reason for this velocity variation is due to the anisotropic behaviour of the shale. P-wave generally travels faster horizontally, along layers, than vertically for anisotropic shale formations. Besides that the magnitude of velocity anisotropy is high in compacted, low–porosity Cretaceous shale than compared to their high porosity equivalents caused by rearrangement of clay particles.

Draupne shale.

The organic matter (kerogen) and the clay mineral illite commonly occur in lamina in the Draupne source rocks. In rich source rocks (>1–2 % total organic carbon) the lamina commonly form continuous 3-D (three dimensional) networks as illustrated on Figure 49. The illite and kerogen lamina networks are commonly anisotropic with a preferred orientation parallel to the bedding plane. Normally the organic material kerogen in the Draupne shale is quite soft compared to the mineral matrix, illite. In this condition kerogen in the rock will be a

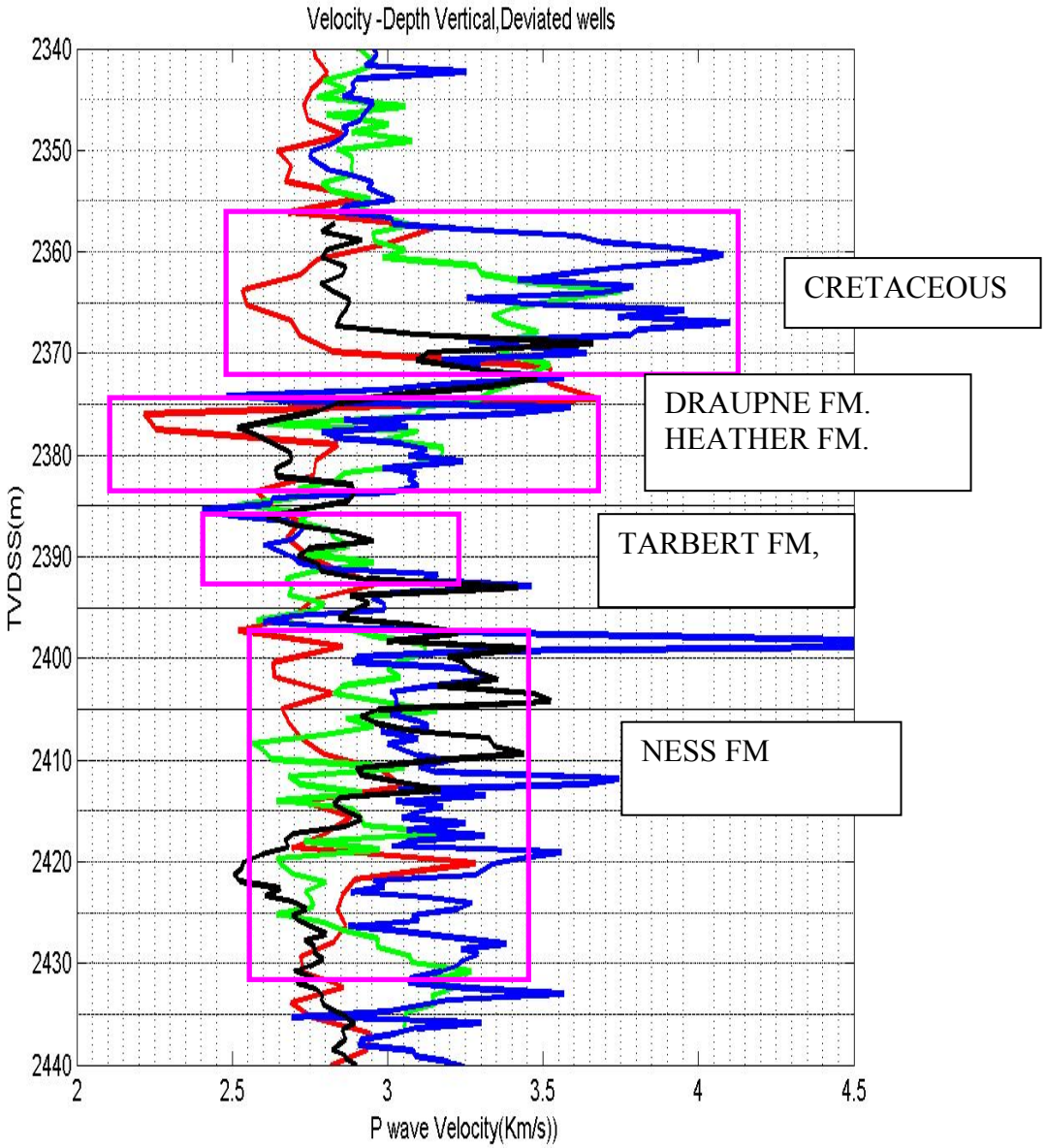

Figure 48: Velocity versus depth for one vertical and three deviated well.

load bearing together with the illite in the rock. This contributes to the strong elastic stiffening in the bedding direction. These factors, together with the sedimentological anisotropy normally found in shales, result in a strong velocity anisotropy where the velocity measured perpendicular to the layering is significantly reduced (Vernik and Liu, 1997).

The other likely reason as explained by many authors is microfracturing in the source rocks. (Vernik and Liu, 1997). Because of the laminar occurrence of kerogen in the source rocks, fractures or low aspect ratio pores parallel to the bedding may be generated when solid

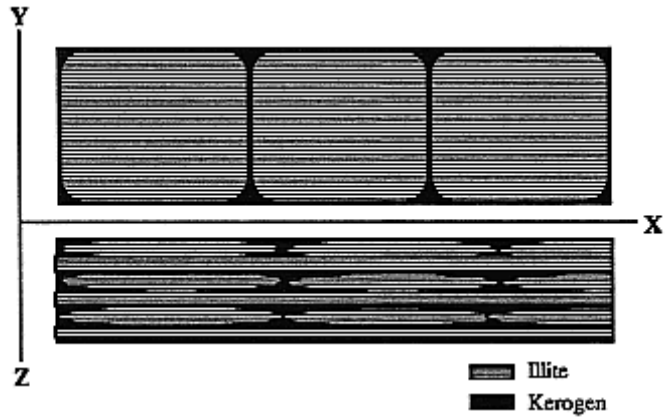

Figure 49: Schematic fabric topology of kerogen-rich (K > 0.15) shales showing discontinuity of some of the clay (illite) layers separated by kerogen in X Y plane. Z-direction corresponds to the symmetry axis (Vernik and Nur, 1992).

kerogen is transformed into hydrocarbons, also enhancing the anisotropy. When hydrocarbon is generated and expelled from the source rock, the illite/kerogen supported structural matrix will collapse and micfractures will develop. The fractures reduce the rigidity and enhance the anisotropy of sedimentary rocks and may be contributing to the low velocities observed in the source rocks.

Heather shale

The offshore marine silty deposited shale the Heather Formation has also showed velocity anisotropy when the velocity in vertical and deviated sonic well logs are compared at different depth for the same lithological level. The degree of anisotropy in the Heather shale is less than the Draupne shale above because of the presence of silt which affects the alignment of the

Figure 50: A) Core picture of Draupne shale drilled from well 33/9-A-37B. The picture shows the alternating lamination of Kerogen (black stuff) and Iillte (brown) layers and it logical to assume Draupne shale is VTI. The black shale is also observed in this picture.
B) ***Heather shale core picture taken from well 33/9-11 at the depth around 2.45 Km. It shows small lamination in some part of the sample.***

clay platelets in the sheet like structure in the bedding plane and also the small content of organic matter. The velocity varies between 2.75 km/s for vertical well and 3.25 km/s for highly deviated well. Heather shale acts as a transverse isotropic cap rock for the underlying hydrocarbon bearing Brent Group sandstone reservoir found in the Tarbert Formation. The measured anisotropy properties of this shale will help to the correct anomalous of AVO signature and migration. If this cap rock is assumed to be isotropic, a different AVO response is expected in the Tarbert Formation, and the sand might not be identified as an oil bearing reservoir. The effect on overburden shales on a reservoir unit will be discussed in the next section together with detailed numerical examples.

Tarbert Sandstone.

The Tarbert Formation gamma ray and velocity logs trends shows a very small deviation in all wells, this is due to intrinsic isotropic behaviour of the formation. It is one of the good hydrocarbon reservoirs in the Brent Group. As shown in the lithostratigraphic column of Brent Group in Figure 51, the Tarbert Formation is often defined by a sharp-based coarse- to very coarse-grained sandstone interpreted as a transgressive lag deposit (a transgressive phase in which the delta and the barrier sediments have been reworked)(Vollset and Dore, 1984). Overlying bioturbated coarse sands, in turn succeeded by fine grained micaceous sands resembling the storm–laid Rannoch shoreface sands lower in the sequence.

. The Tarbert Formation shows a range of compositions ranging from pure quartz to complexes of minerals, similar to those of Ness sands. Some sands contain more mica than is found in the Rannoch Formation. The matrix density values of these sands lie in the range of 2.65-2.8 gm/cc. The resultant variability in the sediments mineral composition and fabric gives rise to a very wide range in pore size distributions and grain size geometries.

Ness Formation

The fluvial dominated Ness Formation seen Figure 51 is heterogeneous and has a variable gamma ray profiles. The gamma ray responses are both complex and characteristically represented by upwards–diminishing patterns over the major sand bodies (= channel fills). The Ness Formation is the most mineralogical complex interval within the Brent Group (Morton, 1992). The Ness Formation comprises with many different environmental settings found on the delta plain e.g. interbedded sandstones, siltstones, mudstones and coals.

The sediment deposited on the proximal part of the over banked delta Ness Formation resulted mineralogical combination of clay silt mudstone, sandyshale. The orientations of the

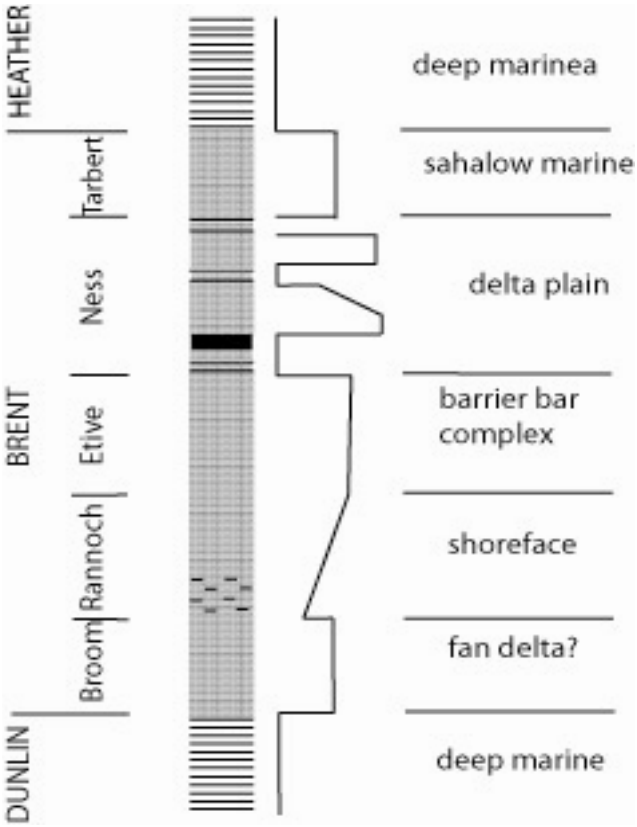

Figure 51: Stratigraphic of Brent Group modified from Harris (1992).

clay mineral is weak which is showed as a general decrease in velocity anisotropy at large well deviation angles. The detailed explanation for this slight anisotropy decrease needs further study on SEM, XRD and other methods which can give supplementary information about the intrinsic anisotropy behaviours of the shale sample.

The lower formation of the Brent Group such as Etive, Rannoch and Broom Formations of was not indicated on Figure 48. The upper part of Etive has a similar depositional environment as the Ness Formation. The Rannoch and Broom Formations are calcite cemented sandstones, where the cementation effect reduces intrinsic isotropy. For example in the previous chapter (chapter 4) a core samples from the Gullfaks area only a very small velocity anisotropy was found for Broom Formation.

Anisotropy well log

The P-wave anisotropy for the four wells used in Figures 48 predicted using the method established by Li (2002). The anisotropic well log can be predicated from the sonic log and clay volume.

The predicated well log (Figure 52) showed that the maximum anisotropy is found in the Draupne shale for all four wells. The value of the predicated P-wave anisotropy ($\varepsilon \approx 0.3$) was larger in well 33/12-B-23A, which was deviated an angle of 75^0. The minimum predicted anisotropy was observed on the vertical well ($\varepsilon \approx 0.1$). For the Brent Group sandstones the predicated P-wave anisotropy are approximately equal to zero.

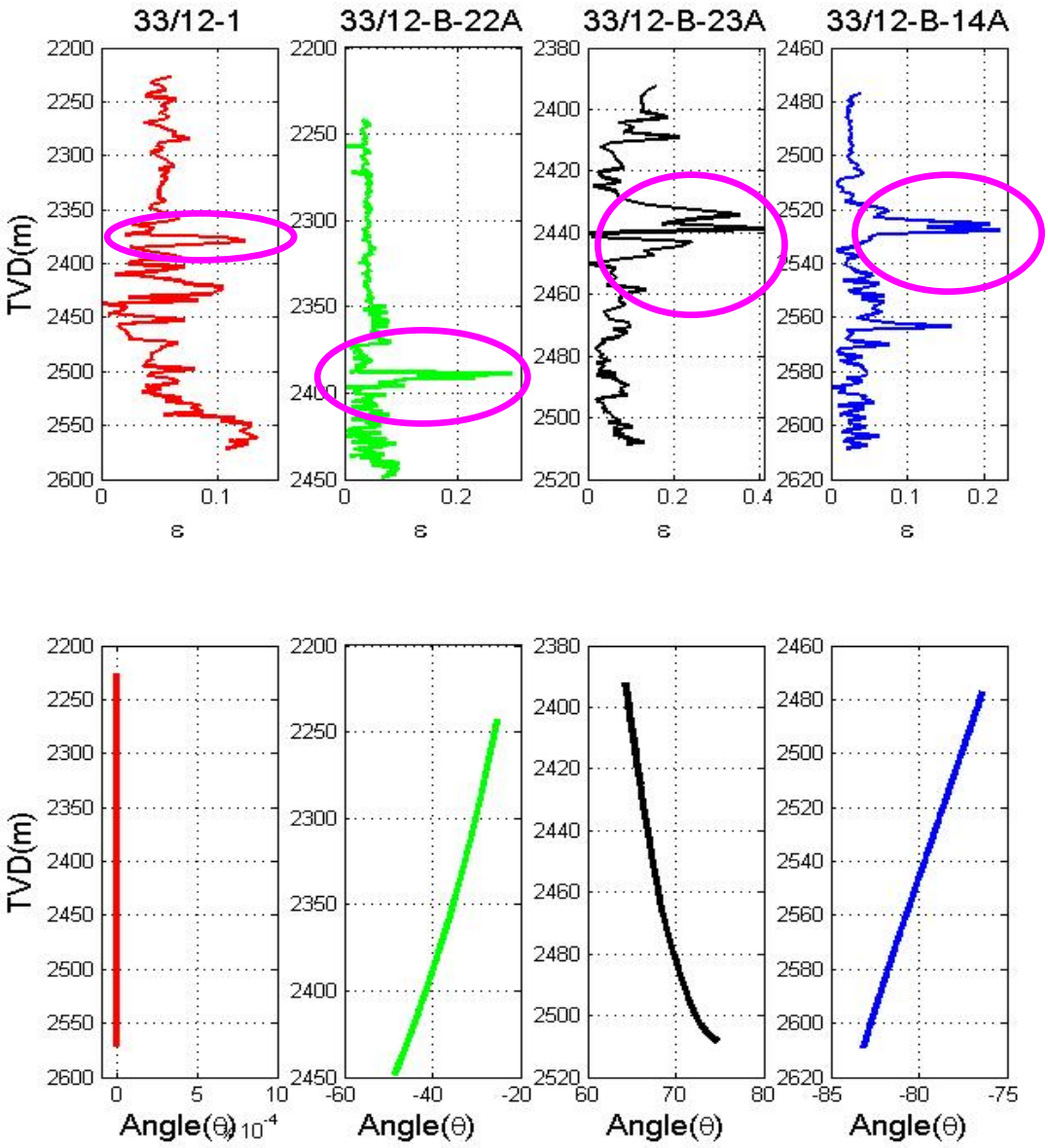

Figure 52: The predicated P wave anisotropy well the four wells. The anisotropy well log is derived from the Volume of shale and P-wave velocity (top). The well deviation angle for the four wells (bottom).

5.4.2 Velocity versus well deviation angle

Factors affecting velocity and anisotropy in shales include stress state, stress history, smectite content, organic content, microstructure and physicochemical interactions with pore fluids (Vernik and Liu, 1997). It is difficult to know all these parameters in situ.

For discussion purpose this study classifies the observed velocity anisotropy in to two: a good correlation of P-and S-wave velocity up to 75^0 well deviation angle and slight decrements in velocity anisotropy after 75^0 well deviation angle. The likely explanations are given as follows:

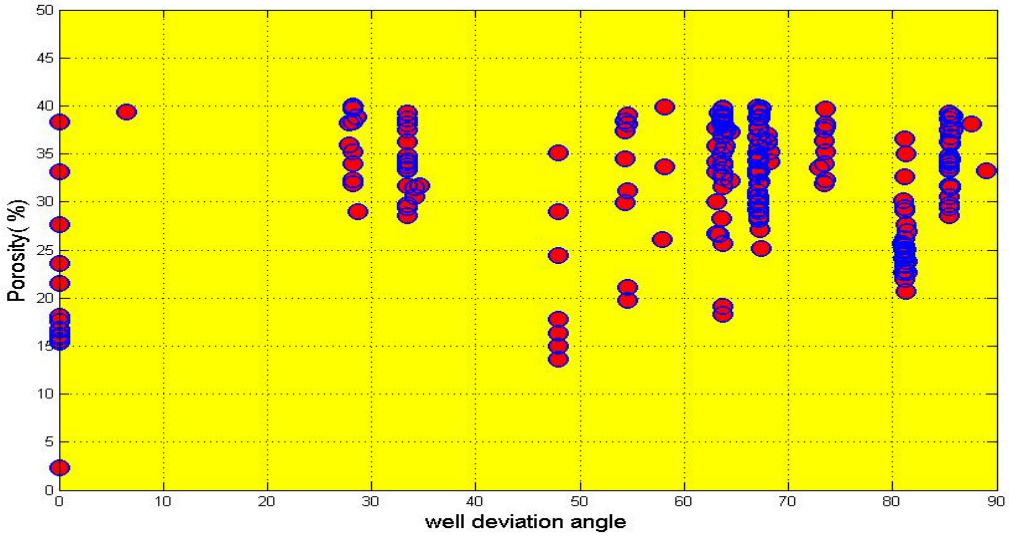

Figure 53: Corresponding values in pure shales of porosity and well deviation angle in all formations at the Statfjord Field. In the vertical well the porosity varies from 5 to 40 %, where as in the scattered decreased for deviation angle more than 30^0 and all having between 15 to 40 %.

The first is that, as shown in the distribution histogram in Figure 45, most of the selected shale samples were taken from an intermediate depth (2-2.5 km). At these depths in the North Sea mechanical compaction will have a more important role than chemical compaction for alteration of the rock properties. Shales without calcite or quartz cement are subjected to mechanical compaction down to a burial depth of 2-3 km (Bjørlykke and Høeg, 1997). Mechanical compaction increases the anisotropy of the clay structure of uncemented sediments, as initially more randomly orientated particles become more horizontal and parallel with increasing effective vertical stress (Nygård et al, 2004). The role of chemical diagenesis has the effect of reducing porosity without significantly affecting the orientation of the particles, i.e. chemical diagensis appears to reduce the spacing between particles but do not cause particle reorientation. (Nygård et al 2004). What observed in Figure 53 is that no

significant reduction of porosity can be detected. Then the observed general increase in anisotropy for the selected shale samples may be mostly related to mechanical compaction compared to chemical compaction. With increase compaction, clay minerals tend to align in the direction perpendicular to the overburden. The observed velocity anisotropy on the selected shale samples of this study is due to the preferred mineral orientation of the clay particles (Liu, 1994, Johnston and Christensen, 1995).

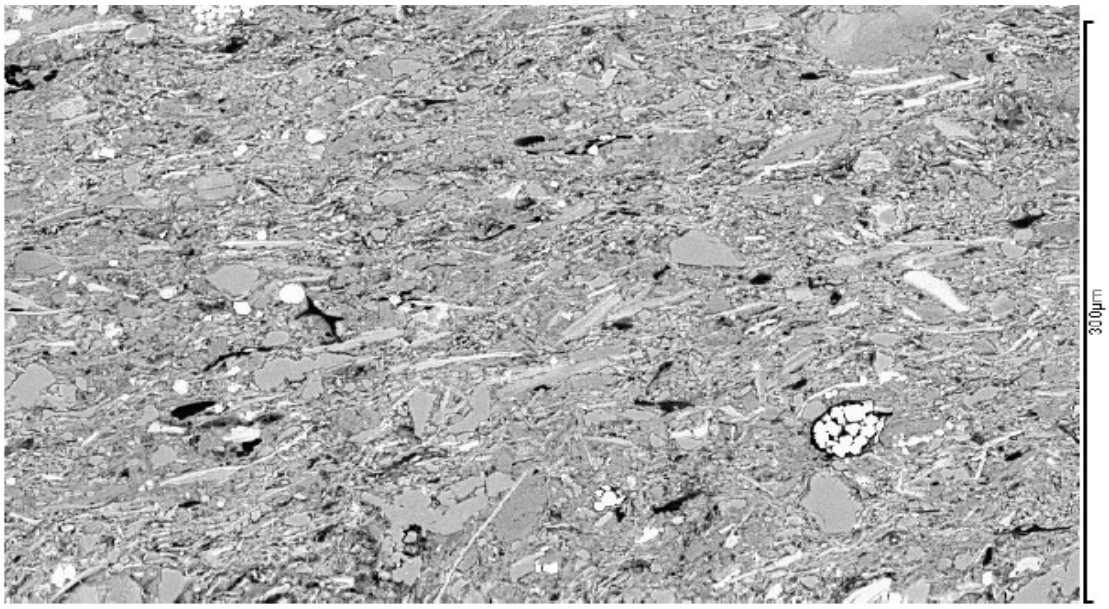

Figure 54: Scanning electron microphotograph) of North Sea shale sample came from the Statfjord Field at: 2451.75 m. TVD. The platy particles are clay minerals while the larger particles are silt, quartz, mica and some pyrite (the photo was taken from Per Moe, 2006).

The second reason is that, any presence of rounder quartz particles leads to deviations from this pattern, for example in Figure 46 up to 75^0 the anisotropy was decreasing slightly. The explanations for the observed velocity anisotropy decrement may be due to physical and chemical processes which have an effect on the alteration of the rock properties. Some of them are describe below:

The clay minerals and its compositions. Clay minerals make up the connected skeleton of the shale and are thus the load-bearing phase. Other minerals, most notably quartz in the form of silt, exist as isolated particles and do not form a connected phases even at relatively high concentrations. Accordingly, these isolated constituencies contribute less to the overall elastic properties of the composite. An example the inclusion of minerals on clay is shown on Figure 4.

The clay platelets seen in Figure 54 show an overall horizontal orientation, however, there is some local disorder or misalignment, with respect to the vertical symmetry axis. This misalignment appears to be controlled largely by the silt. The bedding of the clay platelets tends to drape the larger rounded inclusions. A SEM image from Hornby et al (1994) illustrates that alignment of clay minerals in a shale sample is affected by silts-sized particles.

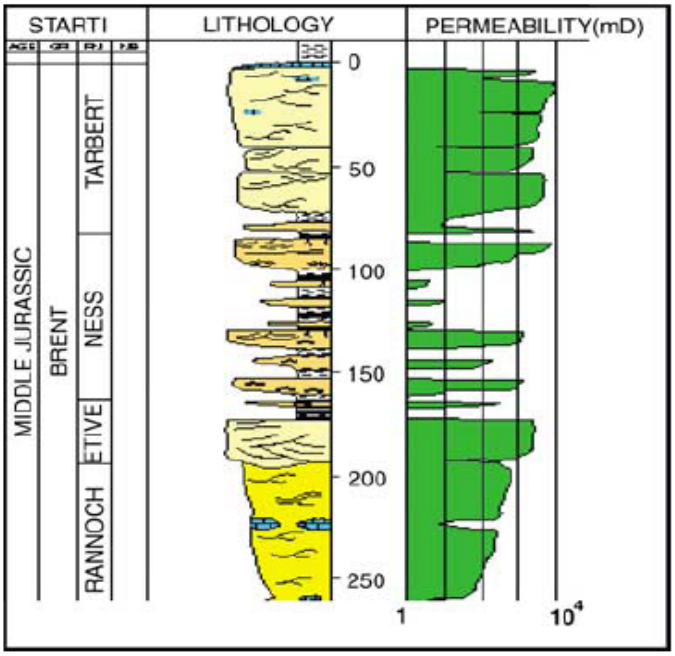

Figure 55: shows the lithostratigraphic section of the Brent group. The Ness Formation has a heterogeneous lithology. Brent Group sandstones typically display wide ranges in porosity and permeability correlated with differences in depositional facies (petrologically expressed principally by variations in grain size and quartz content (Ehrenberg, 1997).

The second is may be related with the effect of external geological processes on the sediments As explained earlier the distributions of clay minerals are dependent on factors such as provenance, depositional environment, climate and, diagenesis. In the Brent Group at the Statfjord Field, the dominant clay mineral is kaolinite (Harris, 1992). The amount of Kaolinite obtained from thin section from type the well 33/12-1 was 80-85 % (Glasmann, 1992). Bjørlykke and Brensdal (1986) have argued that kaolinite at Statfjord Field formed during meteoritic leaching. The Kaoline in the Statfjord is has origin of detrital clay (derived from the mechanical break down of prexisting rocks by weathering and erosion) and authigenic clay (minerals or mineral grow in place with the rock). The clay mineral is mostly detrital which is a result from the dissolution of feldspar and precipitation of kaolinite. Bjørlykke et al (1992) indicated the formation of secondary porosity at shallow burial depth

due to dissolution of feldspars and precipitation of authigenic kaolinite are important features of Brent Group. The secondary porosity comprises 2-7 % of the total rock volume for many fields including the Statfjord Field (Bjørlykke et al, 1992).

The two main reactions which show the dissolution of feldspar and mica and precipitation of Kaolinite as given by (Bjørlykke et al, 1998)

$$2K(Na)AlSi_3O_8 + 2H^+ + 9H_2O = Al_2Si_2O_5(OH)_4 + 4H_4SiO_4^- + 2K^+(Na^+)$$

Feldspar water Kaolinite dissolved silica ions

$$2KAl_3Si_3O_{10}(OH)_2 + 2H^+ + 3H_2O = 3Al_2Si_2O_5(OH)_4 + 2K^+$$

Mica water Kaolinite ions

The characteristic development of secondary porosity and the abundance of kaolinite in the Brent Group are therefore probably related to the depositional environment. The presence of authigenic clays will fill the pores. The pore filling diagenetic processes reduces the net grain alignment and/or the preferred pore orientations which results in decreased anisotropy. Then decreasing feldspar is related to dissolution of feldspar and alteration of feldspar to clay.

A quantitative example of the influence of feldspar on anisotropy was illustrated by (Koesoemadinata and McMechan (2004). What they assumed was that the calcite cement and kaolinite are derived from the feldspars; the expected decrease in feldspar content was used to correlate with the increasing sum of calcite cement and clay (kaolinite).

$$A = -0.743(clay) + 19.262$$

$$A = -0.586(clay + calcite) + 22.594$$

where A is degree of anisotropy coefficient, clay is the volume of fraction of clay and calcite is the volume fraction of calcite if it is resulted from the feldspar dissolution. Anisotropy decrease when the authigenic clay and calcite increases.

The third point may be due to the permeability anisotropy. In the lithostratigraphic column of the Brent Group shown in Figure 55, the permeability is indicated by the green colour. For the Ness Formation the permeability is very small due to a variable lithology. The decrease in permeability (low permeability) has an effect on decreasing the velocity anisotropy. This may be most likely associated with the net reduction of the grain alignment or preferred pore orientations by the increase of calcite cementation and pore-filling kaolinite. The low permeability may be due to complete or partial leaching of feldspar. If the leaching is complete the resultant void space either remains open or acts as the precipitation site of later

phases. If these voids remain open, such secondary porosity can give rise to highly porous but poor permeable sands.

Analytical Quantifications of the observed velocity anisotropy

Following Thomsen's (1986) approximation for weak anisotropy, the angle dependency of the P-wave and vertical and horizontal shear wave S wave Phase velocity can be expressed as:

$V_p(\theta) = V_{po}(1 + \delta \sin^2\theta \cos^2\theta + \varepsilon \sin^4\theta)$, The P wave phase velocity

$V_s(\theta) = V_{so}(1 + \gamma \sin^2\theta)$, The fast shear wave phase velocity

$V_s(\theta) = V_{so}(1 + \sigma \sin^2\theta \cos^2\theta)$ The slow shear wave phase velocity

where θ is well deviation angle, V_{po}, V_{so} are P- and S-wave velocity in the vertical direction, ε, γ and σ are dimensionless formation anisotropy parameters. On the other hand if the angle of deviation and vertical P- and S-wave velocities are known in advance, it is possible to use the above three equations to extract estimates of δ, ε and γ by applying a simple best fit the Thomsen's curve.

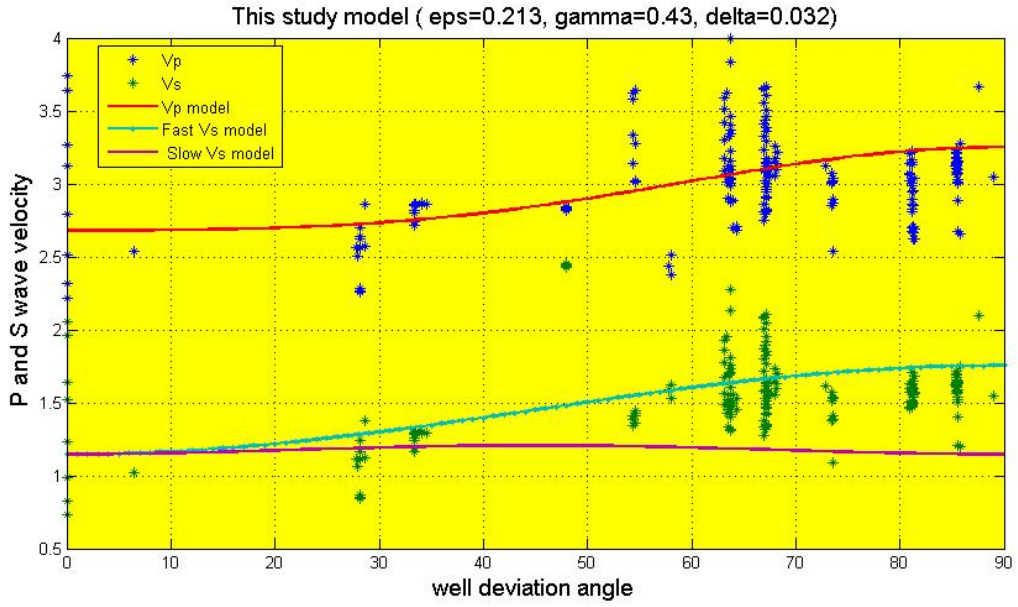

***Figure 56: shows the Best fit phase velocity model for pure shale estimated by regression method and the predicted formation anisotropy parameters are:* ε=0.213, γ=0.43 and δ= 0.032.**

The estimated formation anisotropy parameters for pure shale sample plotted on Figure 56 is to the order of ε=0.213, γ=0.43 and δ= 0.032. The velocities at vertical are V_{po}=2.7

km/s, V_{so}=1.25 km/s and the density used $\rho = 2.4 g/cm^3$. For a VTI media if five elastic parameters V_{po}, V_{so} δ, ε and γ are known, then the five stiffness constants can be calculated by the formulae (Liner and Fei, 2007).

$C_{11} = (1+2\varepsilon)\rho V_{Po}^2$,

$C_{33} = \rho V_{Po}^2$

$C_{13} = \rho[(V_{po}^2 - V_{So}^2)(V_{Po}^2(1+2\delta) - V_{So}^2)]^{1/2} - \rho V_{So}^2$

$C_{44} = \rho V_{so}^2$

$C_{66} = (1+2\gamma)\rho V_{so}^2$

The corresponding stiffness components calculated from the above equation are: $C_{11} = 24.9$ $C_{33} = 17.5$, $C_{13} = 10.6$, $C_{44} = 3.75$, $C_{66} = 6.9$, all units are in GPa.

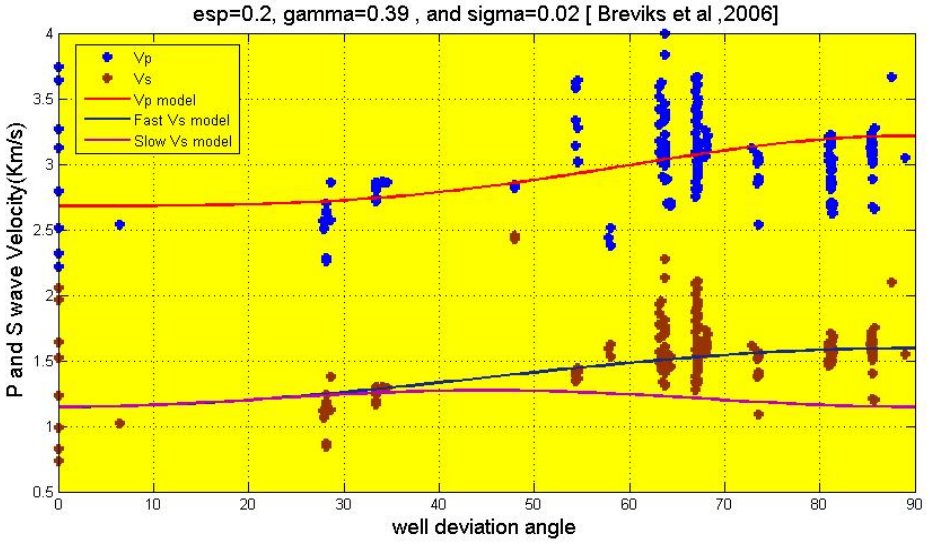

Figure 57: Phase velocity surface for shale sample ($API \geq 180$). Well log shale velocities are shown by blue dots_(Vp) and brown dots_(Vs), , the corresponding calculated velocities are shown as solid lines red (Vp), light brown(Vsv) and green (Vsh). The calculated velocity model formation parameters (ε = 0.2, γ=0.39 and δ= 0.02***, taken from Brevik et al, 2007).***

From these five independent stiffness constants and $C_{12} = C_{11} - 2C_{66}$ the shale data analyzed here is anisotropic. For anisotropic rock, the stiffness constants hold the relation: $C_{11} > C_{33}$, $C_{66} > C_{44}$, $C_{12} > C_{13}$ (Wang, 2002).

To evaluate the method employed in this study, the estimated formation anisotropy parameters were compared with previously estimated and published values from the North

Sea. The values of the elastic parameters showed a good correlation with published data especially with a recently published paper by Brevik et al (2007) on North Sea shale. This article discussed a study using a large number of wells from two producing fields. The method they used was similar with the one used in this study, i.e. documentations and quantification of velocity anisotropy with the corresponding estimation of the formation anisotropy parameters by comparing velocity data from vertical and deviated wire line logs. For one specific formation, their method estimated the anisotropic parameters as ε = 0.2, γ = 0.39 and δ= 0.02 and the elastic constants $C_{11} = 27.1, C_{33} = 19.4, C_{13} = 12.0$, $C_{44} = 3.9$, $C_{66} = 6.9$ (all value are in units of GPa).

5.4.3 Purse shale

From Figure 47, P-wave velocity showed scatter of data points at higher angle of deviation, but it is small as compared with the previous anisotropy analysis (Figure 46). The scatter of the data points may be due to the mineralogical complexity of the upper part of the Brent Group. The S-wave velocity a good agreement is observed between calculated fast shear velocity (Vsh) and data points of well log velocities.

The correlation between calculated fast S-wave velocity and data points can be explained two ways. When S-wave passes through anisotropic medium, the shear wave will be splitting in the fast and slow S-wave. But hear the selected shale has less degree of anisotropy at high well deviation angle, and this is observed also on the P-wave. The second explanation may support the suggestion given by Tsuneyama and Mavko (2005), i.e. for S-waves, when the well deviation exceeds 50°; the logging device measures *Vs* horizontal, which is the fast *Vs* in this angle range. Then the Thomsen's approximation equation for the correction of *Vs* horizontal is as follows:

$$V_s(\theta) = V_{so}(1 + \gamma \sin^2 \theta),$$

Estimated formation anisotropy parameters collected from published articles on North Sea shales is given in Table 9.Velocity models calculated from these data sets plotted together with the result from this study is shown in Figure 58 ,59 and 60. The purpose of these comparisons was to investigate the range of ε, γ and δ and also to get additional evidence on the role of ε and δ at small and large well deviation angle. Five out of six P-wave velocity (Vp) curves almost were overlap each other up to 30^0 well deviation angle, since the contribution from the extra term($[(1 + \delta \sin^2 \theta \cos^2 \theta + \varepsilon \sin^4 \theta]$) on the vertical direction was very small. After 30^0 the contribution of the extra term showed deviation between each of the

curves. These deviations mainly came from the different value of ε. At small angle of incidence the wave propagation is not very much affected by anisotropy, but at large incidence angles (far offsets) the contribution of anisotropy is big and correction for this anisotropy is recommended for reliable subsurface seismic imaging.

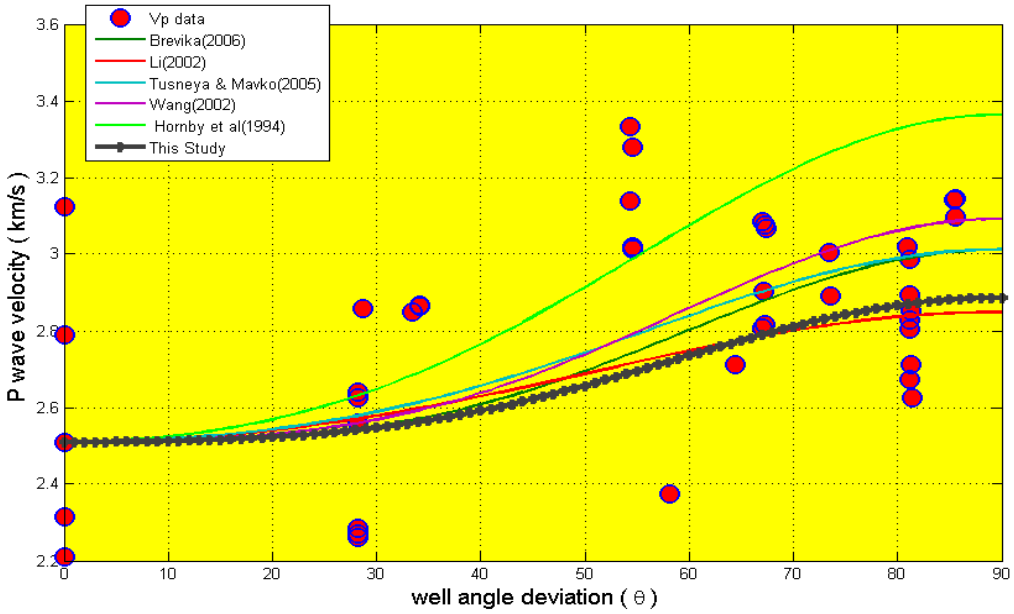

***Figure 58**: P wave Phase velocity surface for the pure shale sample. Well log shale velocities are shown as dot symbols together with six calculated velocities. The formation anisotropy parameters (ε and δ) for the calculated velocities were taken from published articles on North Sea shale data (Table 1). A good correlation is observed between this study and Li (2002). The estimated value of anisotropy parameters are ε=0.15, and δ = 0.028.*

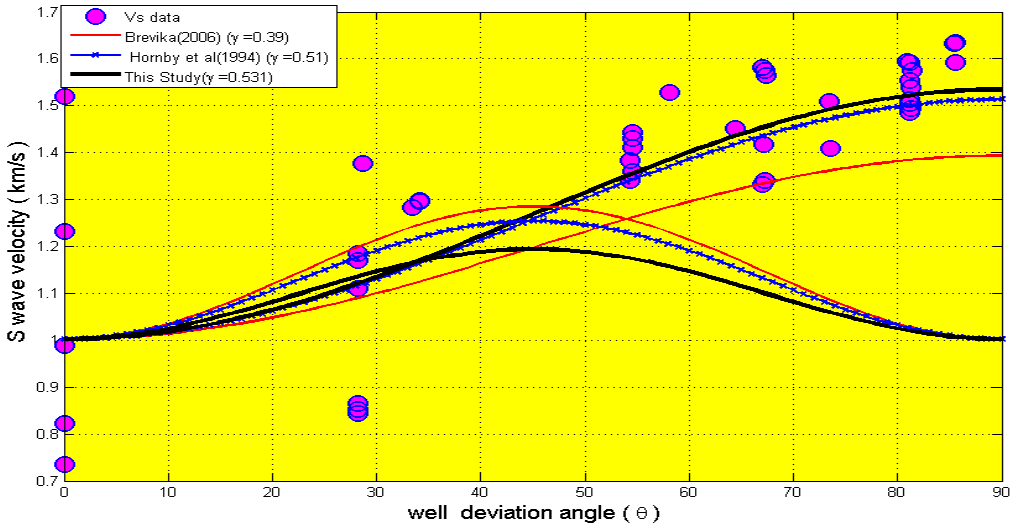

Figure 59: The fast (Vsh) and slow (Vsv) S wave Phase velocity surface for the pure shale sample. Well log shale velocities are shown as pink dots symbols together with three calculated velocities. For the calculated velocities were taken from published articles on

North Sea shale data (Table 1). A good correlation observed this study and Hornby (1998). The estimated value of anisotropy parameters are ε=0.15, γ=0.531 and δ = 0.028.

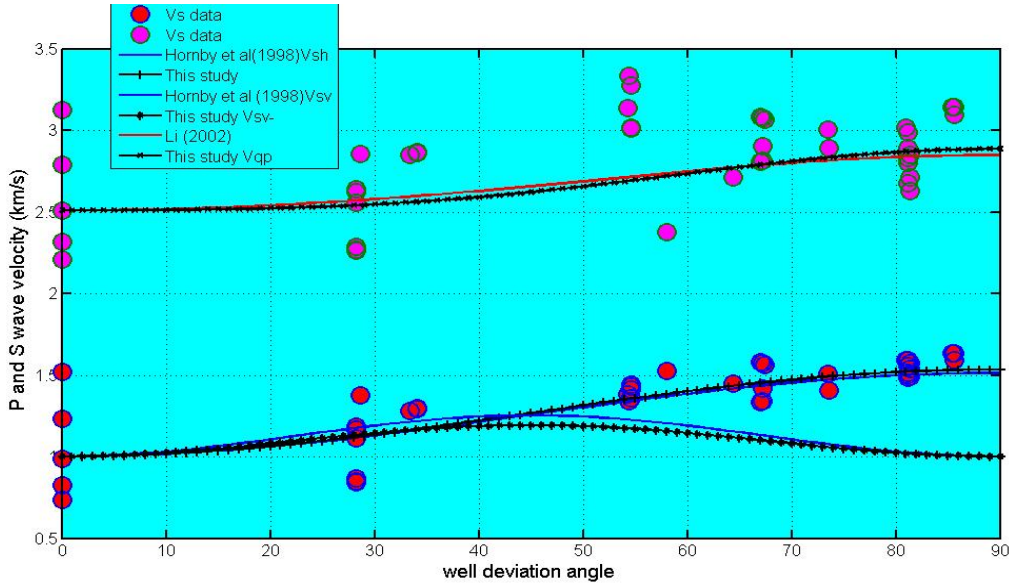

Figure 60: Phase velocity surface for the pure shale sample (dots) and calculated velocities. A good correlation observed this study and Li (2002) for Vp and Hornby (1998) for Vsh. The estimated value of anisotropy parameters are ε=0.15, γ = 0.531 and δ = 0.028.

Table 9: North Sea shale formation parameters (Thompsen parameters) from published articles.

Authors	*Data base*	ε	γ	δ
Li, (2002)	*VSP*	*0.135*	*0.153*	0.0432
Brevik et al(2007)	*Well log*	*0.200*	*0.390*	0.020
Tsuneyama and Mavko (2005)	*Well log*	*0.200*	*0.210*	0.100

Wang (2002)	*Core sample*	*0.232*	*0.226*	0.046
Hornby et al(1994)	*Kimmeridge hot shale*	*0.340*	*0.510*	0.180
	Jurassic shale	*0.230*	*0.380*	0.090
Vernik & Liu (1997)	Brine saturated shale (2.1 km)	0.290	0.420	-0.090
		0.240	0.220	0.020
This study	Dry sample1(4.4 km) Well log (Statfjord field)	0.150	0.531	0.028

5.4.4 The relationship of P-and S-wave anisotropy with porosity and volume of shale

Predication of anisotropic well logs method taken from Li (2002) was applied on the pure shale sample. The P- and S- wave velocity anisotropy parameters derived by:

$$\varepsilon = 0.60\frac{V_{clay}\times\left(V_P - V_{Pwater}\right)}{V_{Quartz} - V_{Pwater} - 2.65\times V_{clay}}, \quad \gamma = 0.67\frac{V_{clay}\times V_S}{V_{SQuartz} - 2.29\times V_{clay}}$$

where V_{clay} = volume of clay (shale), V_P (or V_P *(0))* = P-wave velocity perpendicular to bedding, V_{Pwater} = an approximation of P-wave velocity at critical porosity, $V_{PQuartz}$ = P-wave velocity of quartz, V_S (or $V_S(0)$) = S-wave velocity perpendicular to bedding, and $V_{SQuartz}$ = S-wave velocity of quartz. The result is given on Figure 61.

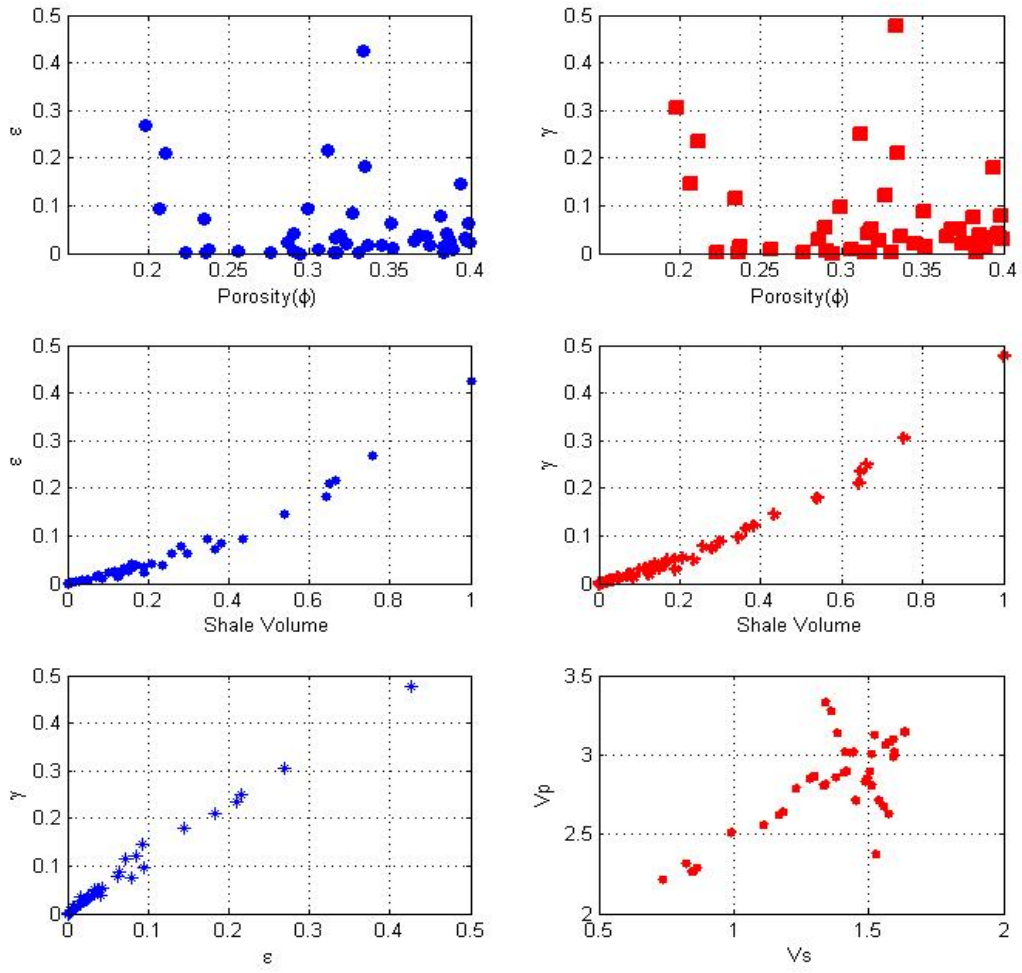

Figure 61: The Anisotropy parameters (a) ε , (b) γ versus porosity, Anisotropy parameters (c) ε , (d) γ versus volume of shale (clay) and (e) ε versus γ , (f) Vp versus Vs

Anisotropy relations

The general relation of P- and S-wave anisotropy derived by:

$$\gamma = 0.0044 + 1.100\varepsilon$$

This linear relationship was compared with formulas derived by Tsuneyama and Mavko (2005) and Wang (2002). These formulas are given as:

$$\gamma = -0.0282 + 1.2006\varepsilon \qquad \text{Tsuneyama and Mavko(2005)}$$

$$\gamma = -0.01049 + 0.9560\varepsilon \qquad \text{Wang (2002)}$$

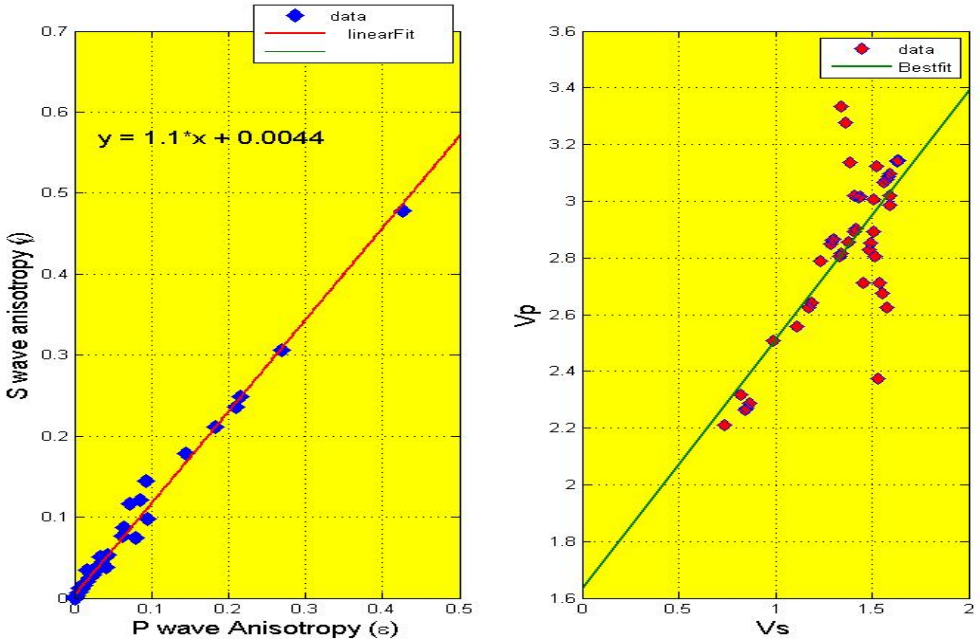

Figure 62: the relation between a) ε and γ b) Vp and Vs. The solid lines are the best fit to the data and the small square dots correspond to one to one relationships between ε and γ and between Vp and Vs.

For example for a laminated Viking Group, Draupne Formation shale specimens from well 33/9-A-37B (Statfjord Field) documented a weak intrinsic P-wave velocity anisotropy which was the order of $\varepsilon = 0.11$. The S-wave velocity anisotropy estimated as by this method is 0.1254, 0.1039 Tsuneyama and Mavko (2005) and 0.0947 and using the equation from Wang (2002). Another example is from a black organic shale (with 15 -20 % TOC) which has documented a substantial intrinsic anisotropy value of 0.4 -0.5 (Vernik and Liu, 1997). For this strong P-wave anisotropy ($\varepsilon = 0.4$) the S-wave anisotropy estimates are 0.44 using the equation from this study, 0.4520 from Tsuneyama and Mavko (2005), 0.3719 from the Wang (2002) method. The remark from these two examples is that the formula derived by this study and Tsuneyama and Mavko (2005) is in good correlation but not with Wang (2005) method. Additionally both this study and the study of Tsuneyama and Mavko (2005) methods used well log data from North Sea. This study method used well from Statfjord Field and Tsuneyama and Mavko (2005) used wells from the Snorre Field. Both the Statfjord and the

Snorre Fields have a similar geological setting. Wang (2002) results was based on data from data was based on laboratory brine saturated core samples.

The relationship between ε and γ in all the three formulas forwarded by Tsuneyama and Mavko (2005), Wang (2002) and this study result may be used to estimate S-wave anisotropy from P-wave anisotropy, or vice versa. Such estimations are independent of pressure, pore fluids, and lithology. It is particularly useful when S-wave anisotropy is available but P-wave anisotropy is not (Wang, 2002). The method applied to estimate the relation between δ with ε and γ, was not successful and for practical purpose may be the formula derived by Li (2002) helpful i. e $\delta = 0.32\varepsilon$

From Figure 12(b) the relationship between Vp and Vs for the selected shale sample was estimated by the formula

$$V_P = 1.126V_S + 1.31$$

The results obtained for Vp and Vs relationship is close to the well know Castagna mudrock line equation given by $V_P = 1.16V_S + 1.36$ (Castagna et al, 1985).

Porosity and anisotropy parameters.

Despite the observed scatter in the anisotropy versus porosity in Figure 64, the P-wave anisotropy shows a slight dependence on porosity using Wang's best-fit line based on brine-saturated core samples. It appears that the S-wave anisotropy shows a poor correlation on porosity. The possible causes of these weak relations between anisotropy parameters and porosity may be due to data selection, estimation of velocity, and logging tool operations.

Considering data selection Brevik et al (2007) used a normalization method to reduce the scatter of velocities which was a result of size and geographical representation. Their methods showed a lack of observed P-wave anisotropy or the apparent increase in anisotropy with increasing porosity, which was in strong contrast to the best-fit line from Wang(2002) based on brine-saturated core samples. But the observed S-wave anisotropy was, however, in reasonable correspondence with Wang (2002).

The other likely reason for the poor correlation between anisotropy and porosity may be due to the mineralogical complexity of the Brent Group (Morton, 1992), since of the samples came from this reservoir zone. The effect of mineralogical variation on logging tools is most obvious on assessment of porosity and density (Moss, 1992). For example the Rannoch

Formation contains significant quantities of micas which increase average matrix density to about 2.75 -2.8 gm/cc. Therefore the use of 2.65 gm/cc as an average matrix density produces erroneously low porosity. Note that also the logs are affected by the thin bedded nature of parts of the Ness Formation and the gradual zone between the sands (simple or complex) and the interbedded mudstones and silts can also complicate the interpretation

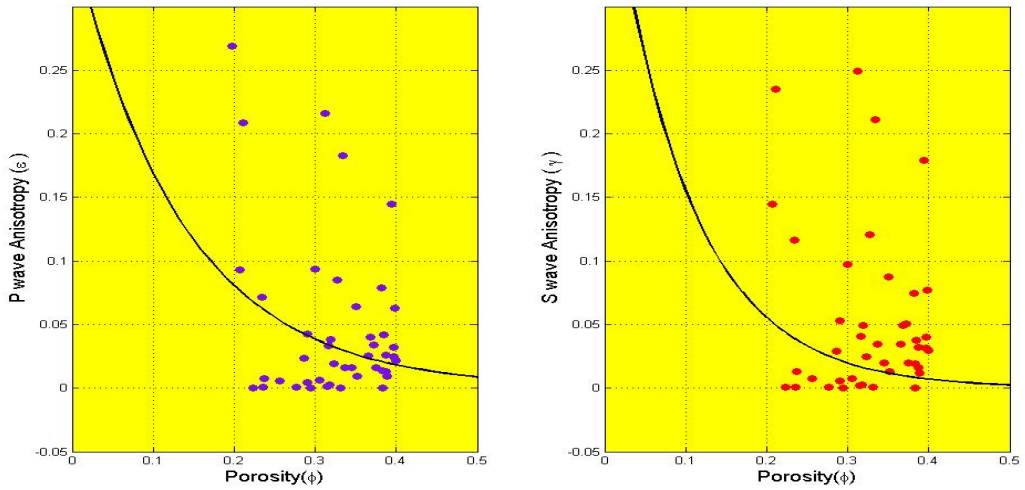

Figure 63: Anisotropy parameters (a) ε , (b) γ versus porosity. The solid lines parabola line in (a) and (b) are Wang (2002) best fit formula. Although large scatter exists; both P- and S-wave anisotropies seem to decrease exponentially with increasing porosity. However, ε and γ are only weakly related to porosity; they seem to decrease as porosity increases.

The volume of shale and anisotropy parameters.

The volume of clay is often considered equivalent to the volume of shale in well log analysis. The orientations of clay minerals are affected by clay volume and compaction. Figure 64 showed the effect of volume of shale for P- and S-wave anisotropy parameters. At first order approximation both P-and S-wave anisotropies showed that there seem to be an exponentially increase with increasing volume of shale..

From the second degree best fit solid line, the relation between the volume of shale (V_{shale}) and P- and S-wave anisotropy parameters are expressed as:

$$\varepsilon = 0.29V^2{}_{shale} + 0.18V_{shale} \quad , \quad \gamma = 0.31V^2{}_{shale} + 0.11V_{shale}$$

The relationship between the anisotropy parameters and volume of shale (clay) using the above equations, is that anisotropy increases exponentially with volume of shale. But at higher volume of shale the exponential relationship is based on few data points. Because of

this shortage of data points, the exponential relationship between anisotropy parameters and volume may not hold for pure shale.

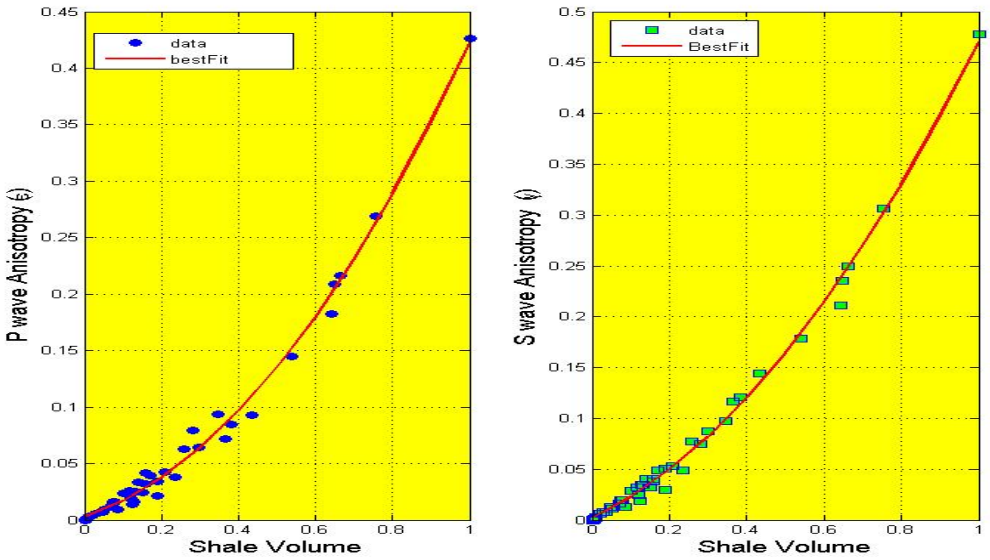

Figure 64: The P and S wave anisotropy parameters versus volume of shale for pure shale. Both P- and S-wave anisotropies seem to increase exponentially with increasing porosity. The solid red lines are best second degree fit and blue dots (P wave) and green dots(S wave) data anisotropy points.

Chapter 6

6. The Use of Velocity Anisotropy for Exploration and Exploitation

Introduction

Laboratory and field experiments in the 1950 detect velocity anisotropy. Despite fifty years of observations in laboratory experiments and over a century of theoretical work, it is only in the past decade that the geophysicists, and exploration community, tried to use anisotropic correction on seismic data.

Previously anisotropy was taken as noise and or it was treated as noise to be removed from the reservoir. Recent research has changed this perception. Especially the intense research on the field of anisotropy and modern techniques and tools able to detect and use the small variation in velocities which are found in sonic and seismic studies.

Taking cap rock variation into account can be very important when explorations are trying to asses target formation. If an Amplitude Verse Offset (AVO) survey does not take account of the transverse isotropic (TIV) in shale cap rock, the underlying gas bearing sandstone may be overlooked because the modelled AVO curve (for an oil sand overlain by anisotropic shale) would not fit the observed AVO response from the survey(Avesth et al,2004).

Anisotropy can make huge difference to reservoir performance. Anisotropy of oil and gas reservoirs starts to develop during the deposition and mostly after deposition diagnesis of the sediments. Reservoir sand can develop anisotropy features during and after deposition. Additionally un-balanced (non-uniform) stress also has effect on changing an isotropic reservoir to anisotropic reservoir.

This chapter will focus on two practical examples of seismic velocity anisotropy research as well as anisotropic corrections on exploration seismic data–and where they apply to exploration problems. The examples are Anisotropic Depth Migration (ADM) for a dipping interface and Anisotropic AVO analysis.

6.1 Anisotropic Depth Migration (ADM)

If there is disturbance on the subsurface geology like tectonic activity, then the TIV anisotropic assumption breaks down (Vestrum and Muenzer, 1997). The resulting dipping layers have tilted symmetry axis or bedding-plane normal. We call this case tilted transverse isotropy (TTI). Several researchers have observed lateral position errors on structures below TTI media (Alkhalifah, 1995, Vestrum and Muenzer, 1997). Correcting imaging and

positioning errors on events below TTI media requires anisotropic depth migration (ADM). A practical example of this misposition problem is illustrated below *(*Vestrum, 2003*)*.

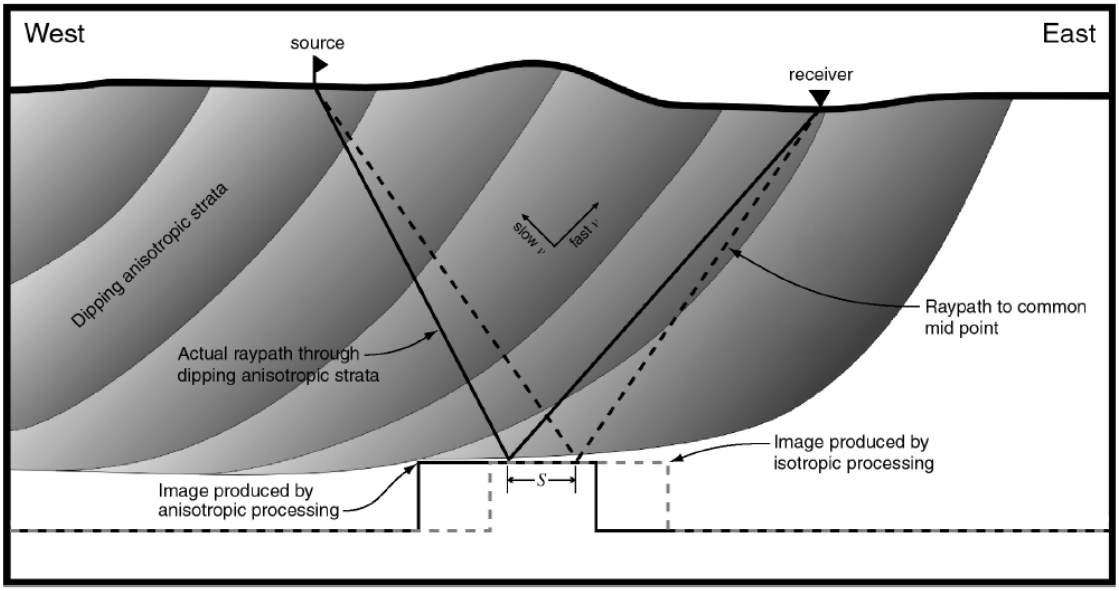

Figure 65: Cross-section showing lateral movement predicted from isotropic processing of data where transverse isotropy with a tilted axis of symmetry is present. The dashed lines represent the result of isotropic processing. S is the distance between the actual subsurface reflection point and the reflection point when isotropy is assumed (Vestrum et al, 1999).

Figure 65 shows the shift one can expect on a subsurface structure below dipping shales. Because the velocity parallel to the shale bedding is higher than the velocity perpendicular to bedding, rays from the eastern or up-dip side of the structure will travel in the fast direction and rays from the western or cross-dip side of the structure will travel in the slow direction. The least-time ray path will have a longer travel path in the faster direction. As seen on Figure 65 for isotropic assumption the lateral position is shifted by S to the right. The correct of this lateral shift can be done by Anisotropic Depth Migration (ADM).

6.2 Anisotropy AVO analysis

Amplitude variation with offset (AVO) is one the few exploration methods that is used for widely for direct detection of hydrocarbon, lithology identification and, more recently, for reservoir monitoring. The improved acquisition design and higher quality of seismic data have allowed the AVO methodology to become more quantitative and sometimes provide us with estimates of important reservoir characteristics including porosity and crack density.

The reflection amplitude depends on the angle of reflection, or offset between the source and receiver, and the contrast between P-and S-wave velocities on either sides of the reflector. The presence of elastic anisotropy on either side of the reflector may significantly distort the angular dependence of reflection coefficients (Banik, 1987). In isotropic rocks, some reflectors especially those where hydrocarbons are involved have amplitudes that vary with angle of reflection. Some operators use this property as a hydrocarbon indicator.

In anisotropic rocks, there is the additional complication that the P and S wave velocities themselves may vary with the angle of propagation, again causing AVO. If a favourable AVO signature is encountered, it is vital to know how much is due to hydrocarbon and how much is due to anisotropy (Armstrong et al, 1994). This dilemma can be resolved modelling, which simulated the seismic response to a given rock or fluid contrast. Modelling requires knowledge of elastic properties, and correct modelling should include anisotropy (Kim et al, 1993).

If the velocity above the reflector is angle-dependent, the behaviour of body-wave amplitudes becomes much more complicated, and the isotropic correction becomes inadequate. The presence of anisotropic layers above the target horizon may be quite typical for sand-shale sequences commonly considered in AVO analysis (Kim et al., 1993). While reservoir sands can be expected to exhibit very weak anisotropy (if any), shale formations are often characterized by strong transverse isotropy, i.e., pronounced velocity variations in the incidence (vertical) plan (Kim et al, 1993).

The main goal of this section is to study the influence anisotropy in transversely isotropic media AVO analysis. To illustrate the problem a weak- and strong anisotropy approximation for shale and isotropic and anisotropic sand layer models used (Storvas and Landrø, 2005). Elastic parameter data are taken from the Gullfaks Field 4D AVO analysis (Landrø and Strønen, 2003). The formation anisotropy parameters (ε and δ) are derived from one of production well bore at Statfjord field.

6.2.1 Reflection coefficients in TI media

Under the plane-wave assumption, Daley and Hran (1977) derived theoretical formulas for reflection and transmission coefficients in TI media. The *P-P* reflectivity in the equation can be decomposed into isotropic and anisotropic terms as follows

$$R_{anis}(\theta) = R_{iso}(\theta) + R_{aniso}(\theta)$$

where $R_{iso}(\theta)$ is the reflection coefficient in the absence of anisotropy (ε=δ=γ= 0) and given by

$$R_{pp}(\theta) = \frac{1}{2}\left[\frac{\Delta Z}{Z}\right] + \frac{1}{2}\left[\frac{\Delta V_P}{V_P} - \left(\frac{2V_S}{V_P}\right)^2 \frac{\Delta\mu}{\mu}\right]\sin^2\theta + \frac{1}{2}\frac{\Delta V_P}{V_P}\sin^2\theta\tan^2\theta \qquad (1)$$

and where $Z = \rho V_P$, denotes the vertical P-wave impedance and θ *is* incident angles for the P-wave and S-wave, respectively, $\mu = \rho V_S^2$ denotes the shear modulus.

$R_{aniso}(\theta)$ is the anisotropic reflection coefficient given by

$$R_{anis}(\theta) = \frac{\Delta\delta}{2}\sin^2\theta + \frac{\Delta\varepsilon}{2}\sin^2\theta\tan^2\theta \qquad (2)$$

where $\Delta\delta = \delta_2 - \delta_1$ and $\Delta\varepsilon = \varepsilon_2 - \varepsilon_1$, the subscripts 1 and 2 refer to the media above and below the reflector, respectively. One of the convenient features of equation (1) is the separation of the "isotropic" and "anisotropic" parts of the reflection coefficient. Assuming weak anisotropy and small offsets, Banik (1987) showed that the anisotropic term can be simply expressed as follows:

$$R_{anis}(\theta) \cong \frac{\Delta\delta}{2}\sin^2\theta \qquad (3)$$

where θ denotes the average of angles of incidence and transmission, $\Delta\delta$ and $\Delta\varepsilon$ denotes the difference in anisotropy across the boundary. $\Delta\delta$ enters the $\sin^2\theta$ term and hence describes the influence of anisotropy on the small angle reflection coefficient and the AVO slope, while $\Delta\varepsilon$ responsible for $\sin^2\theta\tan^2\theta$ term and hence are more dominant at larger incidence angle. This is the manifestation of the well known fact that δ controls the influence of anisotropy for a near vertically travelling P waves while ε dominates near horizontal wave propagation. The influence of ε, δ on the AVO examined by Kim et al (1993) based on the relationship derived by Thomsen(1986) on the variation of phase velocity as a function of incidence angle on the AVO behaviour since phase velocity is one of the most important factors controlling the reflectivity in TI media. This approximation equation for the phase velocity of P–waves in TI media is given by:

$$V_p(\theta) = V_{po}(0)(1 + \delta\sin^2\theta\cos^2\theta + \varepsilon\sin^2\theta) \qquad (4)$$

Since $\sin^2\theta$ is small compared with $\cos^2\theta$ for small θ, the above equation clearly indicates that δ an important parameter for small offsets while ε is important for far offset.

For near offset and weak anisotropy the anisotropy AVO formula in equation (1) reduce to the form

$$R_{aniso}(\theta) = R_{PP}(0) + \left\{ G + \frac{\Delta\delta}{2} \right\} \sin^2\theta \qquad (5)$$

For a planar interface between two VTI layer anisotropic media, the gradient term in the linearized approximation, is given by say G'

$$G' \equiv \left\{ G + \frac{\Delta\delta}{2} \right\} = \frac{1}{2}\left[\frac{\Delta V_P}{V_P} - \frac{2\Delta V_S}{V_S} - \frac{\Delta\rho}{\rho} + \Delta\delta \right] \qquad (6)$$

From the above equation the leading (isotropic) terms are the fractional jumps across the interface of Vp and Vs, which are commonly small in practice, and assumed to be small in the analysis. The anisotropic term δ change or jump is not necessarily small compared to other terms especially at the shale-sand interfaces, where $\delta_{sand} << \delta_{shale}$, and should not be neglected.

6.2.2 Numerical Example for VTI AVO analysis

Most hydrocarbon reservoirs are contained in anisotropic rocks and for a better model description on this study a TVI media assumed, which is the simplest anisotropic model typically used to describe thinly layered media and shale sequences (Armstrong et al, 1994). Provided that the model accounts both the cap rock and reservoir rocks can be anisotropic. In this work, the study focus on to what extent the anisotropic properties of both the cap rock and reservoir rocks influence the ability to distinguish between how much is due to hydrocarbon and anisotropy rock.

Storvas and Landrø (2005) suggested a model which accounts both shale and sand anisotropy which is used here. Consider a plane interface between two homogeneous media with a shale as the upper layer (representing the cap rock) overlaying a sandstone layer (representing the reservoir rock). For the shale three models used:

- Isotropic,
- Weak anisotropy, and
- Large anisotropy.

The large anisotropy model is defined by doubling the anisotropy parameters ε and δ from the weak-anisotropy model. In all cases, the shale is assumed to be anisotropy, and the sandstone is assumed to be elastic.

For the sandstone layer, two models have been used:

- Isotropic and
- TIV

On the previous chapters' velocity anisotropy were observed on the North Sea shale taken from Statfjord. The shale formation was Cretaceous, Draupne and Heather. The over burden rock which consisted of these three anisotropic shale formation sealed the underlying Brent group, Tarbert reservoir.

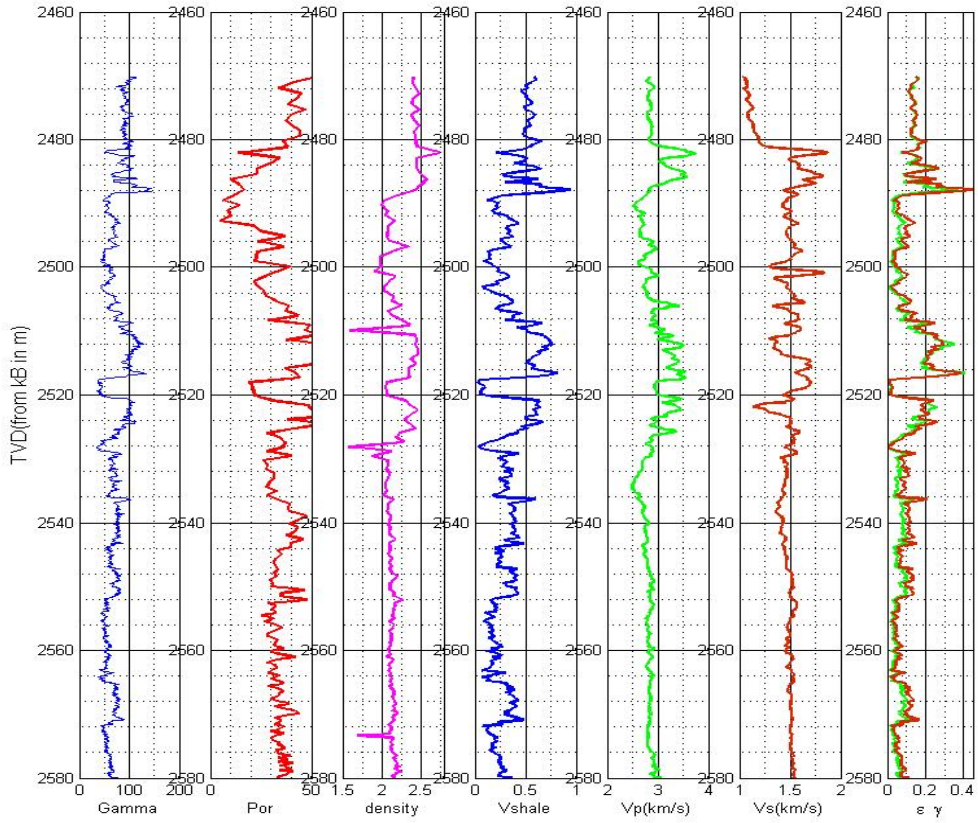

Figure 66: Well logs of a deviated well 33/12-B-23A. The seven columns from the left shows estimated epsilon (gray) and gamma (black) by Li (2002) method.

The whole Statfjord field (similarly for the neighbouring Gullfaks field) the reservoir zone (oil water contact for a seismic) is clearly visible for the good reservoir sands, like the Tarbert Formation. For example Figure 66 shows acoustic and other well logs parameters from well 33/12-B-23A which is a deviated production well**.** On the fifth column where distinct increases in S wav velocity can be observed both at the top Cretaceous and the top reservoir interfaces. This deviated well log was used as input for a simple two layer AVO modelling. Estimated well log elastic parameters for the two layer models are given in Table 10. For computation purpose of the AVO response and to reduce uncertainties due to up calling of

well log data, the data from Landrø and Stronen (2003) used (Table 11). The value of δ is estimated from the formula suggested Li (2002), $\delta = 0.32\varepsilon$ for both shale and sand. To ensure that the combination of the computed value of δ and ε and the model is physically feasible, δ and ε are compared with published anisotropic parameters for North Sea shale and they are in a reasonable range. Figure 67 and 68 shows the modelled AVO curve based on theses data.

Table10: well log derived average AVO analysis parameters for the cap and reservoir rock.

	Vp	Vs	ρ(kg/m^3)	δ	ε
Shale	2.8	1.3	2.1	0.032	0.1
Sandstone	2.25	1.25	2.01	0.016	0.05

Table 11: Seismic derived elastic parameters used for 4D Gullfaks Field study. (The data taken from Landrø and Strønen, 2003).

	Vp(km/s)	Vs(km/s)	ρ (kg/m^3)
Shale	2.9	1.14	2.1
sandstone	2.2	1.24	2.05

6.2.3 The AVO response

The AVO response on Figure 67 and 68 shows reflectivity variation with incidence angle for the three models. The gray solid curve for each model represents the isotropic case. The black solid curves represent the effects of anisotropy where δ_1 = 0.032 in overlying shale and are δ_2 = 0.016 for the underlying sand. The AVO effect generally increases with the angle of incidence and the reflectivity at zero-offset. For all three models, the anisotropy increases the AVO effect. The percentage change of AVO response in the case of weak/ large anisotropy shale sands sequence interface is higher than the where the sand is represented by anisotropic model.

For the near offset anisotropy analysis in Figure 67(a), there was no observed difference between isotropic and anisotropic AVO response up to 5^0. But after around 10^0, the observed difference increased and this due to the extra term $\Delta\delta/2$= [0.016-0.32]/2 = -0.008, which controls the increased AVO effect. In Figure 67(b) the model was done by taking the overlying shale as large anisotropy and anisotropic sand. The large anisotropic model is

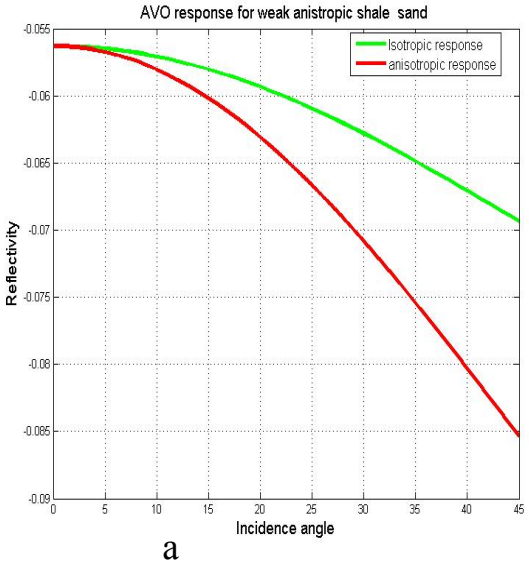

a

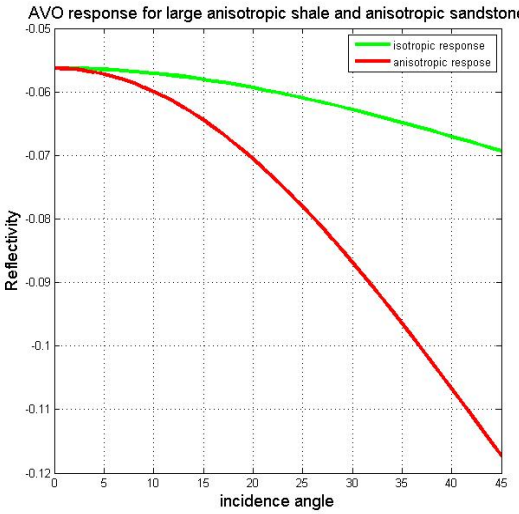

b

Figure 67: Model reflectivity assuming a two layer model at the reservoir interface (input parameters given in Table 1 and 2) The interface model is a) weakly anisotropic shale and anisotropic sandstone sequence, b) large anisotropic shale and anisotropic sandstone sequence. The inclusion of anisotropy leads to the increased reflectivity both at near offset and far offset.

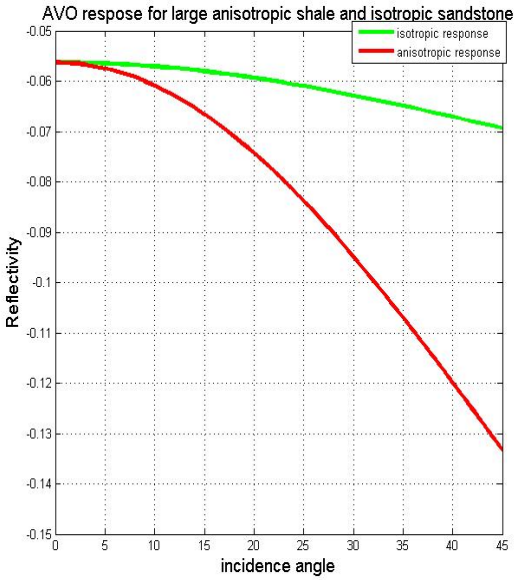

a

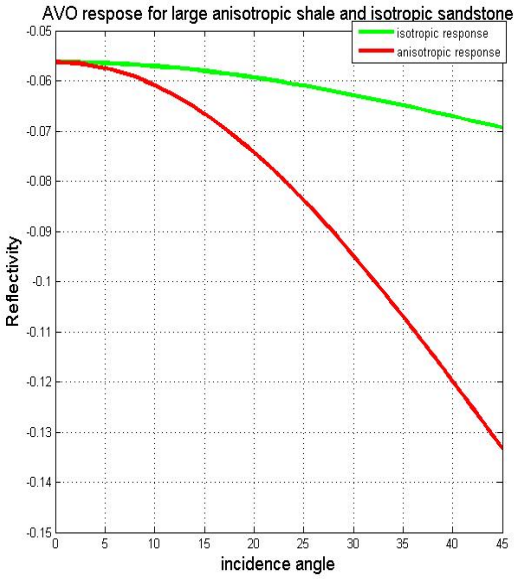

b

Figure 68 a) Model reflectivity assuming a two layer model at the reservoir interface (input parameters given in Table1. The interface model is a) weakly anisotropic shale and isotropic sandstone sequence, b) large anisotropic shale and isotropic sandstone sequence.

defined by doubling the value of δ from the weak anisotropic model (i.e. for large anisotropic model δ for shale is 0. 0.064). In this case also the observed difference in AVO response stared from around 10^0 and at far offset the difference was large than the weak anisotropy model. Figure 68 is the AVO response from a) weakly anisotropic shale and isotropic sandstone sequence, b) large anisotropic shale and isotropic sandstone sequence. The deviation of the AVO response curve is more pronounced as compared with Figure 67.

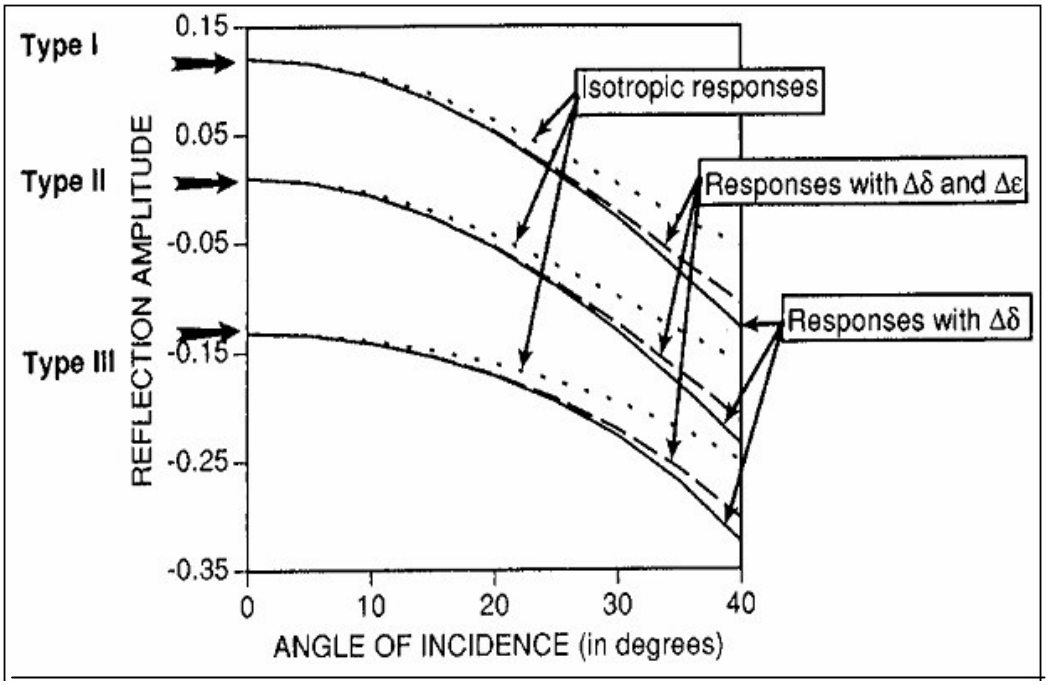

Figure 69: A conventional example of the elastic reflectivity variation with angle of incidence for the three classed of gas sand reflectors. The heavy curves are for anisotropic AVO response and light dotted curves are for isotropic AVO response. The observed difference between the curves is due to the term $\Delta\delta$ which increase the reflectivity at the near offset and $\Delta\varepsilon$ at the far offset (Balngy, 1994).

More illustration of the effect of AVO on gas sand is given on Figure 69. It is a conventional example of the elastic reflectivity variation with angle of incidence for the three classed of gas sand reflectors. In weakly anisotropic TI media with a vertical axis of symmetry, the effect of anisotropy on AVO response have examined for Statfjord field shale and sand sequence. The analysis started from the formulation of isotropy and anisotropy AVO equation at near and far offset. Consideration was given only to P-wave reflection coefficients. The ranges of elastic parameters for computational purpose were taken from the work of Landrø and Strønen, (2003). Provided that anisotropy is a scale dependent effect, and

it is best if measured at a scale similar to the VSP or surface seismic experiment being modelled, such as with VSP.

Chapter 7

7. Conclusions and recommendations

The research in this study was directed on finding the evidence of anisotropy, quantification of the observed degree of anisotropy for VTI media and the use of anisotropy for exploration and exploitation. The study was applied on shale and sandstones formations from the Norwegian Continental Shelf. Some of the findings on this study are:

1. The core sample velocity anisotropy analysis of the Viking shale (Draupne Formation) showed weak anisotropy of the order of 0.11 for P-and S-wave velocities. The observed weak anisotropy was due to state of immaturity of the formation. It is in an early stage of maturation even if it contains an organic matter. Observation indicated that TOC (Kerogen content) exerts a control on the Thompsen velocity anisotropy parameters ($\varepsilon, \gamma, \delta$) however others factors such as clay type and alignment must also contribute. The study demonstrates that anisotropy of wave velocity is linked strongly to kerogen content and maturation. Inversely, velocity may be used as indicator of the detection of kerogen rich shells having different maturation levels.

2. The calcite cemented Broom Formation documented very small degree of velocity anisotropy which is to the order of ε=0.02 and γ= 0.07. This may emphasis the general concept for reservoir sands and sandstone which are essentially clay free have little anisotropy or intrinsically isotropic.

3. The core sample from Haltenbanken Area, the Lange Formation comprise of thick shale column has documented weak velocity anisotropy of ~ ε=0.15 for P-wave and γ= 0.27 for S-wave. The observed pronounced S-wave velocity anisotropy may be due to the space between the pores on the clay minerals may be very small. Then the pores may not contain fluid in their pocket.

4. The observed P-wave velocity anisotropy from two core samples from the Haltenbanken Area of the Not Formation showed that the clayey siltystone ($\varepsilon \approx 0.09$) has less anisotropy than the silty claystone ($\varepsilon \approx 0.15$). Since the silty claystone has contained more clay mineral than clayey siltystone. The lithological variation effect on

these two samples was not observed on the S- wave anisotropy. The type and amount of clay minerals control the degree of anisotropy on the deeply buried Not shale which (buried depth around 4.4 to 4.9 km).

5. The comparison on the sonic velocity between vertical and deviated well bores from the Statfjord Field area showed that the velocity in deviated well is higher than in the vertical well around the shale formations. The predicted anisotropy well log documented strong velocity anisotropy in the organic rich Draupne shale. The Cretaceous shale and the Heather shale showed weak anisotropy compared to the Draupne shale. The value of the predicated P-wave anisotropy ($\varepsilon \approx 0.3$) was larger in well 33/12-B-23A, which was deviated an angle of 75^0. The minimum predicted anisotropy was observed on the vertical well ($\varepsilon \approx 0.1$). The Brent group sandstones below the three shale formations studied is more or less intrinsically anisotropy. For the Brent Group sandstones the predicated P-wave anisotropy are close to zero.

6. From the well log velocity anisotropy analysis, generally the velocity increases with well deviation angle increase for pure shale formation. P- and S-wave a velocity which appears to increase with the well deviation angle ~70^o due to the pure shale sheet-like structure of clay platelets. For higher well deviation angles the result showed the decrease in P-and S-wave velocity due to the inclusion of other mineral on the clay and the mineralogical complexity of the Brent Group reservoir sand. The depositional environment variously affects elastic properties of rock. For example authigenic and detrital clays affect velocity and velocity anisotropy differently. The rate and the source of depositional energy also affect layer induced velocity anisotropy. For example the sand/shale sequences in the Brent Group, Ness Formation are result of alternating depositional energy, rate, and source. Also this result may give additional information to identify the cap rock and reservoir rocks or in general for lithology identification.

7. The estimated velocity anisotropy parameters for pure shale was ε=0.213, γ=0.43 and δ= 0.032 for 80% clay volume and ε=0.15, γ=0.531 and δ= 0.028 for 95 % clay volume. A good correlation was observed with many published North Sea shale anisotropy parameters. The estimated linear relationship between P–and S- wave

success full and it is particularly useful when S-wave anisotropy is available but P-wave anisotropy is not or vice versa.

8. Anisotropic parameter derived from this study was applied on the Anisotropic Depth Migration (ADM) and Amplitude versus Offset (AVO) analysis. The result showed that anisotropy can make a huge difference in reservoir performance and seismic imaging if anisotropic correction is not handled properly.

9. In play and prospect evaluation, source rock, reservoir rock and cap rocks are the three main elements of petroleum system. Accounting the anisotropy feature of these three rocks may help to reduce uncertainties and decrease the number of dry wells. The elastic property (velocity and density) and anisotropy of rock can be potential indicator of remote detection of source rocks, reservoir rock and cap rocks.

10. The Statfjord Field area velocity anisotropy study not only improves an understanding of the Statfjord Field itself, but also adds to the general knowledge of velocity anisotropy in the North Sea area and similar rift systems.

11. If anisotropy is a common subsurface feature, the VTI might be good approximation and representative of medium mainly for computational reasons, not because it is commonly observed in nature and encountered in oil exploration. For a shale layer overlaying a reservoir unit, the VTI assumption might be reasonable, given that the bedding is close to horizontal. However, for the reservoir sand, it is less likely that the VTI assumption is valid. Since mostly hydrocarbon reservoirs are intrinsically isotropic.

Recommendations for Future study.

For the precise quantification and documentation of the velocity anisotropy with small or without uncertainty, this study will recommend the following points.

1. Thorough understanding of the anisotropic should be developed in relation with geological process which influences the subsurface. Such as provenance, sediment transport and deposition, diagensis, compaction.

2. Velocity measurement from different scale of wave length should be integrated to get access for parallel information about the primary anisotropic controlling factors. Shale rock properties like mineralogy, porosity, and texture and environmental conditions like temperature, pore pressure, and external stress vary between the penetrated shale sections. Some of the scales of measurements are XRD, SEM, VSPs, Walkaway VSPs, cross well bore, Ocean bottom seismic (OBS) data

3. Petroleum Industries not only include anisotropy on their rock physics model but also there must be one position which is supposed to be specialist in anisotropy, we call it *anisotropist*. The anisotropist will create new chance of integratation between the Geologist, Geophysicist, petrophysicist and reservoir and drilling engineers. The participation of anisotropist and accounting anisotropy in rock physics model in the Exploration and Production will enhance recovery, decrease the number of dry wells, decreases the risk.

References

Alkhalifah, T., and I. Tsvankin, 1995, Velocity analysis for transversely isotropic media: Geophysics, **60**, 1550–1566.

Anderson et al, 1994, Oil Filed Anisotropy: Its origin and Electrical Characteristics: Oil field review, Schlumberger.

Armstrong et al, 1994, The Promise of Elastic Anisotropy:Oil filed review, Schlumberger.

Avseth P, Tapan M., and Mavko G., 2004, Quantitative seismic interpretation: Applying Rock Physics Tools to Reduce Interpretation Risk; Cambridge University Press, 34-37

Backus, G. E., 1962, Long-wave elastic anisotropy produced by horizontal layering: Journal of Geophysical Research, **67**, 4427–4440.

Badley, M. E., J. D. Price, C. R. Dahl, and T. Agdestein, 1988, The structural evolution of the northern Viking Graben and its bearing upon extensional modes of basin formation: Journal of the Geological Society (London), **145**, 455– 472.

Banik, 1983, Velocity anisotropy of shales and depth Estimation in the North Sea basin: Geophysics, **49,** 1411-1419.

Banik, N. C., 1987, An effective parameter in transversely isotropic media: Geophysics, **52**, 1654-1664.

Berryman, J. G., 2005, Fluid effects on shear waves in finely layered media: Geophysics, **70**, N1–N16.

Berryman, J. G., V. Y. Grechka, and P. A. Berge, 1999, Analysis of Thomsen parameters for finely layered VT1 media: Geophysical Prospecting, **47**, 6, 959–978.

Bjørlykke, K., 1998, Clay mineral diagenesis in sedimentary basins - a key to the prediction of rock properties. Examples from the North Sea Basin: Clay Minerals, **33**, 15 - 34.

Bjørlykke K, 1999, Principal aspects of compaction and fluid flow in mudstones: Physical and Fluid Flow Properties, Geological Society, London, Spec. Publ. 158, 73 - 78.

Bjørlykke, K. and Brendsdal, A., 1986, Diagenesis of the Brent Sandstone in the Statfjord field, North Sea. In: Gautier, D.L. (ed.), Roles of Organic Matter in Sediment Diagenesis. SEPM Special Publ., no. **38**, 57 - 166.

Bjørlykke, K. and Høeg, K., 1997, Effects of burial diagenesis on stresses, compaction and fluid flow in sedimentary basins: Marine and Petroleum Geology, **14**, 267 – 276.

Bjørlykke, K., Nedkvitne, T., Ramm, M. and Saigal, G.C., 1992, Diagenetic processes in the Brent Group (Middle Jurassic) reservoirs of the North Sea - an overview. In: Morton, A.C., Haszeldine, R.S., Giles, M.R. & Brown, S. (eds.), Geology of the Brent Group. Geological Society Special Publication, no. **61**, 263 - 287.

Blangy J.P., 1994, AVO in transversely isotropic media-An overview: Geophysics, **59**, 775-781.

Brandsberg-Dahl, S. and Berkved, O.I., 2002, Anisotropy P-wave velocity derived from deviated wells at the Valhall Field, 64th Mtg.: Eur. Assn. of Expl. Geophys. Expanded Abstract, 135.

Brevik I., Reza A. and Hatteland T., and Alejandra R. M, 2007, Documentation and quantification of velocity anisotropy in shales using wireline log measurements: The Leading Edge, **3**, 272-277.

Byun, B. S., 1984, Seismic parameters for transversely isotropic media: Geophysics **49**, 11, 1908-1914,

Castagna, J. P., Batzle, M. L., and Eastwood, R. L., 1985, Relationships between compressional-wave and shear-wave velocities in silicate rocks: Geophysics, **50**, 571–581.

Daley P. F., and Hran, F., 1977, Reflection and transmission coeffients for transversely isotropic media: Bull., Seis. Sot. Am., **67**, 661-675.

Dalland, A., D. Worsley, and K. Ofstad, 1988, A lithostratigraphic scheme for the Mesozoic and Cenozoic succession offshore mid- and northern Norway: Norwegian Petroleum Directorate Bulletin, **4,** 65.

Deegan, C. E., and B. J. Scull, 1977, A standard lithostratigraphic nomenclature for the Central and northern North Sea: Norwegian Petroleum Directorate Bulletin, **1**, 35.

Ehrenberg, S. N. 1993, Preservation of anomalously high porosity in deeply buried sandstones by grain-coating chlorite: Examples from the Norwegian continental shelf: AAPG Bulletin **77**, 1260–1286.

Furre, A., and Brevik, I., 1998, Characterization of angle dependency in sonic logs: 68th Ann. Intenat. Mtg., Soc. Expl. Geophys., Expanded Abstracts.

Færseth, R. B., Sjsblom, T. S., Steel, R. J., Liljedahl, T., Sauar, B. E., & Tjelland, T. 1995, Tectonic controls on Bathonian-Volgian synrift successions on the Visund fault block northern North Sea. Sequence stratigraphy on the Northwest European margin. In R. J. Steel (Ed.), NPF Special Publications, 5, 325-346.

Gabrielsen, R. H., 1986, Structural elements in graben systems and America Bulletin, 93, 606612.their influence on hydrocarbon trap types. In A. M. Spencer (Ed.), Habitat of hydrocarbons on the Norwegian continental shelf (pp. 5-60). London: Norwegian Petroleum Society, Graham and Trotman.

Gassmann, F., 1951, Elastic waves through a packing of spheres: Geophysics, **16**,673-685.

Glasmann J.R., 1992, The fate of feldsapre in Brent Group reservoirs, North Sea: a regional synthesis of diagensis in shallow, intermediate, and deep burial environments: The Geology of Brent Group, Geological Society Special Publication no, **61**, 329-350.

Glennie, K. W., 1990, Introduction to the petroleum geology of the North Sea: Oxford, United Kingdom, Blackwell Scientific Publications, 403.

Harris B. N., 1992, Burial diagensis of Brent sandstones: a study of Statfjord, Huttom and Lyell fields. The Geology of Brent Group, Geological Society Special Publication No, **61**, 351.

Helbig k., 1994, Foundation of Anisotropy for Exploration Seismic, Handbook of Geophysical Exploration Section 1. Seismic Exploration, Volume 22 Oxford, England: Elsevier Science Ltd.

Helbig and Thomsen, 2005, 75-plus years of anisotropy in exploration and reservoir seismic: A historical review of concepts and methods: Geophysics, **70**, 9-23.

Hesthammer J. and Fossenb H., 1999, Evolution and geometries of gravitational collapse structures with examples from the Statfjord Field, northern North Sea: Marine and Petroleum Geology, **16** , 259-281.

Hesthammer J., Jourdan C.A., Nielsen P.E.,Ekern T.E and Gibbons K.A., 1999, A tectonographic framework for the Statfjord Field, northern North Sea: Petroleum Geosciences, **5** ,241-256.

Hornby, B. E., Miller, D. E., Esmersoy, C., and Christie, P. A. F., 1995, Ultrasonic-to-seismic measurements of shale anisotropy in a North Sea well: 65th Ann. Intenat. Mtg., Soc. Expl. Geophys., Expanded Abstracts, 17–21.

Hornby, B. E., Schwartz, L. M., and Hudson, J. A., 1994, Anisotropic effective-medium modelling of the elastic properties of shales: Geophysics, **59**, 1570–1583.

Hornby BE., 1998, Experimental laboratory determination of the dynamic elastic properties of wet, drained shales,:J Geophys Res, 103(B12)

Hornby B.E., Howie J.M., and Ince D.W., 2003, Anisotropy correction for deviated-well sonic logs: Application to seismic well tie: Geophysics, **68,** 464–471.

Jones, L. E. A., and Wang, H. F., 1981, Ultrasonic velocities in Cretaceous shales from the Williston basin: Geophysics, **46**, 288–297.

Johnston, D. H., 1987, Physical properties of shale at temperature and pressure: Geophysics, **10**, 1391–1401.

Johnston, J. E., and Christensen, N. I., 1995, Seismic anisotropy of shales: J. Geophys. Res., **100**, 5991–6003.

Kaarsberg, E. A., 1958, introductory studies of natural and artificial argillaceous aggregates by sound-propagation and X-ray diffraction methods: J. Geol., **67**, 447–472.

Kim Y. K, Wrolstad K H., and Aminzadeh F., 1993 Effects of transverse isotropy on P-wave AVO for gas sands: Geophysics, **58**, 883 -888.

Koesoemadinata A.P. and McMechan G.A., 2004, Effects of diagenetic processes on seismic velocity anisotropy in near-surface sandstone and carbonate rocks: Journal of Applied Geophysics **56,**165– 176.

Landrø M., and Strønen L.K., 2003, 4D study of fluid effects on seismic data in the Gullfaks Field, North Sea, Geofluid, **3**, 233-244.

Liner C., and Fei T., 2007, The Backus number:The Leading Edge, **4**, 420-426

Li Y., 2002, Anisotropic well logs and their applications in seismic analysis, SEG Expanded Abstracts.

Li Y., 2002, An empirical method for estimation of anisotropic parameters in clastic rocks: The Leading Edge, **6**, 706-711.

Lo, T. W., Coyner, K. B., and M. N., 1986, Experimental determination of elastic anisotropy of Berea Sandstone Chicopee Shale and Chelmsford Granite: Geophysics, **51**, 164-171.

Mancini F., 2004, Converted wave imaging in anisotropic media using sea-floor seismic data, Thesis submitted for the degree of Doctor of Philosophy School of GeoSciences University of Edinburgh.

Moss B, 1992, Petrophysical characteristics of the Brent sandstones: The Geology of Brent Group, Geological Society Special Publication, **61**,471-494.

Morton A.C., 1992, Provenance of Brent Group sandstones: heavy mineral constraints:The Geology of the Brent Group , Geological Society Special Publication , **61**, 227-244.

NPD factmaps and factpages. Retrieved 2006.05.31 from http://www.npd.no/. Norwegian Petroleum directorate.

Nygård, Gutierrez M., Høeg K., and Bjørlykke K., 2004, Influence of burial history on microstructure and compaction behaviour of Kimmeridge clay", Petroleum Geoscience, **10**, 269-270.

Oil field glossary. Retrieved 2007.04.08 from http://www.glossary.oilfield.slb.com/. Schlumberger.

Pearson, M.J., 1990, Clay mineral distribution and provenance in Mesozoic and Tertiary mudrocks of the Moray Firth and Northern North Sea: Clay Minerals, **25**, 519–541.

Per Mo, 2006, Velocity - Depth trends: A comparison between laboratory and log derived measurements for wells from the Norwegian shelf, Master Thesis in Geoscience, University of Department of Geology, Norway.

Rai, C. S., and Hanson, K. E., 1988, Shear-wave velocity anisotropy in Sedimentary rocks: A laboratory study: Geophysics, **53**, 800–806.

Ruiz D. S., 2004, Intrinsic and stress induced velocity anisotropy in unconsolidated sands: PhD thesis, Stanford University, USA.

Roberts, A. M., G. Yielding, N. J. Kusznir, I. M. Walker, and D. Dornlopez, 1995, Quantitative-analysis of Triassic extension in the northern Viking Graben: Journal of the Geological Society (London), **152**, 15– 26.

Rowbotham et al, 2003, the implication of anisotropy for seismic impedance inversion", First Break, Abstract.

Sam M.S and Andrea A., 2001, the effect of clay distribution on the Elastic properties of sandstones, Geophysical Prospecting, **49**, 128-150.

Sayers, C. M., van Munster, J. G., and King,M. S., 1990, Stress-induced ultrasonic anisotropy in Berea Sandstone: Internat. J. Rock Mech. Min. Sci. & Geomech. Abstr., **27**, 429–436.

Song I., Suh M, Woo Y. H, Hao T, 2004, Determination of the elastic modulus set of foliated rocks from ultrasonic velocity measurements: Engineering Geology, **72**, 293–308.

Stovas A. and Landrø M., 2005, Fluid-pressure discrimination in anisotropic reservoir rocks - A sensitivity study: Geophysics, **70**, O1–O11.

Storvoll, V., Bjørlykke, K., Karlsen, D. and Saigal, G, 2002, Porosity preservation in reservoir sandstones due to grain-coating illite: a study of the Jurassic Garn formation from the Kristin and Lavrans Fields offshore Mid-Norway: Marine and Petroleum Geology, **19**, 767-781

Storvoll, V. and Bjørlykke, K**.**, 2004, Sonic velocity and grain contact properties in reservoir sandstones: Petroleum Geoscience, **10**, 215-226.

Storvoll, V., Bjørlykke, K. and Mondul, N.H., 2005, Velocity-depth trends in Mesozoic and Cenozoic sediments from the Norwegian Shelf: AAPG Bull., **89**, 359-381.

Thomsen, L., 1986, Weak elastic anisotropy: Geophysics, **51**, 1954-1966.

Tosaya, C., and Nur, A., 1982, Effects of diagenesis and clays on compressional velocities in rocks: Geophys. Res. Lett., **9**, 5-8.

Tosaya, C., 1982, Acoustical properties of clay-bearing rocks: Ph.D. thesis, Stanford Univ**,** USA

Tosaya, C., and Nur, A., 1989, Effects of diagenesis and clays on compressional velocities in rocks, *in* Nur, A., and Wang, Z., Eds., Seismic and acoustic velocities in reservoir rocks: Soc. Expl. Geophys, 116–119.

Tsvankin llya, 1995, Body-wave radiation patterns and AVO in transversely isotropic media: Geophysics, **60,** 1409-1425,

Tsvankin, I., and Thomsen, L., 1994, Nonhyperbolic reflection moveout in anisotropic media: Geophysics, **59**, 1290-1304.

Tsuneyama F. and Mavko G., 2005, Velocity anisotropy estimation for brine-saturated sandstone and shale: The Leading Edge, **24,**882-888.

University of Oslo, dept of Geology class fronter. https://blyant.uio.no/

Vernik, L., and Nur, A., 1992, Ultrasonic velocity and anisotropy of hydrocarbon source rocks: Geophysics, **57**, 727–735.

Vernik, L., Liu, X., and Nur, A., 1994, Effect of kerogen on velocity anisotropy in source rocks: 64th Ann. Internat. Mtg., Soc. Expl. Geophys., Expanded Abstracts, 323–326.

Vernik L., 1997, Predicting porosity from acoustic velocities in siliciclastics: a new look: Geophysics **62**, 118-128.

Vernik L. and Nur A., 1992, Petrophysical classification of siliciclastics for lithology and porosity prediction from seismic velocities: Bulletin of the American Association of Petroleum Geologists, **76**, 1295-1309.

Vestrum, R., 2003, Imaging Below Dipping Anisotropic Strata, PhD Theses, University of Calgary, Canada.

Vestrum, R. W., D. C. Lawton, and R. Schmidt, 1999, Imaging structures below dipping TI media: Geophysics, **64**, 1239–1246.

Volleset, J., and A. G. Dore, 1984, A revised Triassic and Jurassic lithostratigraphic nomenclature for the Norwegian North Sea: Norwegian Petroleum Directorate Bulletin, **3**, 53.

Wang Z., 2001, Fundamentals of seismic rock physics: Geophysics, **66**, 398–412.

Wang Z., 2002, Seismic anisotropy in sedimentary rocks, part 1: A single-plug laboratory method: Geophysics, **67**, 1415–1422,

Wang, Z., 2002, Seismic anisotropy in sedimentary rocks, part 2: Laboratory data: Geophysics, **67**, 1423–1440,

Winterstein, D. F., 1990, Velocity anisotropy terminology for geophysicists: Geophysics, **55**, 1070-1088.

Appendix

Abbreviations used in this thesis

MD	Measured Depth
RKB	Relative Kelly bushing (zero-level used during drilling)
SEM	Scanning Electron Microscopy
XRD	x-ray diffraction
TVD	True Vertical Depth
Vp	Compressional velocity (P-wave velocity)
Vs	Shear wave velocity (S-wave velocity)
TI	transverse isotropic
VTI	Vertically transverse isotropic
HTI	Horizontal transverse isotropic
TTI	Tilted transverse isotropic
CID	isotropically consolidated drained test
CIU	isotropically consolidated undrained test
NGI	Norwegian Geotechnical institute
VSP	vertical seismic profile
TOC	total organic carbon
AVO	amplitude versus offset
NCS	Norwegian Continental Shelf
ε	P-wave velocity anisotropy parameters (Thomopsen parameters)
γ	S-wave velocity anisotropy parameters (Thomopsen parameters
δ	anisotropy parameters related with energy of wave propagation (Thomopsen Parameters
A	the degree of anisotropic coefficient